



SCUOLA DI DOTTORATO
UNIVERSITÀ DEGLI STUDI DI MILANO-BICOCCA

Department of Materials Science

Ph.D. program in

Materials Science and Nanotechnology

Cycle XXIX

ORGANIC MATERIALS FOR ENERGY

Ph.D. candidate

SALAMONE Matteo Marco, M.Sc.

Registration number 040086

Tutor: Prof. RUFFO Riccardo, Dr.

Coordinator: Prof. BRIVIO Gian Paolo

ACADEMIC YEAR 2015/16

Organic Materials for Energy

A dissertation submitted to
Università degli Studi di Milano Bicocca
for the Degree of
Doctor in Materials Science and Nanotechnology
Cycles XXIX
Presented by
Matteo Marco SALAMONE, M.Sc.
Student # 040086

Tutor: Prof. Dr. Riccardo RUFFO, Università di Milano Bicocca

Referee: Prof. Dr. Mauro PASTA, University of Oxford

Referee: Prof. Dr. Fabio LAMANTIA, Universität Bremen

a.a. 2015/16

To Laura and Giacomo

Life Is What Happens to You
While You Are Busy Making Other Plans

J. Lennon

Table of Contents

Abstract	12
Riassunto	13
Chapter 1 Introduction	15
Motivation	16
Electrochemical Energy	20
Electrochemical Energy Storage Devices.....	23
Battery	27
Selection Criteria for Commercial Battery Systems	31
Lithium-ion Batteries - LIBs.....	32
Primary Li Batteries	33
Secondary, Rechargeable, Li Batteries	35
Reaction Mechanisms.....	37
Negative Electrodes.....	38
Positive Electrodes	42
Issues with Current Li-ion Batteries.....	47
Possible Improvements for Li-ion.....	48
Beyond lithium-ion	49
Aim of This Work	52
Chapter 2 Organic Materials for Energy.....	54
Pigments	61
Organic Small Molecule Working Principle	66

Factors Influencing the Electrochemical Performance	67
Prussian Blue Analogues.....	67
Chapter 3 Characterization Methods	72
Active Material Characterization.....	73
Thermal Gravimetric Analysis – TGA	73
Differential Temperature Analysis – DTA	74
Mass Spectrometry - MS	75
Scanning Electron Microscopy – SEM.....	76
Transmission Electron Microscopy – TEM.....	78
Energy Dispersive X-ray Spectroscopy – EDX	80
X-ray Diffraction – XRD	80
Electrochemical Cell preparation	83
Slurry Formulation.....	83
Electrode Casting.....	84
Cell: Flooded, Swagelok™, Coin.....	86
Battery Characterization.....	88
Cyclic Voltammetry – CV	89
Galvanostatic Cyclation with Potential Limitation – GCPL	92
Electrochemical Impedance Spectroscopy – EIS	94
Chapter 4 Discussion	97
Pigments – Small Molecules.....	98
Early steps.....	98

Perylene Pigments.....	101
Indanthrone.....	114
Quinacridone Pigments	123
Pigments – Prussian Blue Analogues.....	133
Manganese Hexacyanochromate – MnHCCr.....	133
Chromium hexacyanochromate - CrHCCr	142
Chapter 5 Conclusions and Future Work.....	152
Conclusions.....	153
Outlook	156
Annex.....	158
Bibliography.....	159
Table of Figures	172
List of Symbols, Fundamental Constants and Abbreviations	180
Publications, Posters, Conferences	183
Curriculum Vitae.....	186
Acknowledgements	189

Abstract

Energy storage systems are of high interest and in the last decades their demand grew exponentially. In particular mobile devices, Full and Hybrid Electric Vehicles and smart grids are looking for tailored solutions. Because of new energy efficiency and environmental guidelines, researchers are called to find new solutions for energy storage taking in account costs, availability and environmental impact. Nowadays inorganic materials for LIBs needs scarce and, occasionally, toxic elements. Furthermore, the production and process of mixed oxides materials involves energy-demanding fabrication routes. LIBs technology is at the pole since decades and big improvements were made mainly in the field of process and engineering optimization. No breakthrough technology seems to be close to enter the market in the next years. Organic materials offer different advantages over inorganic ones. E.g., they are easy to tailor and composed mainly of C, H, N, O and S, all abundant elements. It has been also reported that organics can be synthesized from reactants produced from biomass wastes. Among them all, pigments are cheap, crystal and insoluble. Another family of pigments is the one of Prussian Blue Analogues. Their affinity to either organic, because of the similarities with MOFs, or inorganic compounds is still debated. PBAs offer several advantages: inexpensive, open framework structure and tailorable electrochemical properties. In this work, we are going to present the results of the studies realized on three different organic small molecule pigments, perylene diimide, Indanthrone and quinacridone, as well as two chromates based PBAs.

Riassunto

Negli ultimi decenni gli apparati per l'immagazzinamento dell'energia riscuotono elevato interesse e la loro richiesta è cresciuta esponenzialmente. In particolare i dispositivi mobili, gli autoveicoli sia elettrici sia ibridi e la nuova rete di distribuzione dell'energia elettrica richiedono soluzioni su misura che soddisfino specifiche esigenze. A seguito di nuovi regolamenti sull'efficienza energetica e ambientali, i ricercatori sono chiamati a sviluppare nuove soluzioni per lo stoccaggio dell'energia che tengano conto del costo, della disponibilità delle materie prime e dell'impatto ambientale. I materiali inorganici utilizzati oggi nelle batterie Litio-ione sono costituiti spesso da elementi rari e talvolta tossici. Inoltre, la produzione e la lavorazione degli ossidi misti richiede molta energia. Da diversi decenni, la tecnologia Li-ione è essenzialmente ferma e i miglioramenti sono arrivati principalmente dall'ottimizzazione del processo produttivo e al momento, non è attesa l'introduzione di nessuna nuova tecnologia innovativa. I materiali organici offrono diversi vantaggi rispetto agli omologhi inorganici: infatti sono semplici da modificare e sono costituiti da C, H, N, O e S, tutti elementi abbondanti. E' noto inoltre che i materiali organici possano essere sintetizzati da precursori prodotti riciclando le biomasse. Fra tutti i composti organici, i pigmenti sono economici, cristallini e insolubili. Una famosa classe di pigmenti è quella degli analoghi del Blu di Prussia (PBA) la cui appartenenza ai composti organici o inorganici è ancora dibattuta. I PBA possiedono i seguenti vantaggi: convenienza, struttura cristallina 3D, facile ottimizzazione e stabilità. In questo lavoro presenteremo i risultati ottenuti dallo studio di tre differenti pigmenti organici, perylenediimide, indantrone e chinacridone, e due PBA contenenti esacianato di cromo.

Chapter 1

Introduction

Motivation

Energy is necessary for different reasons, starting from the most basic and ancestral needs as the preparation of food and the provision of heat, passing through illuminating a light bulb and ending to supplying energy to portable devices ¹.

The kind and the nature of energy changed depending on the application, scientific and technological progress and the century.

Wood has been the only source of energy, once burned, for thousands of years since coal and, more recently, oil derivatives became more appealing because of their higher energy density.

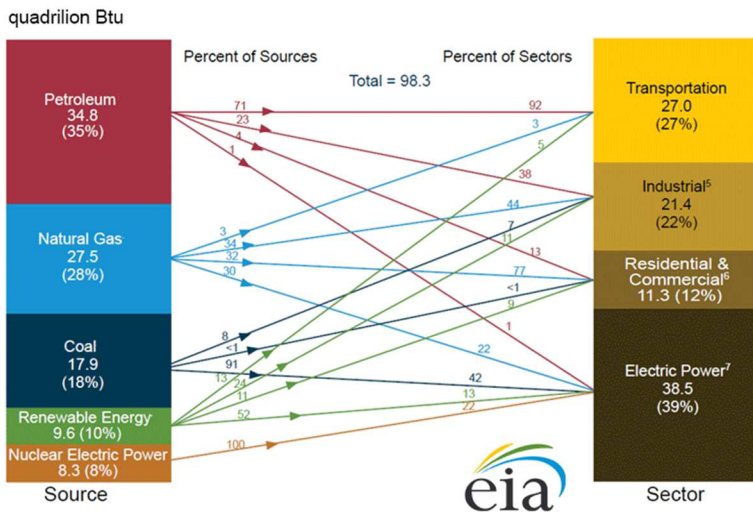


Figure 1 Primary energy consumption by source and sector in US in 2014 ².

With the progression of Physics, Chemistry and, in particular, Thermodynamics scientists discovered the fundamental relationship between Energy, Heat and Work:

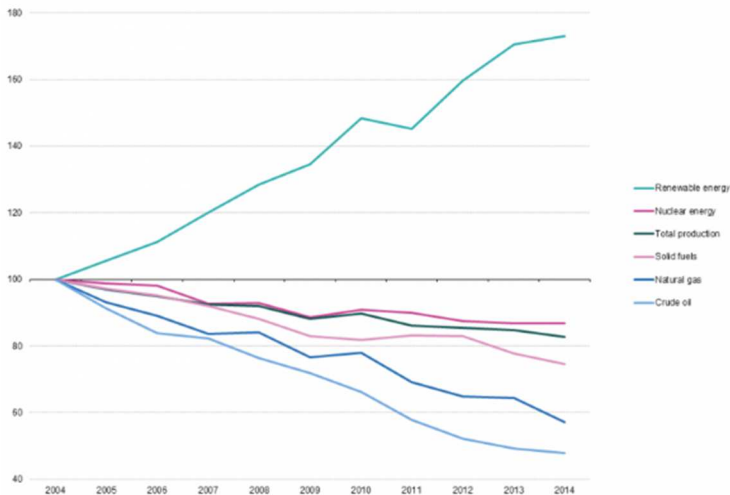
$$\Delta U = q + w \quad [\text{eq. 1}]$$

Eq. 1st Law of Thermodynamics for closed system: U, Internal Energy, q, Heat, and w, Work. IUPAC sign convention.

This relation is crucial in understanding that U, q and w are of the same nature and therefore we can transform one into the other. Making it in a reversible or efficient way is the challenging part.

Nuclear power could have been the answer to energy needs of modern society, but, unfortunately, both catastrophic faults (e.g. Chernobyl 1986 and Fukushima 2011) as well as the not fully addressed problem of safely store the radioactive waste are gradually pushing the public opinion, especially in Europe, to abandon this technology. Anyhow, some countries (e.g. France, USA, Russia, India and China) still rely on nuclear technologies up to 70% in energy production and they still invest in it.

The problem of the depletion of fossil fuels as well as the growing of environmental consciousness moved the interest towards “green & renewable” energy sources as wind, water, solar and others challenging, as in Figure 2, and unlikely applicable sources like tidal waves, geothermic heat and rainfall.



Source: Eurostat (online data code: nrg_100a)

Figure 2 Development of the production of primary energy in EU-28 during 2004-2014 timespan. ³.

However, all the aforementioned energy sources share the same common limitations: time dependence and portability.

Traditional fossil-fuel run power plants need time to switch on and off or, simply, vary the amount of energy produced. The availability of water, strength of wind, intensity of solar irradiation is not constant, periodic and not evenly distributed on earth. It is also obvious that none of these technologies can be pocket-size.

Moreover, depending on the months, weeks, days and hours the need of energy continuously varies respect to the mean request. Surplus or lack of energy consumption can seriously damage the distribution power grid leading to costly blackouts. Matching supplies with the demands is called load/resource management ⁴. Computers

can help in foreseeing these fluctuations, but short-term transient cannot be faced without the use of fast energy buffer apparatus.

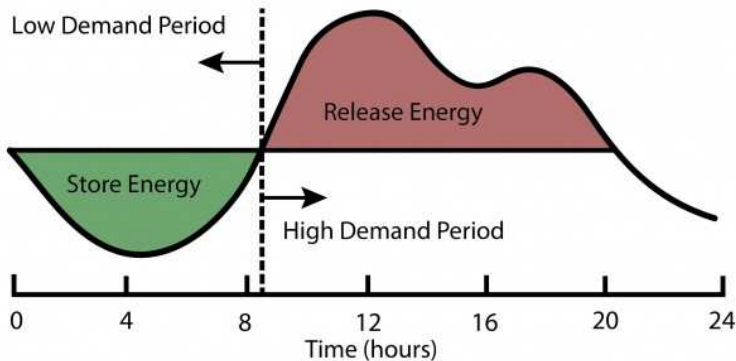


Figure 3 Offer and demand of energy fluctuations and buffer mechanism ⁵.

The more efficient and easy-to-make approach to store energy is Pumped-Storage Hydroelectricity (PSH). As in Figure 3, in “Low Demand Period” there is an under-consumption of energy in the grid, so water is pumped uphill converting electrical energy (surplus from the grid) in mechanical energy (pump) and finally potential energy (pumped water) with an efficiency claimed to be up to 85% ⁶. It is clear that PSH as others mechanical approaches (e.g. flywheels and pressurized air) are slow responding systems and need impressive infrastructure to be practically and economically valuable ⁷.

Portable application is another key market in which conventional energy system cannot be applied because of the impossibility of shrinking the storage and converting apparatus. Mobile applications are Micro Electromechanical Systems ⁸, semiconductor memories, portable devices (e.g. mobile phones, tablets, laptops, shavers, cordless tool, ...) as well as the high demanding FEVs and HEVs.

Another source of energy is the one involved in chemical reactions, mainly heat. There are congruent chemical reactions, in which there is no change in composition (e.g. phase change), and non-congruent ones, in which products have different compositions respect to the reagents. Examples of non-congruent reactions are:

- Insertion reaction (i.e. intercalation) of a guest species $x\text{A}$ in the unoccupied crystallographic sites of an existing stable host material B forming a solid solution A_xB .
- Formation reactions. $\text{A} + \text{B} = \text{AB}$

$$\Delta G_r^0 = \sum \Delta G_f^0(\text{products}) - \sum \Delta G_f^0(\text{reactants})$$
- Decomposition reaction: $\text{AB} = \text{A} + \text{B}$
- Displacement reaction: $\text{A} + \text{BX} = \text{AX} + \text{B}$
 This happens spontaneously if phase AX is more stable than BX (i.e. $\Delta G_f^0_{\text{Ax}} \ll \Delta G_f^0_{\text{Bx}}$).

Generally, in chemical reaction the chemical energy is transformed in heat and, if reversible, vice versa. Therefore, reversible chemical reactions can be used to store energy, but the heat is not a “portable” source of energy and it must be converted into a usable form to run electronic apparatus. Conversely, electrochemical energy is ready to use.

Electrochemical Energy

Electrochemical energy involves the conversion, or transduction, of chemical energy in electrical one and, if the reaction can be inverted, the opposite. In order to define the electrical energy we must combine the first and second laws of thermodynamics and add a generic work term to the resulting equation:

$$dU = TdS - pdV + dw_{\text{other}} \quad [\text{Eq. II}]$$

The Gibbs' free energy and the enthalpy are described as follow:

$$G = H - TS \quad [\text{Eq. III}]$$

$$H = U + pV \quad [\text{Eq. IV}]$$

Combining the eq. III and eq. IV, we obtain:

$$G = U + pV - TS \quad [\text{Eq. V}]$$

Taking the total differential of eq. V and substituting eq.II gives:

$$dG = -SdT + Vdp + dw_{other} \quad [\text{Eq. VI}]$$

For a process at constant temperature and pressure:

$$dG_{T,p} = dw_{other} \quad \text{and} \quad \Delta G_{T,p} = w_{other,max} \quad [\text{Eq. VII}]$$

Where $w_{other,max}$ is the maximum work done on the system for a reversible process and in electrochemistry this work corresponds to the electrical one.

In general work done on the surroundings is a force F acting through a distance dx and in case of electrical work the force depends on the charge Q and the electric field \mathbf{E} , thus:

$$dW_{surr,el} = Fdx = Q\mathbf{E}(x)dx \quad [\text{Eq. VIII}]$$

Nevertheless, the electric field is the derivative of the electrical potential ϕ :

$$\mathbf{E} = -\frac{\delta\phi}{\delta x} \quad [\text{Eq. IX}]$$

$$dw_{surr,el} = -Q\frac{\delta\phi}{\delta x}dx = -Qd\phi \quad [\text{Eq. X}]$$

$$w_{surr,el} = - \int Qd\phi = -Q \int d\phi = -Q(\phi_f - \phi_i) = -QE \quad [\text{Eq. XI}]$$

And

$$w_{sys,el} = -w_{surr,el} = +QE \quad [\text{Eq. XII}]$$

With E the electrical potential through which the charge Q moves. However, for electrochemical reactions, the moving charges are moles of electrons and Q can be rewritten:

$$Q = -nF \quad [\text{Eq. XIII}]$$

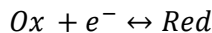
Where F is the Faraday's constant F=96485 coulomb/mole. n is negative because the charge of electrons is minus as well. We can then rewrite w_{sys} and the Gibbs' free energy like this:

$$w_{sys,el} = -nFE = \Delta G_{p,T} \quad [\text{Eq. XIV}]$$

At constant p and T, the van't Hoff equation identifies the Gibbs' free energy for a chemical reaction in non-standard conditions as follows:

$$\Delta G_{p,T} = \Delta G^0 + RT \ln \frac{a_p}{a_r} \quad [\text{Eq. XV}]$$

Where R is the gas constant, T the absolute temperature and a_p and a_r the activity of the products and reagents, respectively. Combining this latter equation with eq. XIV, for a general electrochemical redox reaction:



We can write the Nernst equation for diluted solutions:

$$E = E^0 - \frac{RT}{nF} \ln \frac{[Ox]}{[Red]} \quad [\text{Eq. XVI}]$$

The Nernst equation gives the electromotive force (emf) of a cell when no current is flowing (i.e. at open circuit potential) and [Ox] and [Red] are in non-standard conditions (i.e. non-unit activity)^{9,10}.

When the current flows through an external circuit, the available emf is always lower than the theoretical one because of the overpotential η , a kinetic parameter:

$$E_{practical} = E_{theoretical} - \eta \quad [\text{Eq. XVII}]$$

$$\eta = \eta(i) \quad [\text{Eq. XVIII}]$$

Where i is the flowing current and η represents the potential drop in the chemical-electrical transduction of energy, hence the “loss” of efficiency. Depending on the involved mechanisms, η is composed of one or more contributes: ohmic, charge transfer, diffusion and reaction overpotentials. This loss depends not only on the nature of the materials involved but also on others factors as well: for example, morphology (e.g. shape, size and porosity of the material) can be a key parameter to play with to improve performance.

Electrochemical Energy Storage Devices

Storing energy by electrochemical means, or transforming chemical energy in usable work, has been known to men for many centuries¹¹.

The first example of battery was discovered in 1936 near Baghdad. It is a terracotta jar with two electrodes made of iron and copper probably immersed in an acidic electrolyte of natural origin, like lemon juice. It is believed to be 2000 years old and its real use is still debated¹².

electrochemically to produce a steady current. This apparatus has been lately named fuel cell ¹⁵.

The third way to store energy using electrochemistry are capacitors, invented in 1745 by Ewald Jürgen Georg von Kleist. That concept was then updated and improved in 1957, when General Electric applied for a patent describing a device that would store larger amounts of energy than conventional capacitors: supercapacitors or electrochemical double layer capacitors (EDLC) were born ¹⁶.

Despite being based on three diverse principles, batteries, fuel cells and EDLCs are generally grouped when discussing energy storage systems. Nonetheless, all three serve different purposes, according to their energy and power density characteristics, often represented in the well-known Ragone chart.

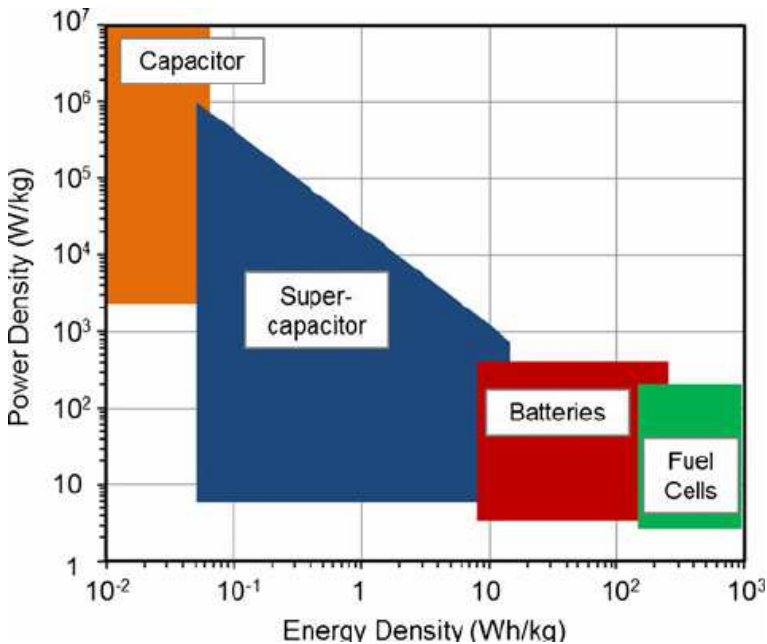


Figure 5 Ragone chart. Different electrochemical storage technologies are plotted against their power and energy density¹⁷.

In Figure 5, different electrochemical storage technologies are plotted respect to their power and energy density and their key characteristics are clearly identifiable. Capacitors are in the left top part of the plot, as they are likely to provide high burst of power for a very short time, while fuel cells stay in the right bottom area, as they are willing to deliver low current for a long time. In electric vehicles, high power means fast acceleration; otherwise, high energy gives longer range. Batteries, depending on the technology and materials they are made of, lie somewhere in between capacitors and fuel cells. In the real world, it is possible to combine two or more

technologies, thus coupling their benefits. Among all electrochemical devices, battery is the most widely and more reliable technology used nowadays.

Battery

Batteries are stand-alone units that store chemical energy and, on demand, convert it into electricity to “fuel” different of applications. Batteries, generally, do not need time to start-up and, at low drains, can efficiently (up to 95%) convert the stored energy in useful one.

They do offer clear advantages compared to other energy storage technologies: wide working temperature range, different chemistry/voltage choices, can operate in any orientation, portable, no moving parts, up/down-scalable, standardized form factors, high power rate and application-adaptable. On the other hand, they have low energy density and they are expensive compared to fossil fuels as well as there is not an “universal” battery that can fit all the purposes¹³.

Depending on the application, there are four main parameters for judging a battery:

- Cost
- Performance
- Reliability
- Appearance

These parameters can be controlled by specific factors in the development and production pipeline:

- Technology
- Cell Design

- Manufacturing

Fulfilling the application requirements decreases the success of one technology over others. Clearly, technology is the answer to a specific request, the application, and sometimes some applications cannot be realized because of the lack of proper technical solutions. For example, in the last two decades notebooks market grew double digit because of the availability of new reliable, compact and cheap Li-ion batteries while automotive market was following the average gross national product growth because of no new breakthrough technological achievements.

Nowadays, the battery market is worth approximately 50 billion USD, so the interest in entering it is high.

In Figure 6, the Daniell's Zinc-Copper battery is represented showing the general configuration of a modern Solid-Liquid-Solid accumulator.

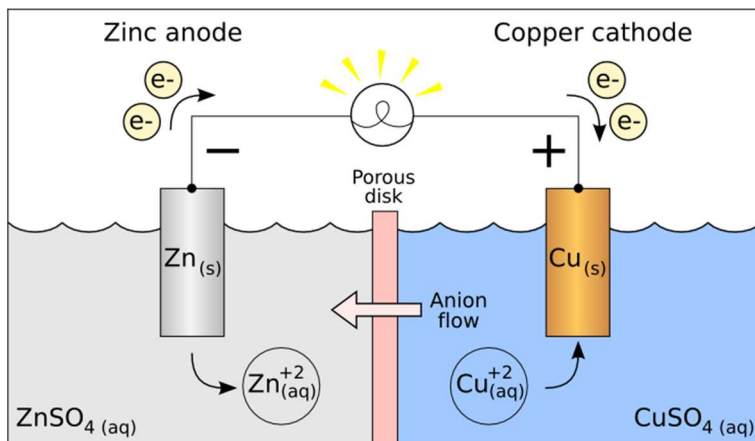


Figure 6 Daniell's Zinc-Copper Solid-Liquid-Solid Battery ¹⁸.

In practice, a porous electrical insulating material containing the electrolyte is placed between the cathode, the positive pole, and the anode, the negative counterpart. Metals such as lithium, sodium, Zinc or Lead (i.e. low redox potential materials) are good anodes and acts as reducing agents giving electrons during the discharge, while cobalt, manganese and lead oxides (i.e. high redox potential compounds) can accept electrons and are well performing examples of cathodes. Electrolytes provide ionic conductivity nor electronic one and they are usually liquids (at room temperature solvent-based while at high temperature molten salts) or solids. They physically separate the cathode and the anode and liquid ones are often supported by a solid separator, namely a membrane (e.g. fiberglass, ceramic or polypropylene based) permeable to the electrolyte solution and electron insulating. Liquid electrolytes are a concentrated solution of a salt into a solvent. Either water or organic solvents can be used, by itself or in mixtures. Aqueous solutions possess high ionic conductivity up to 1 S/cm but the thermodynamic stability window is narrow, 1.2V (kinetically stable up to 2V) ¹⁹; alternatively, organic solvents can be used, widening the kinetic stability window up to 4.6V. However, non-aqueous solvents have low solvating power and dielectric constant allowing the formation, even at low concentrations, of ion pairs that lower down conductivity to 10^{-2} - 10^{-3} S/cm ²⁰. Low ionic conductivity translates in slow speed reaction and thus bad (slow) charge-discharge rate, while limited potential window, thus low cell potential, means low quality energy (i.e. less electrical work can be performed by the electrochemical cell). Moreover, most organic solvents are toxic or flammable, therefore unsafe ²¹.

Room temperature solid electrolytes are of high interest, in fact their mechanical stability prevents short circuit between the electrodes as well as the absence of solvents allows the shrinking of volume in the packaging of the battery, thus leading to higher volumetric capacity. However, there are several technological e engineering issues to be addressed and their use is still limited ²².

Batteries are commonly divided into two main classes, primary and secondary batteries. Primary battery are worn once completely discharged, while secondary ones are rechargeable and thus reusable.

A List of common battery systems is found in Table 1:

Common Name	Nominal Voltage	Anode	Cathode	Electrolyte
Primary				
Lanclanchè	1.5	Zn foil	MnO ₂	aq ZnCl ₂ /NH ₄ Cl
Zinc chloride	1.5	Zn foil	MnO ₂	aq ZnCl ₂
Alkaline	1.5	Zn powder	MnO ₂	aq KOH
Zinc-air	1.2	Zn powder	O ₂ 20%	aq KOH
Silver zinc	1.6	Zn powder	Ag ₂ O	aq KOH
Lithium manganese-dioxide	3.0	Li foil	MnO ₂	LiClO ₄
Lithium-carbon monofluoride	3.0	Li foil	CF _x	LiClO ₄
Lithium-iron sulfide	1.6	Li foil	FeS ₂	LiClO ₄
Secondary				
Lead-acid	2.0	Lead	PbO ₂	aq H ₂ SO ₄
Nickel-cadmium	1.2	Cadmium	NiOOH	aq KOH
Nickel metal-hydride	1.2	MH	NiOOH	aq KOH
Lithium-ion	4.0	Li(C ₆)	LiCoO ₂	LiPF ₆

Table 1 List of common primary and secondary, rechargeable, batteries.

There are specialty battery as well, such lithium Thionyl Chloride (3.6V, Li, SOCl₂ (C₆), SOCl₂/LiAlCl₄), and their use is let to high demanding applications and niche markets like military and aerospace.

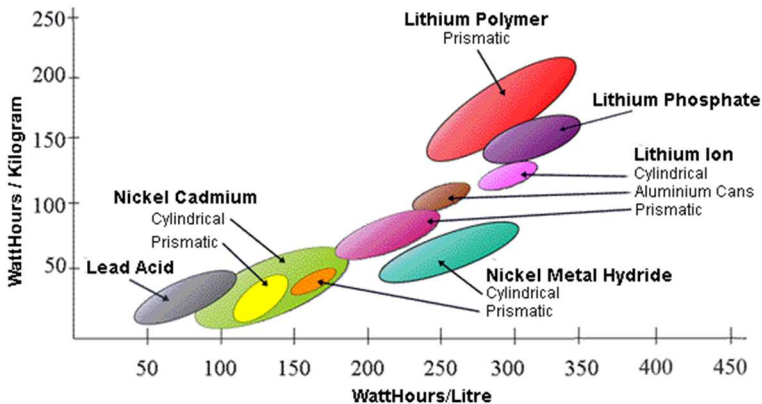


Figure 7 Gravimetric and volumetric energy densities of conventional battery systems
23

Despite Zinc-carbon and Alkaline accumulators outsold lithium based batteries in terms of produced units, Li technology is the one implemented in high-end applications (i.e. ultra-portable devices and electric vehicles). In Figure 7, lithium accumulators occupy the top right part of plot; in fact, lithium batteries outperforms other chemistries thanks to their gravimetric and volumetric energy density.

Selection Criteria for Commercial Battery Systems

Only a few of the many proposed battery systems have been used and commercialized. The fact that after one century from their first introduction Lead – Acid (secondary) and Zinc – MnO₂ (primary) are

still the main player in their category means that very few combinations of chemistries meet all of the criteria for a general purpose power supply.

The criteria to illustrate the characteristics of the materials and reaction follow:

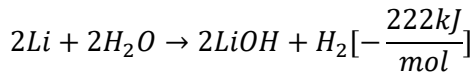
- Mechanical and chemical stability
- Energy storage capability
- Temperature range operation
- Self-Discharge
- Shape of the discharge curve
- Cost
- Safety
- Ability to recharge and deliver power
- Cycle life
- Charge time
- Over-charge/discharge protection

It is obvious that scientists must keep in mind all the criteria listed above, as a successful battery must satisfy as much as possible of those.

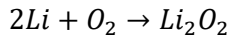
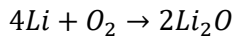
Lithium-ion Batteries - LIBs

The choice of lithium for batteries is not random, but it is dictated by the fact that Li is the lightest metal, Li M_w 6.94 g/mol: meaning that lithium has a theoretical specific charge of 3861mAh/g (e.g. Zn^{2+}/Zn has 820mAh/g and Na^+/Na has 785mAh/g)²⁴.

Unfortunately, lithium, as all alkali metals, reacts violently and exothermically with water to form hydrogen gas:



Moreover, it is oxidized extremely quickly when put in contact with oxygen:



Because of its reactivity, lithium metal is not safe in open atmosphere and therefore its use in batteries has been subjected to finding suitable ways to protect it from oxygen and moisture.

As for all types of batteries, LIBs can be divided in two families:

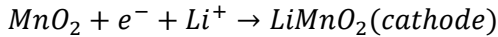
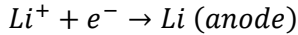
- Primary batteries, not rechargeable, such as the Li-MnO₂, Li-SOCl₂ and Li-FeS₂ systems.
- Secondary batteries, rechargeable, such as Li-ion or Li-polymer systems.

Other interesting lithium battery technologies, the lithium-air²⁵ and Li-sulfur²⁶, have been proposed. Theoretically, they provide the highest specific capacity of all lithium batteries, but being in the research and development phase, they will not be discussed further.

Primary Li Batteries

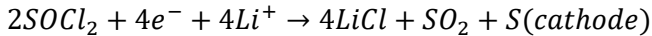
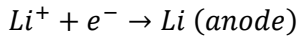
Under the definition of primary lithium batteries, it is possible to find a large number of options of different chemistries that employ metallic lithium at the anode and some kind of reducible compound at the cathode²⁷.

The most common primary lithium battery employs MnO_2 as cathode, and provides a nominal voltage of 3V. Its electrode reactions is:



This battery uses an organic electrolyte (propylene carbonate with LiClO_4) and it is commonly found in wristwatches, calculators, and all sorts of low power and low drain applications.

The lithium-thionyl chloride battery has been developed by the US Army for stationary applications because of the wide range of temperatures in which it can operate (from $-55\text{ }^\circ\text{C}$ to $+85\text{ }^\circ\text{C}$) and the minimal self-discharge. It is built around a liquid cathode with a carbonaceous current collector and the electrode reactions are:

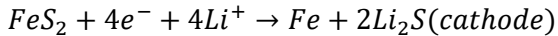
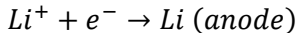


The discharge products (sulfur and sulfur dioxide) are soluble in the electrolyte, generally LiAlCl_4 in thionyl chloride. This battery provides a nominal voltage of 3.5V, a similar energy density to the aqueous zinc air and an extremely long life, but has a major drawback in the constituents. Thionyl chloride is extremely toxic and upon deep discharge, gaseous SO_2 can build up to a dangerous pressure: therefore, they need to be stored properly and are not generally available to the public.

Lithium – sulfur dioxide cell also uses a liquid cathode construction as the thionyl one. The SO_2 is dissolved in an organic solvent, mainly PC

or MeCN, or alternatively pressurized to the liquid state and $\text{Li}_2\text{S}_2\text{O}_4$ being either the SEI at the anode surface and the discharge product at the carbon cathode.

One last example of primary lithium battery is the iron sulfide battery. This system is based on the following reactions:



The electrolyte in this cell is an organic mixture of propylene carbonate, dioxolane and dimethoxyethane.

These batteries are the primary lithium batteries commercialized by many major manufacturers and they are suitable to replace normal zinc carbon and alkaline batteries, while providing a lifetime up to 2.5 times longer²⁸.

Secondary, Rechargeable, Li Batteries

Secondary cells generally have lower energy densities than primary one. The additional requirements of being rechargeable and long operation limit the choice of suitable chemical systems and construction to those that are more robust.

Lead acid battery dominates the rechargeable market since decades but both the toxicity of Pb and H_2SO_4 and the poor gravimetric properties limit the application to some portable application. Because of their very good reliability, outstanding cyclability and long life, they are widely used as stationary energy back up installation, start system in conventional ignition cars and as main energy source in early full and hybrid electric vehicles.

The discovery and optimization of both nickel Cadmium (NiCd) and Ni metal hydride (NiMH) accumulators having bigger energy storage capabilities, allowed the blooming of portable applications such as laptops and mobile phones. NiMHs are nowadays first choice in the HEV and FEV application. The main drawback of such system is the very poor quality of stored energy; in fact, they can provide only 1.2V.

Rechargeable lithium batteries were first proposed by Michael Stanley Whittingham in 1976, when working for Exxon ²⁹. He proposed a system with metallic lithium at the anode and titanium disulfide at the cathode. The mechanism of the battery was the reversible insertion of lithium ions into TiS_2 , but the use of Li at the anode posed great safety concerns. For this reason, it was proposed to use an insertion material also at the anode and in 1981 the first workable graphite anode was patented by the Bell Labs ³⁰. The work of John B. Goodenough led to the first commercial lithium-ion battery, commercialized by Sony in 1991. This cell was based on a graphitic anode and on a layered lithium cobalt oxide cathode ³¹: when assembled, the cell was in the discharged state, another safety advantage.

Sony's lithium-ion batteries were based on the reversible insertion (intercalation) and extraction (deintercalation) of lithium ions in and from host materials. For this property, they are also called "rocking chair batteries". As electrolyte, a solution of a lithium salt in an organic solvent is used. A scheme of the functioning principle is shown in Figure 8.

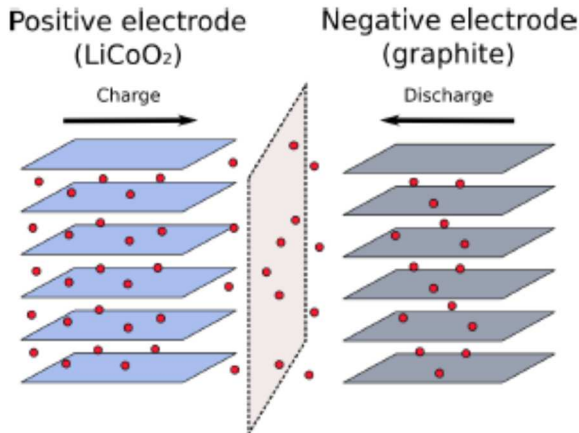
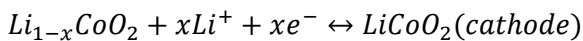
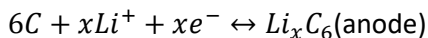


Figure 8 Sony's rocking-chair battery: Layered lithium cobalt oxide cathode, graphitic anode and a Li-salt based organic electrolyte. The black arrows shows the directions of the Li⁺ ions (in red) during the charge and discharge steps³¹.

During the discharge process, the positive electrode, the cathode, is reduced while the negative one, the carbonaceous anode, is oxidized following these reactions:



A polymeric membrane that is permeable to the electrolyte and ensures electrical insulation separates the electrodes. The vast majority of today's Li-ion batteries are still built around this "simple" design.

Reaction Mechanisms

There are three main reaction mechanisms going on in rechargeable batteries:

- Intercalation
- Alloying
- Conversion

While in cathodes intercalation is the main mechanism, anodic materials may follow alloying and conversion reactions as well. In the following subchapters, some materials, both positive and negative, that can be found on the market, are presented and the way they work is described briefly.

Negative Electrodes

In lithium-ion batteries, it is obvious that using pure metal as the negative anode would be the best choice. In fact, as consequence of using metal Li in LIBs, both specific capacity (3840mAh/g) and the activity (1) are maximized and the cell voltage is the lowest possible (0V). Unluckily, several issues arise when bare metal is used as anode. Firstly safety, as pure metal can violently oxidize in contact with water and oxygen. Moreover, during charging the metal can deposit in location where it is not supposed to be, like separators or current collectors; or the metal growth is not even and it tends to increase roughness and form dendrites or filaments that can short circuit the device and lead to fires or explosions³². Furthermore, if the electrolyte is not stable in contact to low potential anode materials, during charging the formation of a decomposition product layer (called Solid Electrolyte Interface, SEI)³³ can happen increasing the overall impedance of the cell. Because the SEI layer is not even, where there are breaches the impedance is low, thus, the local current is high, and filaments or pillars can easily grow forming woven structures. When the process is reversed, this spongy structure can detach from the surface losing electrical contact. Therefore, that

material is “lost” for further cycling lowering the overall capacity of the cell.

Starting from the first Sony’s rocking-chair battery, carbonaceous compounds are first choice as negative electrode reactant in the common LIBs. There are different carbon materials and everyone shows peculiar behavior and performance. Graphite, Figure 9, consists in parallel sheets of graphene stack together in the ABAB configuration. Graphite is amphoteric and can accommodate both anions Br^- , SO_4^{2-} or SbF_6^- and cation Li^+ , Na^+ , K^+ . Early works on this topic demonstrated, using XRD and XPS, the existence of the carbon-lithium alloy while first experiments of reversibly intercalating Li in the carbon structure failed because of the use of the wrong supporting electrolyte^{34,35}. In fact, only polymeric carbonate solutions avoid the swelling and defoliation of the carbonaceous electrode.

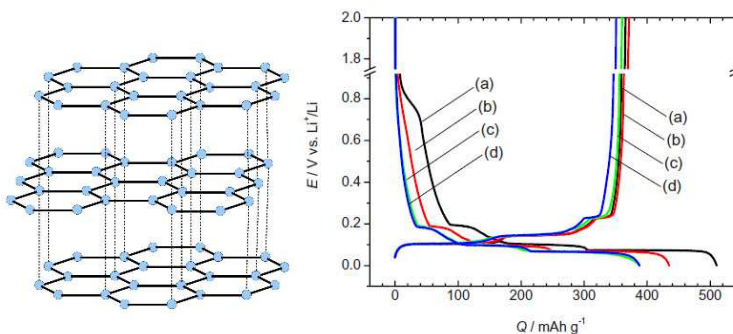


Figure 9 Left: Graphite stacked structure. Right: Initial charge (reduction) and discharge (oxidation) curves of graphite as a negative electrode with several binders, (a) PVdF, (b) PAAH, (c) PAALi, and (d) PAANa, in LiClO_4 1M EC:DMC at 50 mA g^{-1} ³⁶.

In commerce, there are two main types of graphite materials, soft and hard carbons depending on their precursors, e.g., liquid→soft and solid→hard. Soft carbons are agglomeration of small graphitic grains that have large amount of in/inter-plane and rotational defects and their planar orientation differs considerably between grain neighbors. Otherwise, hard carbons are less packed and more porous increasing the surface area and allowing fast charge discharge rates. In both cases, the intrinsic defects can be “corrected” using high temperature, i.e. 1000-2000 °C, annealing. Hard carbons need higher T and longer exposure because of their inter-planar bonds. Low T or amorphous graphite can be used as well, but with low performance and worst charge retention at the first cycle. The theoretical specific capacity of LiC_6 is around 372mAh/g (practical 300-350mAh/g) and it operates at a potential of few hundreds of mV above lithium, 250÷100mV. In carbon-based anodes, low charge retention at the first cycle, due to irreversible absorption of Li in the structure and SEI formation, is common. This inconvenient leads to the necessity to load extra “disposable” negative material in the cell increasing the final weight and volume.

Another intercalation material of big interest is the titanium oxide compounds, Figure 10. In particular, the spinel $\text{Li}_4\text{Ti}_5\text{O}_{12}$ ³⁷ work at quite high voltage, 1.5V, limiting SEI formation, electrolyte decomposition and Li deposition during charge. Titanates are safer and cheaper than carbonaceous anodes but they provide lower capacity, 175-330mAh/g, and lower energy as well as power. Nanostructured titanium oxides deliver improvements in specific capacity, cycle life and rate capability.

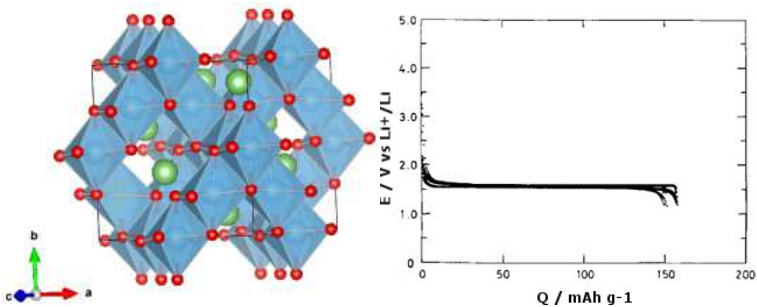


Figure 10 Left: Spinel structure of the $\text{Li}_4\text{Ti}_5\text{O}_{12}$ anode material. Octahedral sites are occupied randomly by lithium (1/6) (not shown in image) and titanium (5/6) atoms. Ti atoms are blue, Li atoms green and O atoms are red. Right: Charge discharge profiles of a 88:6:6 titanate electrode at 0.5mA/g at 30 °C in 1M LiClO_4 EC:DME 1:1v. Capacity fades in 100 cycles from 160mAh/g to 150mAh/g.³⁸

Metal-lithium alloys have been considered, especially in high temperature (i.e. 400-500°C) applications, to avoid the melting of the lithium and its dissolution in the molten electrolyte. Compared to pure Li anodes, metal-lithium alloys have lower Li activity, thus higher potential, and reduced energy density because of the presence of another “inactive” material in the alloy. Several binary alloys have been tested both at high and room temperature and, above all, Li_yAl (0.30V y:0.08-0.9), Li_ySn (T_{high} 0.17-0.57V y:0.57-4.4 ; T_{room} 0.66-0.38V y:0.4-4.4) and Li_ySi (0.33-0.05V y:0-4.4) are those of most interest and they now found use in both military and consumer applications (e.g. Matsushita Corp.). At room temperature, the major drawback of such materials is the phenomenon called decrepitation, or crumbling, happening because of the significant change in volume upon cycling³⁹. The lithiation process is not homogenous and thus some parts increase volume, up to 4 times, causing mechanical stress in the electrode and fracturing it in small pieces that loose electrical contact with the rest of the bulk. This disastrous phenomenon can be easily

identified using imaging techniques like SEM and TEM or XRD. Because of the appeal, several attempts have been made to minimize this issue and efforts have been focused on the design of complex morphologies that can accommodate the strain efficaciously, e.g. : nanofibers, hollow nanotubes, nanopillars, coaxial carbon nanotubes and the fancy yolk-shell approach ⁴⁰.

Fuji Corporation first introduces “convertible” reactant electrodes to the market in the late nineties ⁴¹. Their negative electrode was composed of amorphous alloy made melting together different oxides (e.g. SnO, B₂O₃, Sn₂P₂O₇ and Al₂O₃). During the first discharge cycle, the multicomponent oxide mixture is converted in mainly Li – Sn and other residual “inert” oxides and, therefore, the behavior is equal to the one of normal alloy anodes with the claimed advantage of better stability. Fuji asserts to provide up to 800mAh/g in a potential range of 0.66-0.38V (the longest plateau happens at 0.56V, 0.7-2.23 Li ion for Sn atom). Therefore, conversion materials, after the 1st cycles, share most of the characteristics of standard alloy ones. Moreover, in the case of Li- Sn, a spontaneous displacement reaction (Li₂O, ΔG°_f -562kJ/mol, is more stable than SnO, ΔG°_f -256.8kJ/mol) takes place consuming a discrete amount of Li. The displacement reaction is helped by the good mobility and decent diffusion coefficient of Li ions at room temperature in such solid-state material, $D = 6 \times 10^{-7} \text{cm}^2/\text{s}$.

Positive Electrodes

Commercial positive electrode materials can be divided in three main categories:

- Layered type oxides
- Spinel type oxides

- Olivine type phosphates

All of these types of positive electrode materials have strengths and weaknesses that will be discussed hereafter.

Layered Cathodes

Layered oxides are the dominating material on the market today. They all share a general formula LiMO_2 , where M can be one or more transition metals, and they are all isostructural to NaFeO_2 . They all belong to the R3-m space group and the structure can be described as the periodic distribution of layers of MO_6 and LiO_6 octahedra stacked in an alternate manner, as shown in Figure 11.

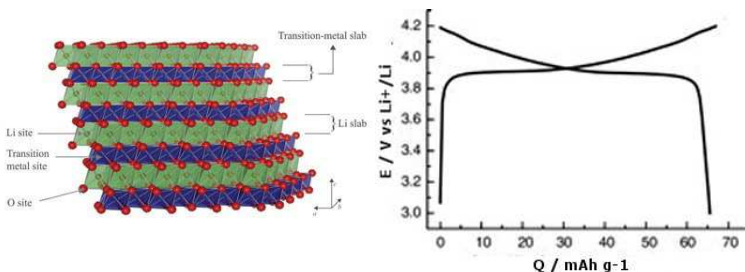


Figure 11 Left: Layered mixed metal oxide crystal structure (MIT's courtesy). Right: charge-discharge curves of LiCoO_2 thin film in half cell test ⁴².

LiCoO_2 , however, has many drawbacks affecting its performance. As major disadvantage, it is possible to extract only half of the intercalated lithium, limiting its charge capacity to 130mAh/g. Above this threshold, $\text{Li}_{0.5-x}\text{CoO}_2$ undergoes phase transitions that heavily hinder the stability of the structure and therefore limit the reversibility of the intercalation process ⁴³.

Moreover, Co is a rare expensive element and finding a substitute is of high interest. It was proposed to substitute cobalt with nickel, but isostructural LiNiO_2 does not work properly⁴⁴.

Therefore, cobalt seemed then almost irreplaceable for a reliable operation of layered oxides, and this observation led the way for the study of compounds containing mixed metals. Many different compositions in the range of $\text{LiNi}_x\text{Co}_{1-x}\text{O}_2$ have been synthesized and studied, and among them $\text{LiNi}_{0.7}\text{Co}_{0.3}\text{O}_2$ showed good behavior. Other examples of cobalt substitution include aluminum, chromium and manganese⁴⁵.

It is clear that every transition metal included in a layered oxide contributes to the overall performance of the final product. After binary combinations of Mn, Ni and Co, it was only logical to mix these three metals in various ratios and test the properties of the ternary oxide. A range of ternary oxides was first reported by Liu in 1999⁴⁶ and it was shown that this family of materials retained the layered structure typical of LiCoO_2 . The electrochemical performance was dependent on the Ni/Mn/Co ratio, with $\text{Li}(\text{Ni}_{0.7}\text{Mn}_{0.1}\text{Co}_{0.2})\text{O}_2$ having the best long-term capacity retention. The manganese is reported to be electrochemically inactive, but its role is to stabilize the structure during cycling. The fully symmetric compound $\text{Li}(\text{Ni}_{1/3}\text{Mn}_{1/3}\text{Co}_{1/3})\text{O}_2$ was reported in 2001, showing a reversible capacity of 150 mAh/g when cycled in a narrow potential window of 2.5V-4.2V vs. Li⁴⁷. It has been shown that upon lithium removal the unit cell volume change in $\text{Li}(\text{Ni}_{1/3}\text{Mn}_{1/3}\text{Co}_{1/3})\text{O}_2$ is less than 2%, so the low strain might explain the high cycle reversibility of this material. This low variation happens without phase transitions, thus further enhancing the stability of the material. The higher thermal stability of this material in its charged

state allows for higher cutoff potentials, therefore enabling the cell to reach up to 20mAh/g more than simple LiCoO_2 .

Overlithiated ternary compounds with layered structure and general formula $\text{Li}_{1+x}\text{M}_{1-x}\text{O}_2$ can be seen as a solid solution of $\text{LiCo}_y\text{Ni}_{1-y}\text{O}_2$ and Li_2MnO_3 . This latter compound is particularly interesting because of its unpredicted electrochemical activity. Upon further experiments it was discovered that the material with the lowest “x” value (therefore with the highest excess lithium) showed the best electrochemical performance, peaking at about 200mAh/g⁴⁸.

From these results it is clear that many factors can influence the electrochemical performance of mixed cation layered oxides and each component of the materials give a particular property: manganese seems to be needed for structure stabilization, nickel offers most of the electrochemical activity, cobalt tends to help the rate capability and excess lithium increases the capacity.

Spinel-type oxides

Spinel is a class of compounds with general formula AB_2X_4 , largely occurring in minerals on a wide range of compositions. They share a cubic unit cell, shown in Figure 12:

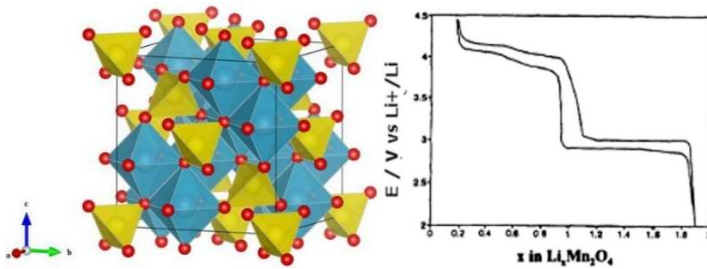


Figure 12 Left: LiMn_2O_4 spinel crystal structure Li in red, tetrahedral Mn in yellow and octahedral oxygen in blue. Right charge/discharge profile of $\text{Li}_x\text{Mn}_2\text{O}_4$ half-cell, both plateaus at 4V and 3V are visible ⁴⁹.

The first spinel to be used as cathode in LIBs was LiMn_2O_4 and Thackeray and Goodenough proposed it in 1983. This spinel exhibits two charge plateaus, one around 3V and another around 4V, but in general only the highest one is used in battery operation. The plateau (Figure 12) at 4V corresponds to a lithium content limited between $x=0$ and $x=1$ in $\text{Li}_x\text{Mn}_2\text{O}_4$. When inserting more lithium in the structure (the plateau at 3V vs. Li), divalent manganese ions are formed and these ions are soluble in acidic conditions. The lithium-manganese-oxygen is an extremely complex system and a comprehensive review was written by Thackeray in 1997 ⁴⁹.

Phosphate-based Olivine Cathodes

Olivine-type phosphates with general formula LiMPO_4 ($M = \text{Fe}, \text{Ni}, \text{Co}, \text{Mn}$) represent a valid alternative of cathode material for Li-ion batteries. They all share the same orthorhombic structure presented in Figure 13. First proposed by Goodenough in 1997 [28], LiFePO_4 has practical advantages such as low cost and low toxicity, thanks to the use of iron as transition metal, good specific capacity of 170mAh/g and great reversibility.

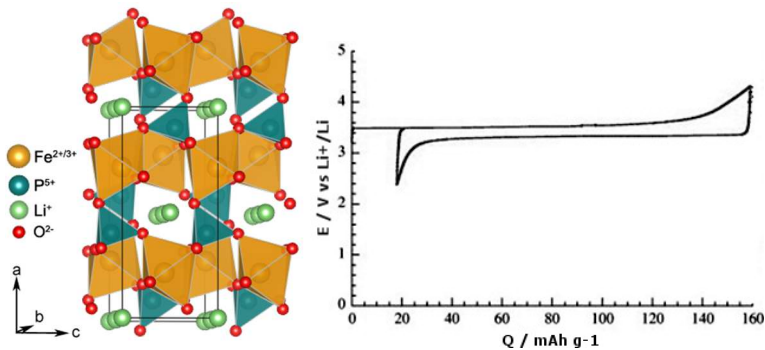


Figure 13 Left: The olivine structure of LiFePO_4 : showing the FeO_6 octahedra (yellow), PO_4 tetrahedra (blue), and the one-dimensional tunnels in which the Li^+ ions reside⁵⁰. Right: First electrochemical cycle of hydrothermal LiFePO_4 at room temperature⁵¹.

One drawback of LiFePO_4 is the relatively low discharge potential observed at about 3.5V, thus lowering the energy that can be extracted from this electrode material.

Other olivine type phosphates have been proposed, such as LiCoPO_4 , LiMnPO_4 and LiNiPO_4 . All these compounds are isostructural and present intercalation potential higher than the one of iron, at 4.8V, 4.1V and 5.1V for Co, Mn and Ni respectively. Unfortunately, lithium intercalation is not as reversible as for the iron compounds.

Issues with Current Li-ion Batteries

Lithium ion batteries are a relatively recent technology, and they are not perfect nor fully established yet. Many issues are still open in all components of the battery and on diverse fronts.

When focusing on electrode materials, performance problems are to be reckoned with, for example the disparity in practical charge capacity between positive and negative materials, or the inherent

danger of overcharging a battery. Electrolytes present issues too: in the current technology a solution based on organic flammable solvents is used. Actions are being taken immobilizing the liquid organic solvent into a polymeric matrix (the so-called “lithium-polymer” batteries, or “LiPO”) but while these polymers are less flammable than the liquid, they do not solve the problem at its roots²¹.

Another big topic is the availability of lithium in the upcoming years. Annual demand has therefore grown by 7–10%, currently reaching about 160k tons of lithium carbonate (Li_2CO_3) per year: about 20–25% of which is for the battery sector. Extracting lithium from hard rocks is laborious and expensive and most of that (roughly 83%) comes from brine lakes and salt pans. Considerable amounts of lithium are present in seawater, but its recovery is tricky and highly expensive.

It is extremely difficult to estimate the world’s lithium reserves. The present production of Li_2CO_3 is about half what would be needed to convert the 50 million cars produced every year into FEVs (40kWh) and HEVs powered by a 7 kWh Li ion battery and a combustion engine.

Hopefully, this alarming situation will push researchers to investigate new battery technologies and, fortunately, the situation improves if one also considers recycling.

Possible Improvements for Li-ion

It is possible to classify the needs for improvement of current Li-ion materials in three big groups:

- Performance

- Safety
- Politic, Toxicity, Economy

Regarding performance, the challenge is to enhance both power and energy density. The former can be improved by finding materials that can guarantee a higher charge/discharge rate, while the latter by enlarging the potential window with positive electrode materials working at 5V or plus. This way, though, is limited by available electrolytes as they start oxidizing around 4.5V. Ionic liquids have been proposed as possible substitutes⁵² but they don't form the SEI on the anode surface.

For safety, two great issues can be addressed. First, using anodes that work at higher potential than carbonaceous material, e.g. titanates; secondly avoiding the use of organic flammable solvents in the electrolyte, e.g. using full polymeric or inorganic solid state materials similar to NASICON⁵³. There are already some options but none can compete with liquid ones in terms of Li⁺ diffusion coefficient.

Lastly, it is important to consider economic and environmental questions, the most pressing of which is the use of heavy metals, like cobalt, in the positive electrode materials. These heavy elements can be easily found in limited areas of planet Earth, mainly politically unstable countries, and, because of their rarity, the price is skyrocketing. Other metals can be used, such as manganese and nickel, which can solve these problems.

Beyond lithium-ion

In the last couple of decades quite often has been read on the newspaper the discovery of a new battery that will solve all the needs

of energy storage, but unfortunately none of them passed over the headlines.

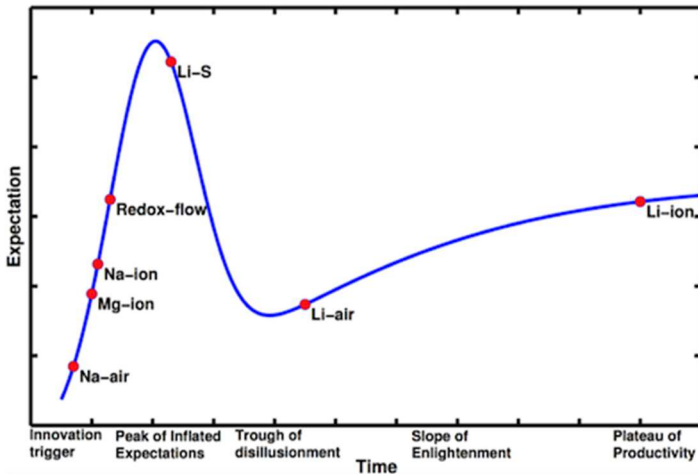


Figure 14 Gartner type hype chart for battery technologies. A typical technology goes through five phases: (i) innovation trigger, (ii) peak of inflated expectations, (iii) trough of disillusionment, (iv) slope of enlightenment and (v) plateau of productivity. Na-air, Mg-ion, Na-ion, redox-flow, Li-S, Li-air and Li-ion batteries are plotted at their respective phase of development [45].

In 2015, Sapunkov et al. tried to summarize the expectation of different battery technologies analyzing the fluctuations of published papers. As shown in Figure 14, except Li ion, none of them reached the plateau of productivity by now. Na-air, Mg-ion, Na-ion and redox flow are at the early stages of interest, Li-S seems to be less appealing than before, while Li-air just exits the “Through of disillusionment”, the “minimum of potential” that can “kill” an idea. Nevertheless, for Li-air the road to the production is still steep and long⁵⁴.

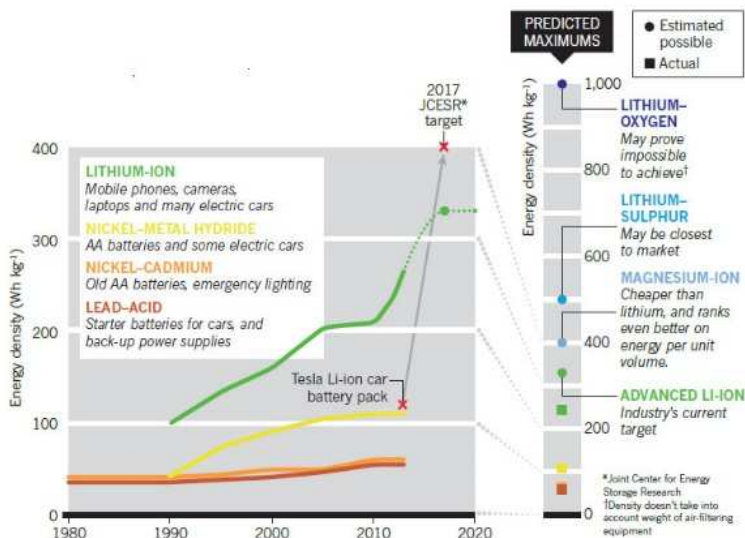


Figure 15 Progresses, left, and expectations, right, in the optimization of storage technologies⁵⁵.

Another interesting chemistry fallen out of Sapunkov's radar uses organic compounds, either polymer or molecules, as electrode material for energy storage. Albeit there are 30 years old papers about electrochemical studies on organic materials, the reason of this forgetfulness is related to the low scientific interest in the topic. During the one week symposium of IMLB (i.e. International Meeting on lithium Batteries) 2014 in Como (Italy) only two posters, out of 750, and no presentations were reporting studies on organics.

Aim of This Work

The development of the next generation of lithium ion batteries is a complex task that involves the cooperation of many different experts. Among them, the material scientist is called to invent and perfection new chemistries and materials. These new compounds cannot be engineered simply by trial and error approach; therefore, the understanding of the processes involved in the operation of a Li-ion battery is of high importance.

The purpose of this work is the scouting, characterization and optimization of novel organic materials to be used as active material in lithium ion batteries. The focus of the thesis is on the investigation of organic pigments: OSMs, containing mainly carbonyls and imides groups, and MOF cyanide-based compounds⁵⁶.

Pigments are good candidates as organic material because they fulfill several selection parameters:

- Electroactive: they can undergo reversible redox reactions
- Low cost: they are already produced in tons for other application
- Low weight: thus high theoretical charge capacity
- Nontoxic: already employed in real world application
- Insolubility: by definition, pigments are not soluble in the media in which they are dispersed
- Processability: they come as powder so they can be processed as other active material for batteries.

This thesis details the study of three small molecule pigments: perylene diimide (PDI), indanthrone (IND) and quinacridone (QA).

Moreover, Prussian Blue Analogue materials have been synthesized and fully characterized.

Chapter 2

Organic Materials for Energy

Lifecycle assessment studies highlighted important issues regarding the environmental impact and resource depletion associated with Li-ion batteries and consequently their competitiveness can be challenged by other storage systems⁵⁷. The manufacturing of conventional LIBs requires non-renewable materials and high-energy consumption during processing. Moreover, recycling strategies are not well established yet and rely on large consumption of energy and toxic chemicals⁵⁸. Lithium is not a rare element, but its resources are far from unlimited, especially if demand will increase rapidly⁵⁹. There are primarily two strategies suggested for future battery chemistries employed to resolve this issue: either the Li-based systems are replaced by more abundant analogues such as Na, or the inorganic non-renewable materials are replaced by organic counterparts, which are—or can be—synthesized from biomass resources.

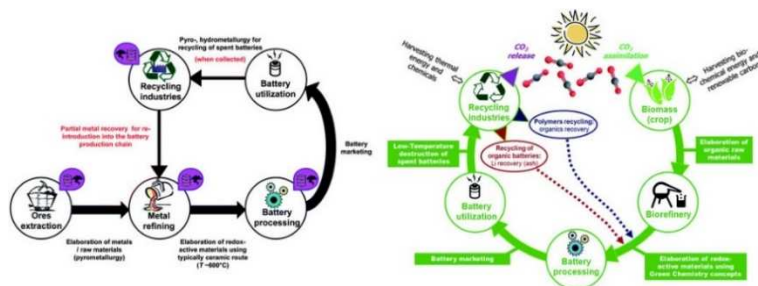


Figure 16 Illustration comparing current technology using metal-based electrode materials with a simplified cycle life of a “greener” Li-ion battery taking benefit of redox-active organic electrode materials deriving typically from biomass⁶⁰.

From a perspective of materials resource sustainability, Na provides a better solution while the organic electrodes provide a better option regarding energy consumption and recycling, Figure 16. Both strategies have shown promising results and cell concepts, utilizing a

broad range of active materials with a large variation in electrode potential and capacity (Figure 17), although significant developments are still required before widespread commercialization can happen.

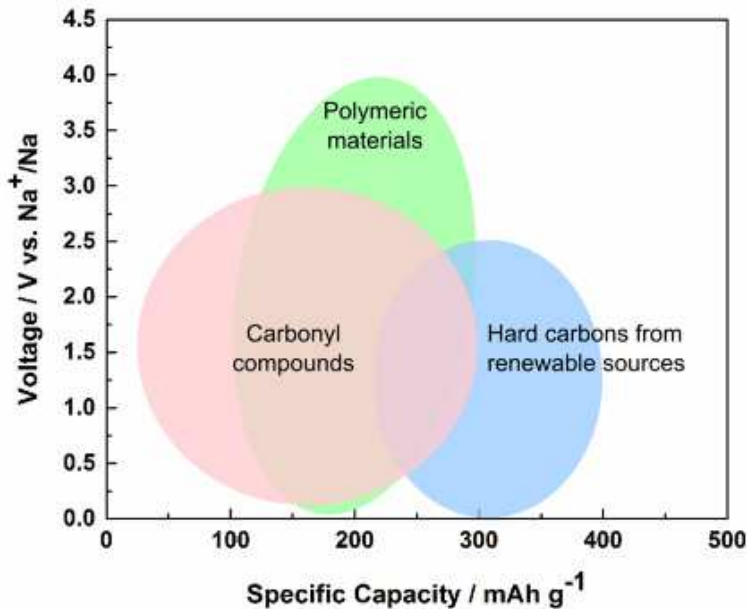


Figure 17 Average voltage vs. Na and capacity for some families of organic electrode materials [17].

Few studies have also tried to combine these two approaches in organic Na-based chemistries, although significant developments are still required.

Nowadays, graphite is the organic material of choice for the anode electrode. Graphite can be natural or synthetic but in both cases the extraction of natural ore and the high temperature annealing of amorphous carbons need a significant amount of energy. In the

recent years, some studies focused their attention to the production of carbonaceous material for energy storage starting from waste products like coconut husk ⁶¹, crops and other organic materials (similar to nanostructured silicon from rice husk ⁶²).

Organic electrode materials display advantages over traditional inorganic Li-ion compounds:

- Organic materials are flexible
- Their redox properties can be tailored using organic synthesis approaches
- They are composed of naturally abundant chemical elements (C, H, O, N, S)
- They, or at least their precursors, can be generated from renewable sources
- They can be disposed by low temperature process
- They are electrochemically active towards different kind of anion e cations
- They have supercapacitor-like kinetics (up to 120 °C)

However, organic compounds did not get all the expected attention because of the following drawbacks:

- Traditional materials rely on well-established technologies
- They need high amount of electron conductivity enhancer, up to 50%
- Reactions are multi-steps and show low production yield
- Reaction and purification steps are challenging

Among all the organic compounds the following are of great interest in electrochemical application because of the promising results they

gave: electroconductive polymers ⁶³, thioethers ⁶⁴, organodisulfides ⁶⁵ and organic radicals ⁶⁶.

Another interesting class of redox-active compounds that has been studied lately are organic carbonyl small molecules. The recent need of finding alternatives to traditional storage system brought back interest over this class of materials. The carbonyl group represents a common organic structural moiety and displays a redox activity. Depending on the molecule structure, carbonyl group can undergoes reversible one-electron reductions, which can be extended to more electrons if further carbonyls groups are in direct conjugation to form multivalent anions. Depending on the stabilization mechanism, see Figure 18, carbonyls can be divided into three distinct groups: vicinal carbonyls to form stable enolates; aromatic carbonyl derivatives sharing the negative charge; vicinal quinone substructures forming additional aromatic system upon reduction.

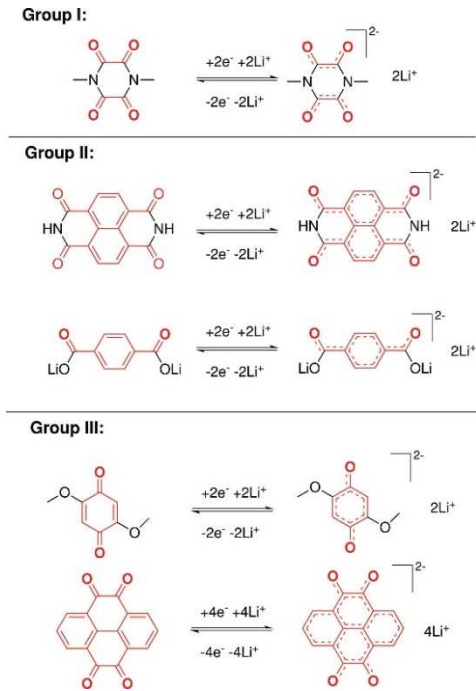


Figure 18 Representative structures of the carbonyl-based active electrode materials and their different stabilization mechanism of the charge ⁶⁷.

Similarly, imide-containing compounds can undergo reversible oxidation reaction and the stabilization of the resulting cation rely on the neighbor groups and the overall molecule structure.

Is of great interest the study of organic molecules having both carbonyl and imide groups and among all the available families of materials, pigments attracted our attention because of the following reasons:

- availability

- inexpensive
- insolubility
- graphite-like crystal structure
- condensed heteroatomic (carbonyl, imide, sulphides,...)
chemical structure

Pigments

Colorants are classified as either pigments or dyes. Pigments are inorganic or organic, colored, white or black materials, which are practically insoluble in the medium in which they are incorporated. Dyes, unlike pigments, dissolve during their application and in the process lose their crystal structure⁶⁸.



Figure 19 Yellow, purple, blue, green and red pigments⁶⁹.

It is thus by physical characteristics rather than by chemical composition that pigments are differentiated from dyes. In fact, both are similar and one structural skeleton may function either as a dye or as a pigment.

The history of pigment use dates back to 30,000 years ago to prehistoric cave paintings, which give evidence of the use of ocher, hematite, brown iron ore, and other mineral-based pigments.

Cinnabar, azurite, malachite, and lapis lazuli have been traced back to the third millennium BC in China and Egypt.

In the early 18th century, Prussian Blue (PB), the first synthetic pigment, was manufactured by chance. It was not until a century later that L. j. Thénard produced cobalt Blue. Ever increasing expertise and technology led to the production of others covering parts of the ranges of yellow, red, and black hues. Currently newly developed inorganic pigments were introduced to the market for fulfilling lead and cadmium free formulations requirements.

The beginning of organic pigment application dates to antiquity as well. It is certain that the art of using plant and animal “pigments” to extend the spectral range of available inorganic colorants by a selection of more brilliant shades had been practiced thousands of years ago. However, for solubility reasons, most of these organic compounds would be classified now as dyes rather than pigments.

The beginning of the era of modern chemistry was marked by the synthesis of large numbers of dyes for textile related purposes. Some of these were also applied to inorganic substrates by adsorption, for use as lakes in toners.

Over the course of the years, scientists have proposed several classification systems for organic pigments and it seemed appropriate to adopt a classification system by grouping pigments either by chemical constitution or by optical properties. However, this approach is not very practical, because the categories tend to overlap; so, it is sometime useful to list pigments according to their basic chemical structure.

There are different “chemical” families of organic pigments and the most representative ones follow:

- Azo pigments, subdivided into the monoazo and diazo pigments, have the azo group (-N=N-) in common. The synthesis of azo pigments is economically attractive, because the standard sequence of diazonium salt formation and subsequent reaction with a wide choice of coupling components allows access to a wide range of products.
- Pigments with condensed aromatic or heterocyclic ring systems are known as polycyclic pigments; only few are produced in large volume. Their main characteristics are good light- and weatherfastness (resistance to light and weather exposure) and good solvent and migration resistance; but, apart from the phthalocyanine pigments, they are also more costly than azo pigments.
- The dioxazine molecule is derived from triphenodioxazine, a linear system of five anellated rings. Apart from Pigment Violet 37, the commercially most representative one is Pigment Violet 23, an extremely lightfast and weatherfast compound with good to excellent solvent and migration resistance.
- There are two groups of triarylcarbonium pigments: inner salts of triphenylmethane sulfonic acids, and complex salts with heteropolyacids containing phosphorus, tungsten, molybdenum, silicon, or iron. The first group is characterized by poor lightfastness and limited solvent resistance. The second group includes the complex salts of basic pigments that are common in the dyes industry with certain heteropolyacids. Despite the disadvantages of comparatively

poor solvent resistance and limited lightfastness, these pigments are used for their excellent color brilliance and clarity of hue; properties which exceed those of any of the other known organic or inorganic pigments. These features make those types whose lightfastness satisfies the commercial requirements suitable candidates for the printing inks industry and especially for packaging inks.

- Quinophthalone pigments have a polycyclic structure derived from quinaldine and phthalic anhydride. A few members of this class have gained commercial recognition for their very good temperature resistance. The main markets for their mostly greenish yellow shades are in the plastics and coatings industries ⁷⁰.

Another interesting class of pigments is the cyanide based Prussian Blue. The classification of this kind of material is ambiguous because of the nature of $-C\equiv N$ group: in organic compounds is called nitrile, e.g. acetonitrile $CH_3C\equiv N$, while in inorganic ones is called cyanide, e.g. the NaCN sodium Cyanide. However, the capacity of creating self-assembled $Fe^{II}-CN-Fe^{III}$ scaffold structures is similar to the one of Metal Organic Framework compounds and consequently PBAs are treated as MOFs in some publications ⁵⁶. Self-assembling MOFs are of big interest nowadays because they show very interesting properties and, despite their complex 3D structure, they can be easily synthesized using simple wet chemistry techniques. MOFs find application in different fields and in recent years their electrochemical performance have been analyzed ⁷¹.

PB was discovered purely by chance through a lucky accident. In c.1704, the German color-maker Diesbach was creating a red lake

pigment to use as a dye, using iron sulphate and potash. On this occasion, the potash was contaminated with impurities (hexacyanoferrate) and instead of a bright red, Diesbach produced a purple, which when concentrated, became a deep blue pigment ⁷². PB has been widely used as pigment in paintings, as in the famous Van Gogh's reported in Figure 20:



Figure 20 The Starry Night -1889 Van Gogh. In this painting Prussian Blue and other blue-hue pigments have been used ⁷³.

Organic Small Molecule Working Principle

In contrast to inorganic materials, with redox reactions depending on the valence charge of the metal, the mechanism of carbonyl compounds is based on the charge state of the carbon and oxygen atoms of the carbonyl group or nitrogen charge state of the =NR imide.

There are three big different groups of organic electroactive materials:

- n-type if can be reduced
- p-type if can be oxidized
- b-type if can undergo both reactions

Pigments contain both groups so they are b-type. Depending on the number of active groups, the molecule can exchange more than one electron. If it is n-doped it becomes an anion, otherwise if it is p-doped it turns into a cation. Every electrons must be counterbalanced by one or more suitable ions coming from the electrolyte solution.

Pigments, in solid state, retain a crystal structure similar to the one of graphite. In fact, they possess a quasi-planar crystal structure and thus the molecule can π - π stacking together.

Factors Influencing the Electrochemical Performance

The redox potential of organic compounds can be tailored by the introduction of electrodonating or electrowithdrawing substituent leading to a higher or a lower reaction potential, respectively. However, adding inert moieties increases the molecule weight lowering the theoretical specific capacity. The charge/discharge cycling stability is dependent on several factors. The most critical factor is the solubility of the molecule in the supporting electrolyte, which leads to a loss of material and a decrease of capacity upon cycling. Because of their intrinsic insolubility in the neutral state, the latter issue should not affect pigments, but the anion or cation forms can be soluble. Furthermore, side reactions or instabilities of anions and cations, e.g. dimerization, also effect the cycling stability. Some other materials, e.g. croconic acid ⁷⁴, suffer of intense volume changes upon redox cycling and thus decrepitation. Because of the low electronic conductivity of organic materials, the choice of the additive in the amount is crucial. It seems that high surface high conductive carbons like nanotubes or graphene ⁷⁵ give performance advantages.

Prussian Blue Analogues

In addition to the application as a colorant in paints and varnishes, PB finds use in other fields as well: in purification and medical treatment as sequestering agent for heavy and radioactive metals ⁷⁶, medical laboratory analysis for cell staining ⁷⁷ and in the smart-window word as electrochromic material ⁷⁸.

Nowadays, electrochromism is of high interest and PB is widely used as counter electrode in blue-colorless switching shading devices.

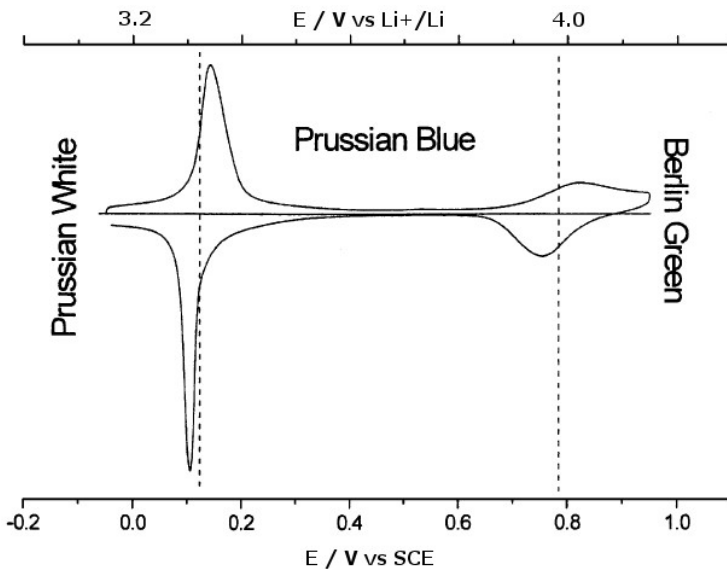
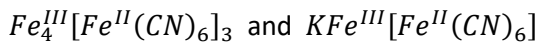


Figure 21 Cyclic Voltammetry of PB, 40mV/s in 0.1M KCl aqueous electrolyte ⁷⁹.

The generic formula of PB in the Fe^{III}/Fe^{II} oxidation state is between:



“Insoluble”

“Soluble”

In addition, it can undergo both reduction, to Prussian White, and oxidation, to Berlin Green. Karyakin et al. propose ⁷⁹ the following redox reactions:

- Prussian Blue \leftrightarrow Prussian White @ 3.3V vs Li
 $Fe_4^{III}[Fe^{II}(CN)_6]_3 + 4e^- + 4X^+ \leftrightarrow X_4Fe_4^{II}[Fe^{II}(CN)_6]_3$
- Prussian Blue \leftrightarrow Berlin Green @ 4.0V vs Li
 $Fe_4^{III}[Fe^{II}(CN)_6]_3 - 3e^- + 3A^- \leftrightarrow Fe_4^{III}[Fe^{III}(CN)_6A]_3$

The theoretical specific capacities of the two processes are 125mAh/g @ 3.3V vs Li and 93mAh/g @ 4.0 V vs Li, respectively; however, due to the high content of vacancies, the practical values can be half of the theoretical ones. Therefore, the PB electrochemical performance are not appealing for commercial applications and alternatives to the Fe/Fe couple are necessary.

It is clear from these numbers that PBAs cannot tackle Li-ion in high energy application but the fast kinetic and inexpensive of PBAs allows them to find space in critical application such smart-grids. In fact in this application the key elements are fast-responsiveness, environmental compatibility and inexpensive.

Pasta et al. have recently extensively investigated this class of materials to optimize their electrochemical performance as energy material in, mainly, aqueous materials for smart-grid leveling system ^{80–86}.

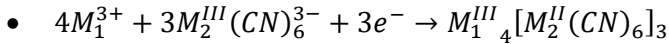
There are four main winning factors in favor of PBAs:

- Inexpensive and facile synthetic routes
- Tunable electrochemical properties
- Open framework structure
- Outstanding stability

PBAs is synthesized via two main wet chemical routes:

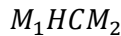
- $4M_1^{3+} + 3M_2^{II}(CN)_6^{4-} \rightarrow M_1^{III}_4[M_2^{II}(CN)_6]_3$
- $4M_1^{3+} + 18(CN)^- + 3M_2^{2+} \rightarrow M_1^{III}_4[M_2^{II}(CN)_6]_3$

Alternatively by electrodeposition:



The use of aqueous solution, commercially available reactants and simple labware as well as the high yield decrease the production costs. The price of Prussian Blue is, depending on the quality, between 1 and 5 \$/kg. The main drawback is the presence of the cyanide group that, in strong acidic conditions, can evolve into poisonous HCN. Therefore, the waste must follow appropriate disposal operations⁸⁷.

In general, we will refer to a generic PBA $M_1^{III}_4[M_2^{II}(CN)_6]_3$ as follows:



The electrochemical properties, in particular the redox potential, can be tailored changing the followings⁸⁸:

- C-coordinated metal M_2 : moves the potential of several hundreds of mV
- N-coordinated metal M_1 : finely tune the redox potential with a linear dependence vs $\phi = Z/r_{eff}$
- The insertion cation (Li^+ , Na^+ , K^+ , Rb^+ , ...): the bigger the ionic radius the higher the insertion potential

Unfortunately, not all the possible permutations are feasible and sometime the C- and N-coordinated metals exchange their position for thermodynamic matters (i.e. $\Delta G_{f M_2HCM_1}^0 \ll \Delta G_{f M_1HCM_2}^0$).

The open framework crystal structure is typical of this self-assembled material sharing the cubic⁸⁹ structure.

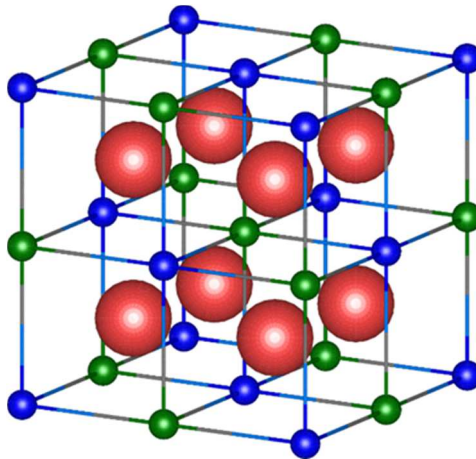


Figure 22 Prussian Blue cubic crystal structure: in blue the N-coordinated Me_1 , in green the C-coordinated Me_2 and in red the intercalated ions ⁸⁹.

In Figure 22, the cubic structure of PB family is reported. Depending on the transition metals the cell parameter a ranges $10\div 11\text{\AA}$ and the inner channels have an width of 3\AA , therefore a multitude of cations can freely move in and out the structure (e.g. naked ionic radius: Li^+ 1.48\AA , Na^+ 2.04\AA , ..., Cs^+ 3.00\AA). Additionally, the cubic structure suffer very low structure strain, $<1\%$, upon insertion and extraction of cations ⁹⁰. Several works described the long term cyclability of this class of materials in various experimental conditions ^{91,92}.

Chapter 3

Characterization Methods

In this chapter, the experimental techniques used are presented. The discussion is divided in three topics: Active Material, Cell Assembling and Battery Characterization.

Active Material Characterization

Thermal Gravimetric Analysis – TGA

Thermogravimetric Analysis is a technique in which the mass of a substance is monitored as a function of temperature or time as the sample specimen is subjected to a controlled temperature program in a controlled atmosphere. A generic schematic follows:

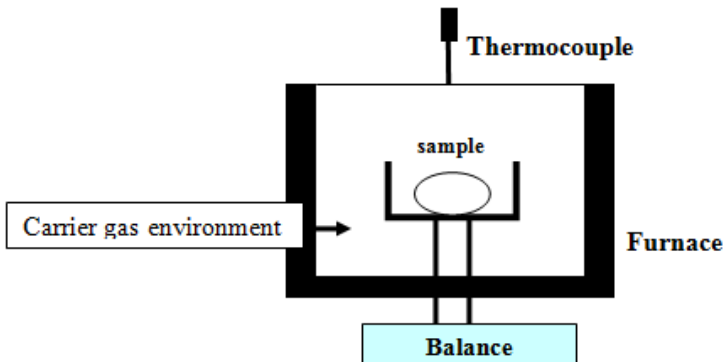


Figure 23 Thermal Gravimetric Analysis general working scheme ⁹³.

A TGA, Figure 23, consists in a precision balance atop of which a sample pan is placed. The balance-pan resides in a furnace and is heated or cooled during the experiment while the whole environment is purged with a flux of inert gas (i.e. N_2 or Ar) or reacting (normally O_2 -based). The mass of the sample is monitored during the experiment.

This technique can be used to measure different properties of the material: thermal stability, content of water or carbon, comparing materials, quality control, find reaction temperatures and others.

TGA is often coupled with other analysis techniques: DTA/DSC, MS, GC, and FTIR.

Differential Temperature Analysis – DTA

TGA comes often coupled with DTA and similarly to the Differential Scanning Calorimetry (DSC), but indirectly, provides information about the heat flux occurring during a reaction.

Calorimetry involves the experimental quantification of heat released in a chemical process. It can be used to determine parameters such as the Heat of Reaction (Δ_rH), which is the change in enthalpy associated with the process of a chemical reaction. So, DSC permits to identify if a process is endothermic or exothermic or if a change in the specific heat happens (e.g. glass transition, T_g).

In DTA the temperature of the chamber, containing both the sample and the reference pans, is varied and the temperature of the two is recorded. Because the sample pan contains the material, a difference of temperatures between the reference and the sample is recorded and the corresponding heat flow calculated. So, DTA is an indirect and, thus, less precise method compared to DSC. The difference between the provided heats plotted vs the temperature is reported in the following Figure 24.

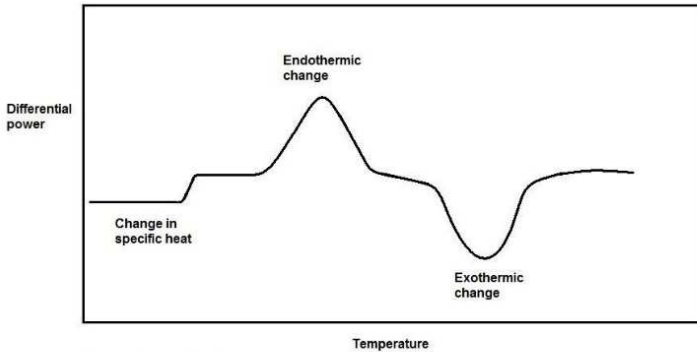


Figure 24 Typical DSC/DTA diagram. Step-like variations are changes in the specific heat, e.g. glass transition. Upwards peaks correspond to endothermic reactions or transitions, while downwards ones are exothermic⁹⁴.

Mass Spectrometry - MS

MS is an analytic method that employs ionization and mass investigation of compounds to determine the mass, formula and, possibly, structure of the tested compound. The mass analyzer is the core component of the mass spectrometer. It takes and separates ionized masses based on the mass to charge (m/z) ratio and outputs them to the detector where they are identified.

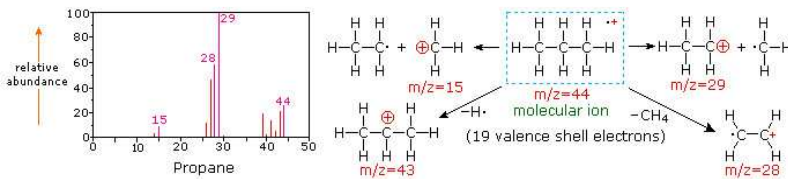


Figure 25 Mass Spectrometry analysis of propane gas. The MS graph represents the relative abundance of the possible m/z decomposition products presented⁹⁵.

When connected downstream to a TGA, the exhaust gas coming from the TGA furnace is the analyte in the MS. The instrument is composed of a turbo pump, an ionizer coupled to an ion accelerator and the revelator. The pump is crucial to clean the analyzing chamber from any unwanted chemical. There are different kinds of detectors, each one with its pros and cons and the given output can be either intensity of the ionic current or counts related to one specific mass to charge ratio.

So, if TGA, DSC and MS are coupled together, it is possible to understand at which temperature a reaction happens, if it is exothermic or endothermic, which, if any, volatile compounds are released and, maybe, how much material is reacting.

Scanning Electron Microscopy – SEM

The SEM uses a focused beam of high-energy electrons to generate a variety of signals at the surface of solid specimens. The signals that derive from electron-sample interactions reveal information about the analyte including surface morphology (texture), chemical composition, crystalline structure and orientation of phases making up the sample.

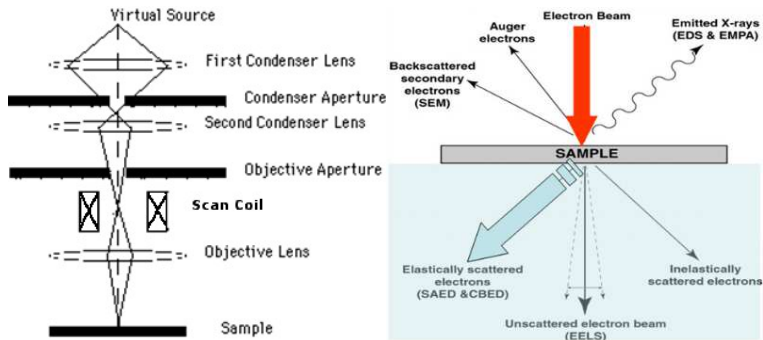


Figure 26 Left: schematic view of a SEM machine. Right: Electron Beam to the sample matter interaction. All of those different signals are peculiar and can be used to both construct the image and analyze the chemical and structural composition of the sample. The beam interacts only with the first few microns from the surface ⁹⁶.

Essential components of all SEMs include the following:

- Electron beam source (aka the “gun”)
- Electron lenses
- Sample stage
- Detectors for all signals of interest

Accelerated electrons in an SEM carry significant amounts of kinetic energy, and this energy is dissipated as a variety of signals produced by electron-sample interactions when the incident electrons are decelerated in the solid sample. These signals include secondary electrons (SE), backscattered electrons (BSE), diffracted backscattered electrons (EBSD), photons, and heat. Secondary electrons and backscattered electrons are commonly used for imaging sampling: secondary electrons are most valuable for showing morphology and topography on samples and backscattered electrons

are most valuable for illustrating contrasts in composition (i.e. for rapid phase discrimination).

SEM strengths are the ease of use, the simplicity in the preparation of the specimen, the relative inexpensive of the machinery, the possibility to couple different revelators in addition to the ones for imaging and the good, nanometric, resolution. Limitations are the necessity of using conductive samples (or sample coated with conductive materials), working in high vacuum, the sensitivity to electromagnetic fields and the limited magnification.

Transmission Electron Microscopy – TEM

TEM is a very powerful tool for material science. A high-energy beam of electrons is shone through a very thin sample, and the interactions between the electrons and the atoms can be used to see high-resolution pictures and observe features such as the crystal structure, dislocations and grain boundaries. Like SEM, TEM can be coupled with different detectors performing chemical and structural analysis.

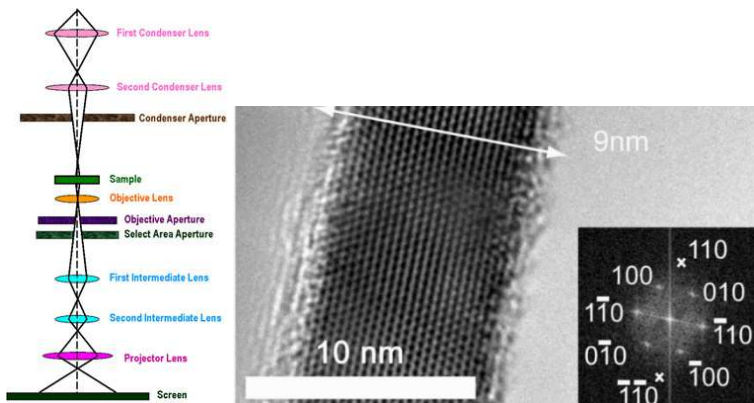


Figure 27 Left: TEM building sketch. The sample is placed between the projector lens and the screen (i.e. the detector), in the beam focus. Right: an example of the TEM analysis. Both morphological and structural information are accessible from a single TEM measure⁹⁷.

The TEM operates on the same basic principles as the light microscope but it uses electrons instead of light. Because the wavelength of electrons is much smaller than that of light, the optimal resolution attainable for TEM images is many orders of magnitude better than that from a light microscope (i.e. in the sub nanometric scale). Thus, TEMs can reveal the finest details of internal structure and in some cases as small as individual atoms.

The beam from the electron gun is focused into a small, thin, coherent beam by the use of the condenser lens. This beam is restricted by the condenser aperture, which excludes high angle electrons. The beam then strikes the specimen and parts of it are transmitted depending upon the thickness and electron transparency of the specimen. This transmitted portion is focused by the objective lens into a revelator.

Energy Dispersive X-ray Spectroscopy – EDX

The EDX sensor is commonly coupled with SEM and TEM machinery because it can detect the X-rays emitted by the atoms following inelastic interaction with an electron beam. It is a nitrogen cooled Si-based detector, positioned close to the sample holder, which can detect X-rays.

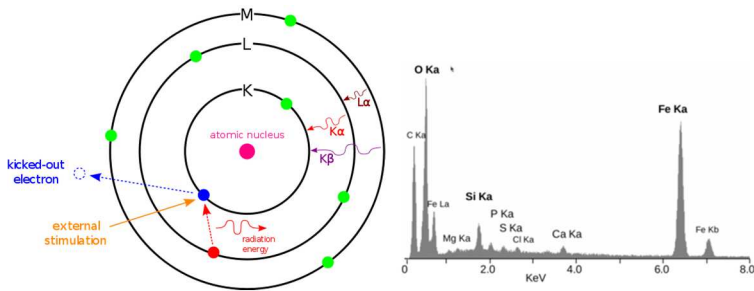


Figure 28 Left: schematic of the mechanism of generation of $K\alpha$, $K\beta$ and $L\alpha$ photo emitted X-rays. Right: EDX plot example. It is clear the overlapping of signals, especially at low keV⁹⁸.

EDX, or EDS, is commonly used to analyze and map the composition of an unknown material. The strengths of this analytical technique are the spot resolution similar to the one of SEM and TEM and the immediate response. Main limitations are the overlapping of K, L, M energy levels of different elements, the need of high-energy beam (i.e. intense accelerating field) and standard detectors are not capable in detecting elements lighter than sodium.

X-ray Diffraction – XRD

X-ray diffraction (XRD) is an analytical technique primarily used for phase identification of a crystalline material and it can provide

information on unit cell dimension and atoms position. The analyzed material can be in either powder or a single crystal form.

In 1912, Max von Laue discovered that crystalline substances act as three-dimensional diffraction gratings for X-ray wavelengths accordingly to the d spacing of planes in a crystal lattice.

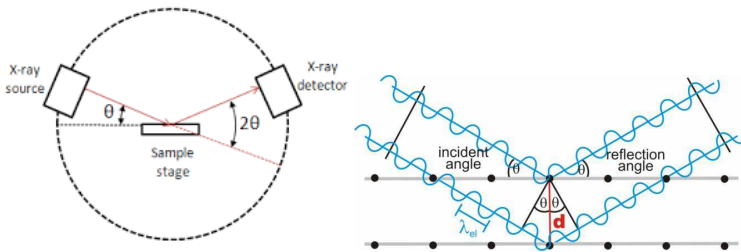


Figure 29 Left: θ – 2θ goniometer configuration, both the X-ray source and detector move following the perimeter of a circumference centered in the sample. Right: Geometrical representation of the incident and reflected beam. If the Bragg's law is satisfied, a maximum of interference happens and a diffraction peak is recorded. Courtesy of ETH Zurich⁹⁹.

X-ray diffraction is based on constructive interference of monochromatic X-rays and a crystalline sample. When conditions satisfy Bragg's Law (i.e. $n\lambda = 2d \sin \theta$), the interaction of the incident rays with the sample produces constructive interference and, thus, a diffracted ray. This law relates the wavelength λ of electromagnetic radiation to the diffraction angle θ and the lattice spacing d in a crystalline sample. In the case of powder samples, by scanning the sample through a range of 2θ angles, all possible diffraction directions of the lattice should be attained due to the random orientation of the powder material. To avoid preferential orientation of crystallites, the sample stage spin around its perpendicular axis.

The conversion of the diffraction peaks to d-spacing allows the identification of the mineral because each crystal material has a set of unique d values.

X-ray diffractometers consist of three basic elements: an X-ray tube, a sample holder, and an X-ray detector. The specific X-ray wavelengths are characteristic of the target material (Cu, Fe, Mo, Cr) used in the source. Filters or monochromators are required to produce monochromatic X-rays needed for diffraction. Copper is the most common target material, with CuK_α wavelength radiation of 1.5418Å. These X-rays are collimated and directed onto the sample. As the sample and detector are moved simultaneously, the intensity of the reflected X-rays is recorded. When the geometry of the incident X-rays hitting the sample satisfies the Bragg Equation, constructive interference occurs and a peak in intensity is recorded and processed.

Applications of XRD:

- Identification of unknown crystal materials
- Identification of single components in mixed materials and their relative concentration
- determination of unit cell dimensions

It is also possible to determine:

- crystal structures using Rietveld refinement
- amounts of minerals and phases (quantitative analysis)
- lattice mismatch between film and substrate
- dislocation density and quality of the film
- superlattices in multilayered epitaxial structures
- thickness, roughness and density of the film

- textural measurements (e.g. orientation of grains, in a polycrystalline sample)

Major strengths are: rapidity, unambiguous results, easy preparation of samples, established technique and straightforward interpretation of data. However, drawbacks are: unknown sample must be pure and single phase, access to XRD database is needed for phase identification, a discrete amount of material is needed, detectability limit is 2%, diffractograms can be complex and, at high angle, peaks overlaps.

Electrochemical Cell preparation

After the production of the material, the powder to be tested is processed into electrodes and the characterization cell is assembled. The main steps are:

- Slurry formulation
- Electrode casting and annealing
- Cell assembly

Slurry Formulation

The slurry, or ink, is obtained mixing three main components with a suitable solvent:

- Active Material
- Electrical conductivity enhancer (carbons)
- Binder
- Active material is the compound to be investigated
- Conductivity enhancer is graphitic carbons. In this work we used independently Timcal Super P and Imerys C-ENERGY™

Super C65 but carbon nanofibers, nanotubes, fullerene and graphene have been used as well

- Binders are inert polymers. We employed PVDF either Kynar™ HSV 900 or Solvay 6020, but PAA, CMC, Agar and SBR are common as well). PVDF is dissolved in anhydrous NMP (Sigma, Merk or Acros) but DMSO is an alternative, while CMC, Agar and SBR are water-soluble.

One very common lab formulation ratio is 80:10:10, but different combination can be possibly used: very low conductive materials can be tested with high content of carbon, while in commercial application the amount of carbons plus binders is lower than 10%.

At lab scale, the active material is grounded in an agate mortar to downsize agglomerates as much as possible, while hard materials can be mechanically ball milled. Carbon is then added and the two powders are mixed together. If the amount of active material is lower than 250mg the PVDF is pre dissolved in NMP and then added to the mortar for mixing; otherwise PVDF powder is transferred in a testing tube along with the others and the NMP and all is mixed together using a homogenizer (30k for 5 minutes). The amount of NMP depends on different factors, mainly the surface area of the powder materials and the amount of PVDF, and its content must be chosen to achieve a honey-like viscosity (i.e. 1000-10000 Poise or g/cms).

Electrode Casting

The obtained slurry, or ink, is casted on different conductive substrates, also known as current collector: metal foils, transparent conductive oxides or graphitic tissues and cloths. Commercial batteries normally use copper and aluminum foil for anode and cathode, respectively. Copper is heavy and expensive but it does not

alloy with Li at low potential so it can be safely used at the negative side, while Aluminum is stable at high potential and fits the positive electrode. 304 or 316 Stainless Steel Alloys are another option available for both sides; in fact, it is stable in the 0-5V range. SS is a good choice for working with aqueous electrolytes. Carbon cloths, mainly used in fuel cells or air-cathode and flow batteries, offer the advantage of a 3D conductive matrix that can be impregnated with high loads of material but its volume and price are high and consequently not appealing for commercial applications.

The obtained ink is casted using a blade or a spin coater and the final dry thickness is in the order of few tens of microns (corresponding to 100-200 micrometers wet thickness) to give 1-2mg/cm² load of material. Commercial batteries have higher loads to diminish as much as possible the active to inert material ratio and thus increase the energy density. In this work, 125 microns of wet ink is deposited on the surface of the current collector or carbon cloths are fully soaked with the slurry.

The casted material is first treated at room temperature or on a hot plate (<100 °C) to remove the excess of solvent and finally at 70 °C in vacuum to completely dry the sample. This two steps process is needed to avoid mechanical stress caused by the formation of bubbles in the bulk and the consequent detachment of active material from the surface of the current collector.

The obtained electrode can be pressed using a calender to improve the adhesion to the current collector and maximize the density of the active layer, thus lowering the grain boundary resistance (i.e. the resistance caused by the limited contact of two neighbor particles).

Depending on the cell used for characterizing the material, the electrodes can be cut in any shape using scissor, hollow puncher, crimping machine or laser cutter. In industry, the use of ceramic blades is compulsory for increasing safety, as metal blades or knives can leave metal debris during cutting, therefore allowing possible short circuits inside the cell.

Cell: Flooded, Swagelok™, Coin

Flooded cell, Figure 30, consist in a glass container in which two or more electrodes can be dipped in an excess of liquid electrolyte. It is the easiest way to perform measurements, in either aqueous or organic electrolyte, but it can be expensive because of the large volume of used electrolyte.

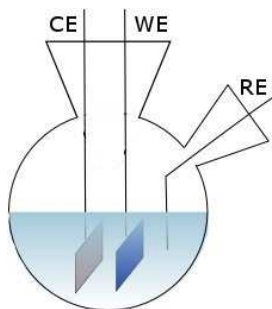


Figure 30 Three electrodes flooded cell. The working, WE, the counter, CE, and the reference electrodes, RE, are submerged in the electrolyte.

Swagelok™ cell, Figure 31, is a good solution and the sketch of both two and three electrodes configuration follow:

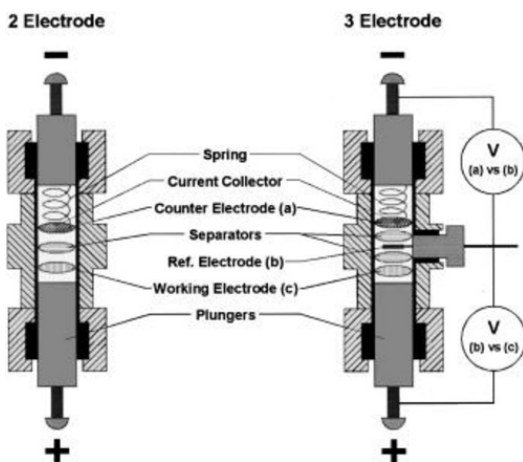


Figure 31 Swagelok™ cells. Two electrodes configuration, left, and three electrodes setup, right. Metal current collectors (SS, Al, and Cu) provide the electrical contact. Note the spring to provide the same pressure to the stacked materials and thus making the experiment reproducible¹⁰⁰.

This kind of cell is reusable and it requires a small amount of electrolyte. The separator is normally a woven fiberglass or a polymeric membrane like Celgard, while the pressure is ensured by the use of one spring. Likewise flooded cell, it can be assembled in either two or three electrodes configuration ensuring, in the latter case, the possibility of following the potential of both electrodes respect to a reference (e.g. Ag/AgCl wire, Na or Li metal). Current collectors are made of SS, Al or Cu. Moreover, Swagelok are air tight allowing the cycling of air sensitive system out of glove boxes or dry rooms. In this work, 10mm and 18mm in diameters three electrodes cells have been used.

Coin Cell, Figure 32, is the laboratory battery configuration closest to the real world application and it requires only the purchase of the

crimping machine to seal the battery. It comes in different sizes but the most used is the CR2032, i.e. 20mm diameters and 3.2mm in height.

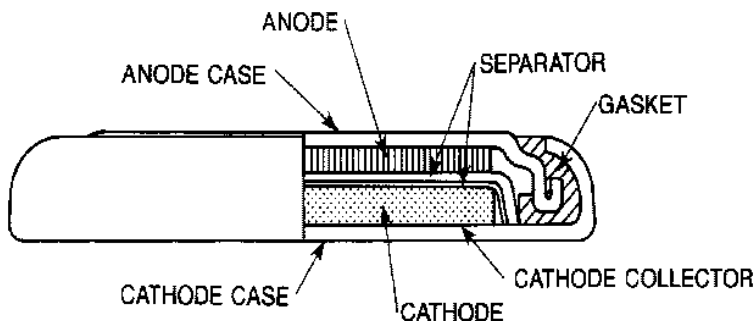


Figure 32 Section view of the coin cell. Note the gasket placed between the anode and cathode cases that provides both electrical insulation and protection from moisture and oxygen¹⁰¹.

The reproducibility of this kind of cell is good, the amount of materials required to the assembly is limited and it is very compact. As Swagelok™, the construction is airtight so it can be used out of controlled environments. The main drawback is that it comes only in two electrodes configuration.

In this work, CR2032 cells are used: lithium or sodium anode and cathodic materials are 16mm discs, while the glass fiber or polymeric separator is 18mm. The cell is assembled and closed in an Argon feed glove box and then cycled in room conditions.

Battery Characterization

Independently to the cell, to perform whatever electrochemical measure, the electrodes must be coupled to a machine that can both

deliver and measure potential and current simultaneously. Potential is measured or applied between the working (i.e. the sample material) and the reference, while current is provided or read amid the working and the counter electrodes. This machine is commonly called potentiostat.

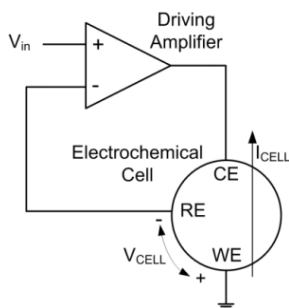


Figure 33 Very basic configuration of a three electrodes cell coupled to a potentiostat. The current flows between WE and CE, while the potential is controlled between WE and CE ¹⁰².

Potentiostats range from simple power supplies to complex frequency response analyzers and they can be stand alone or coupled to computers to setup, visualize and analyze experiments.

Different techniques can be performed and the ones used in this work are described in the following subchapters.

Cyclic Voltammetry – CV

Cyclic voltammetry is a quasi-stationary method. It implicates the imposition of a triangular waveform as the potential on the working electrode, with the simultaneously measurement of the current. Following the European rule, positive current is for anodic oxidative process while negative one for cathodic reductive reaction.

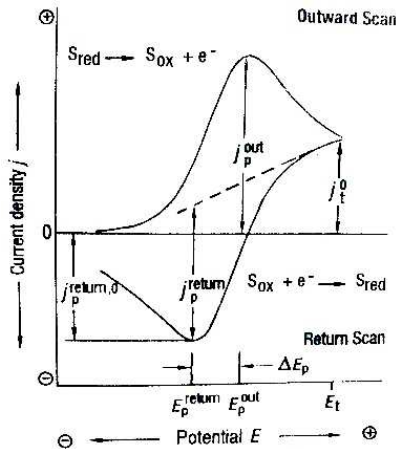


Figure 34 Representation of a single cyclic voltammetry scan, European convention
103.

The potential window, in which the tested material is switched, is normally chosen within the potential stability window of the supporting electrolyte. E.g. in case of aqueous systems the switching potentials should not exceed the ones of water splitting reactions (i.e. $-0.4 < E_{\text{applied}} < +0.8$ vs NHE at pH 7). Doing this, no decomposition species will alter the electrode surface or the electrolyte composition and thus it is possible to obtain high reproducible current-voltage (i.e. i/V) behavior. Another parameter that can be chosen in CVs is the scan rate. Depending on the nature of the leading electrochemical mechanism, diffusion or charge transfer control, either position or intensities of peaks are “dependent” to the scan rate. Other parameters as temperature, concentrations, viscosity of the electrolytes, stirring, nature of the counter electrode can interfere as well. Unfortunately, there is no magic number, but in aqueous solution values between 10mV/s and 100mV/s are quite common,

while solid-state materials suffer of low ion diffusion thus lower rates, e.g. 0.1mV/s, are compulsory.

CV is a very powerful technique that allows the identification of several information in one shot: reaction potential, process thermodynamic reversibility, charge capacity, charge efficiency, limiting reaction mechanism, electrocatalytic (i.e. active) surface area and more.

The current is determined by the coupling of diffusion of species from the bulk to the surface of the electrode and an electron transfer process at the surface thereof. In general, this coupling gives rise to a current maximum, since after the potential, at which electron transfer takes place, is reached, the surface concentration, c_s , of the reacting species falls as the potential moves further, from the bulk concentration, c_0 , towards $c_s=0$. The fall in c_s initially increases the concentration gradient $(c_0-c_s)/\delta_N$ and hence the flux of material to the surface. However, δ_N is also increasing with time according to the expression $\delta_N=(\pi Dt)^{1/2}$, and at higher potentials, when electron transfer is fast and the current has reached its mass-transport-limit value nFc_0/δ_N , it will cause the current to decrease again. Consequently, a peak is formed in the i/V plot. Several parameters can affect the CV plot and a deeper description of the technique is referred to specific publications.

In this work, CVs are mainly used to estimate the potentials at which reactions take place and to evaluate briefly the reversibility and the coulombic efficiency of the transformations of interest.

Galvanostatic Cyclation with Potential Limitation – GCPL

Galvanostatic techniques are stationary methods in which the current is set and the potential changes are followed during the measure. The exit condition can be either the potential or the time.

The current applied to the cell must be defined taking in account the specific theoretical capacity q (mAh/g) for a given material is calculated as follow:

$$q = \frac{nF}{3600M} \quad [\text{Eq. XIX}]$$

Where n is the number of electrons exchanged, F is the Faraday's constant and M is the molecular mass of the active material. q times the mass of the sample and divided by 1h gives the current needed to charge or discharge that amount of material in one hour, that is also known as 1C rate: likewise, in 10h is C/10 while in 0.1h (i.e. 6 minutes) is 10C. A typical discharge plot follows:

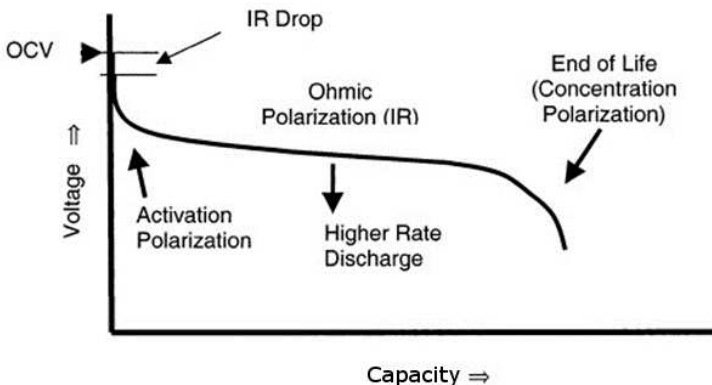


Figure 35 Generic galvanostatic plot. Different polarization contributes as well as IR drop are highlighted. For simplicity the OCV is considered constant¹³.

In Figure 35 is reported a generic variation of potential upon capacity variation of a material that, theoretically, has a constant OCV voltage despite the charge/discharge state. There are several kinetic contributes to the potential delivered by the cell:

- IR drop: $\eta = iR_{\text{cell}}$
- Activation polarization: $\eta = a - b \log(i/i_0)$ [a,b:constants]
- Ohmic polarization: $\eta = iR_{\text{wires+electrolyte+material}}$
- Concentration polarization: $\eta = (RT/n) \ln(C/C_0)$

Where $i_0 = k_0FA$ is the exchange current (K_0 is the reaction rate constant and A the activity product of the reactants), i is the applied current and C and C_0 are the concentrations at the surface and in the bulk respectively. A more exhaustive explanation of these polarization contributes are referred to specific textbooks.

In this work, GCPL is used to evaluate the practical charge capacity, the working potentials, the charge efficiency and retention.

Gibbs' Phase Rule

The shape of the "Ohmic polarization" part of the charge/discharge GCPL curves Figure 35, gives another important information. In fact, some curve are flat while others have slopes or are S-shape. To understand better, it is good to keep in mind the Gibbs' Phase Rule:

$$F = C - P + 2$$

In which C is the number of components and P is the number of phases present in the material during the experiment. F is the number of degree of freedom; namely the number of intensive thermodynamic parameters that must be specified in order to define

the system. One of the thermodynamic parameters in an electrochemical reaction is the potential.

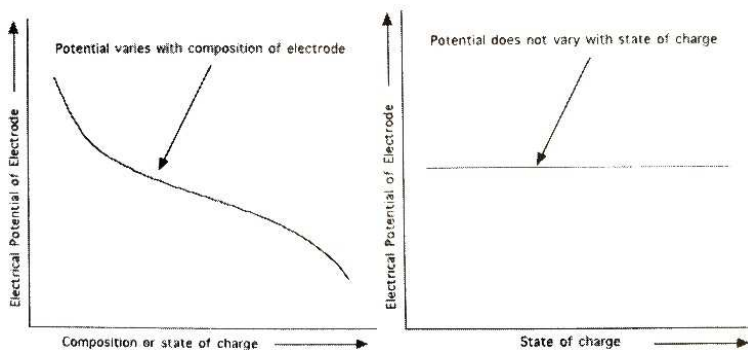


Figure 36 Left: dual components, single-phase transformation. Right: single component, single-phase reaction ¹.

In Figure 36, one component single-phase system, F is equal to two and thus, if the temperature and pressure are specified, there are no more degree of freedom available and the potential cannot change. Otherwise, if the material is two components single phase (e.g. solid solution), F is equal to three and subsequently one degree of freedom is not set and thus E can vary.

Electrochemical Impedance Spectroscopy – EIS

The component steps of an electrochemical process, such as mass transport, chemical adsorption steps, electron transfer and others, all contributes to the total potential drop across the cell and for a DC current can be represented by resistances such as R_E (i.e. electrolyte resistance) and R_{ct} (i.e. charge transfer resistance). However, if an AC current flows, it becomes necessary to distinguish purely ohmic resistance, such as R_E , from non-ohmic, complex and

real frequency-dependent resistances (i.e. impedances). By careful investigation of the frequency dependence of such impedances, it is possible to separate the contribution to the overall electrochemical process. These studies include, in addition to kinetic and adsorption processes, corrosion mechanism, battery behavior, sensor ageing and studies on porous electrode structures. However, despite the simplicity of experiment setup and data, the understanding of this kind of experiment is extremely tricky.

In EIS, a probe signal, often sinusoidal potential V of frequency ω , is applied to the investigated system and a response signal, in this case a current I of frequency ω' , is recorded.

$$Z = \frac{V}{I} = \frac{V_0 e^{i\omega t}}{I_0 e^{i\omega' t}} = \frac{V_0}{I_0} e^{i(\omega - \omega')t} = \frac{V_0}{I_0} e^{i\phi t}$$
$$Z = Z_{real}(\omega) + iZ_{im}(\omega) \quad [\text{Eq. XX}]$$
$$Z_{im} = Z_{im}(Z_{real})$$

Hence, plotting the Z_{im} as function of Z_{real} the Nyquist plot is obtained. In Figure 37, a simulated Nyquist plot and its equivalent circuit are shown.

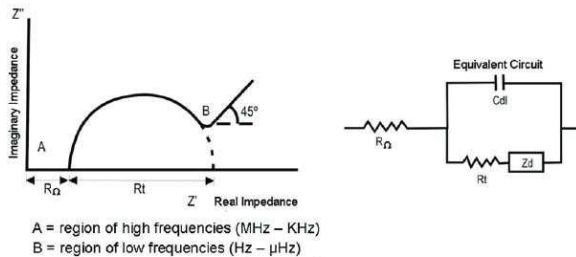


Figure 37 Electrochemical impedance spectroscopy of a mixed diffusion and charge transfer reaction. Left: the obtained Nyquist plot; Left: the equivalent circuit ¹⁰⁴.

When applied to batteries it provides information on reaction and kinetic processes taking place during charge/discharge cycles. It is used mainly to monitor the impedance during extensive ageing tests.

However, it is compulsory the use of well-designed experiment to avoid undesired contributes. For example, coin cell is not a good choice because in two electrodes configurations the contributes of both electrodes are mixed together. Swagelok, as three electrodes configuration is possible, is a better choice since it is possible to decide which of the two electrodes investigate.

In this work, EIS is used to estimate the ionic conductivity of solid-state electrolytes and thus no complex interpretation are needed, as a simple semicircular fit is required. The topic will be discussed in detail in the following chapters.

Chapter 4
Discussion

Pigments – Small Molecules

The idea of investigating organic small molecule carbonyl/imide pigments comes from a long and linear path. In fact, Ruffo et al. are interested in organic electroconductive materials since fifteen years mainly because of projects involving new electrochromic materials for shading application. Being energy storage another hot topic and because electrochromic and battery materials shares core mechanisms, the idea of evaluating and optimizing our materials for energy application was spontaneous.

Early steps

In late two thousands we were working with a derivative of poly(3,4-ethylenedioxythiophene) showing great stability and great optical properties¹⁰⁵.

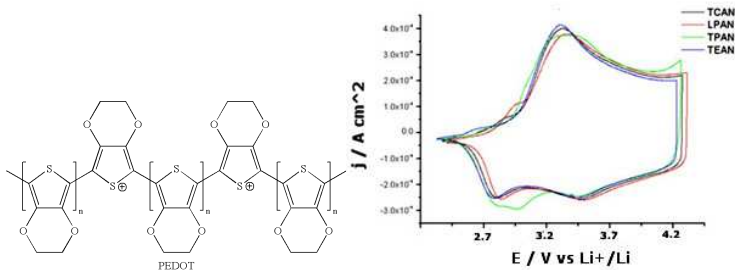
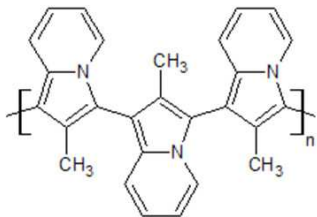


Figure 38 Left: poly(3,4-ethylenedioxythiophene) (pEDOT) polymer structure in the aromatic oxidized colorless state. Right: 10th cycle of electrodeposited pEDOT thin layer, 50mC/cm², on top of gold pin electrodes cycled in different acetonitrile-based electrolytes.

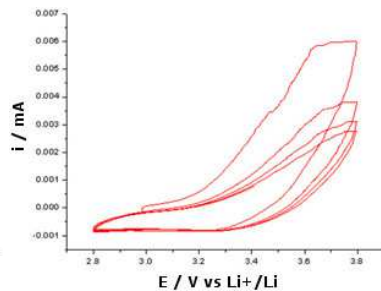
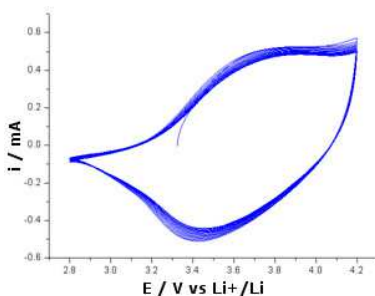
Lately, we used standard pEDOT system, Figure 38, in order to identify some of its kinetic properties¹⁰⁶ and evaluating its charge discharge properties as well.

Electroconductive polymers are very appealing because of their high oxidation voltage $>3.5\text{V}$, high rate capability, b-type mechanism, thermodynamic reversibility and cycling stability but the specific capacity is too low for energy storage applications (i.e. theoretical is 180mAh/g while practical is around 50mAh/g). The low capacity comes from the impracticality of extracting one electron from every monomer unit.

We then changed the monomer unit trying to increase the working potential and the specific capacity and the methyl derivative of Indolizine (IND)¹⁰⁷ has been our choice.



(a)



(b)

Figure 39 (a) polyIndolizine aromatic neutral structure. (b) Cyclic voltammery behaviour of polyIND electrodeposited thin film. (c) Cyclic voltammery response of a thick chemically polymerized bulk polyIND electrode.

The experiment succeeded but major drawback have arisen when bulk electrodes were cycled. In Figure 39 it is clear the capacity fading upon cycling and the given reason for this lies on both morphological issues (i.e. the chemically polymerized material has a bulky non-porous macrostructure) and mechanical instability similar to decrepitation for alloy anodes.

Exploring the world of pigments, we developed a polymeric derivative of the naftalenebisimide NDI pigment^{108–111}.

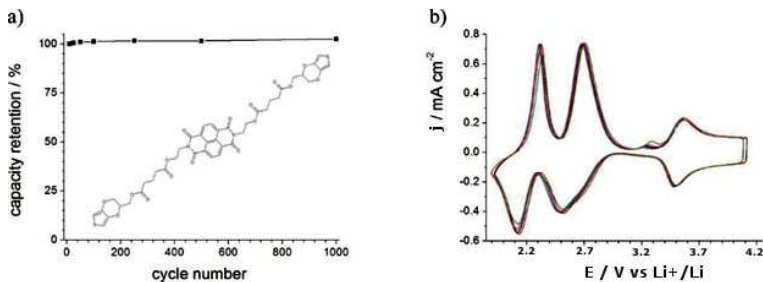


Figure 40 (a) Capacity retention over one thousand cycles; inset the monomer structure. (b) Cyclic voltammetry response over one thousand cycles. Add 3.7V to calculate the potential vs Li.

It is the first material reported to switch reversibly between three different color states: colorless, blue and gray. Its electrochemistry is extraordinary as well reporting good capacity retention after one thousand cycles in the full range. NDI has both carbonyl and imide group, thus being a b-type organic material. If the carbonyls n-doping contributes is clearly visible in Figure 40-b (i.e. the two one electrons redox reaction below -0.5V vs Fc), on the contrary there is no signal from the imide group. In fact, at least in the explored region, the only contribute to the cathodic charge comes from the p-doping process of the pEDOT cross-linked backbone. The main issues reported are

both the intermediate n-doping potential, 2÷3V, and the low theoretical specific capacity, 60mAh/g for two e⁻, due to the very high molecular weight, 891g/mol.

Confident that all the good properties were coming from the chemical structure of the pigment, we decided to explore this family of organic materials as simple small molecule. Our motivation were also endorsed by the good mechanical and chemical stability or properties described in Chapter 2.

Therefore, because of their availability, characteristics and novelty, we decided to focus our attention on the following three pigments: peryldiimide (PDI), indanthrone (IND) e quinacridone (QA).

Perylene Pigments

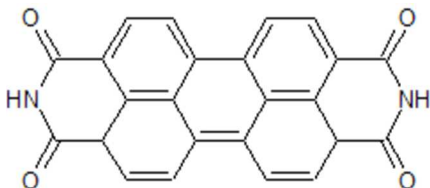


Figure 41 Perylenediimide “Violet 29” structure, M_w 392g/mol. It is a reddish powder.

Perylene pigments include the dianhydride and diimide of perylene tetracarboxylic acid along with derivatives of the diimide. Commercially available types provide good to excellent lightfastness and weatherability; some of them, however, darken upon weathering. A number of these compounds have excellent heat stability, which renders them suitable for spin dyeing. They are also used to color polyolefins, which are processed at high temperatures. The list of applications includes high-grade industrial coatings, such as automotive finishes; and, to a lesser degree, special printing inks

for purposes such as metal decoration and poster printing. The H derivative is named “Violet 29” and has a reddish hue.

PDI has four carbonyl and two imide groups and it is synthesized in the fully aromatic neutral state. If all the heteroatomic groups, four carbonyls and two imides, undergo reversible redox reactions, the theoretical specific capacity of PDI is 134mAh/g in oxidation and 268mAh/g in reduction. Wei et alii, in the same paper¹¹², declare that a molecule similar to PDI can irreversibly intercalates eleven Li⁺ ions when deeply reduced close to 0V. In Figure 42, the proposed doping mechanism for reversible reactions is proposed.

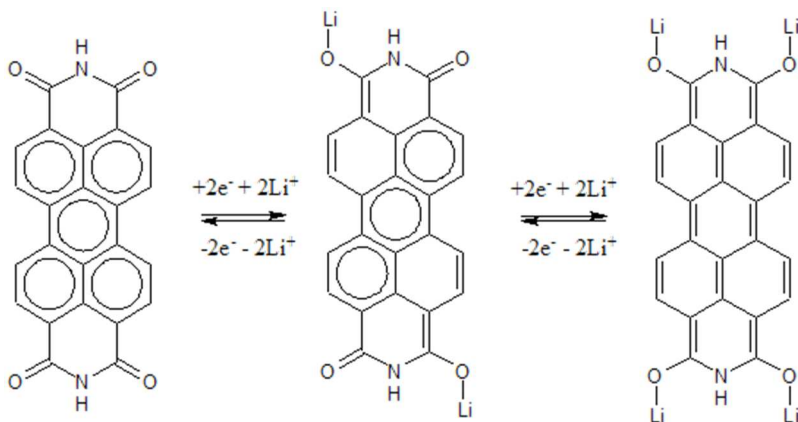


Figure 42 Left: the PDI five rings core preserve its aromaticity and the molecule is in the neutral state. Middle: upon reversible reduction of two electrons at around 2.5V, the electronic configuration changes and O-Li, ionic, groups are formed at the carbonyls. Right: a second reduction happens, all the carbonyls are reduced and the core rings are in quinoid configuration. This reduction reaction is reported to happen close to 0.5V and being not fully reversible.

Materials: PDI (Sigma Aldrich) is used with no further purification, hard carbon SuperP is from Timcal, PVDF model 6020 is from Solvay and LP30 (EC:DMC 1M LiPF₆) electrolyte is from Ferro Inc.

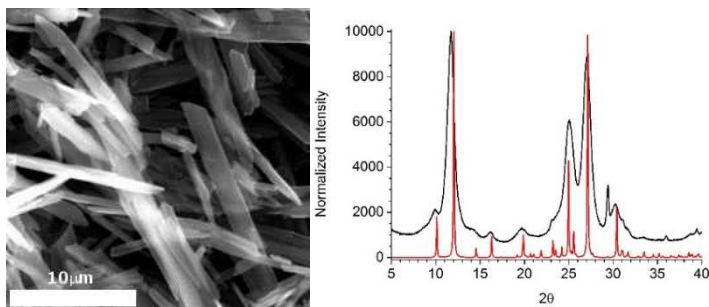


Figure 43 Left: SEM image of commercial untreated PDI showing the needle shape of the micrometric crystallites: length 10 microns, width 2 microns. Right: The XRD spectrum, black, of the commercial sample is compared to the theoretical one, red.

In Figure 43 Left, the needle like macrostructure of the commercial compound is presented. The crystallites are 10 μ m long and 2 μ m wide. The XRD analysis, Figure 43 Right, compares the experimental diffractogram, in black, to the theoretical one. Despite the small shift of some peaks to bigger angles (except the one at 25° that move to the left), the structure is confirmed to be the monoclinic P 2₁/c space group, typical of the β -form. The shifts are due to slight differences in the unit cell parameters (i.e. bigger angle, smaller parameters), while low crystallinity or particle dimensions can cause the broadening of the peaks. It's interesting to observe that both morphology and crystal structure are similar to the perylene-3,4,9,10-tetracarboxylic dianhydride (PTCDA) polymer derivatives reported by Sharma et alii¹¹³.

Firstly, a soluble PDI derivate has been analyzed. The material has been dissolved 10^{-3}M in a 0.1M LiClO_4 solution in $\text{CH}_2\text{Cl}_2:\text{MeCN}$ 1:2 by volume and then studied in a three electrodes flooded cell using a glassy carbon pin as working electrode.

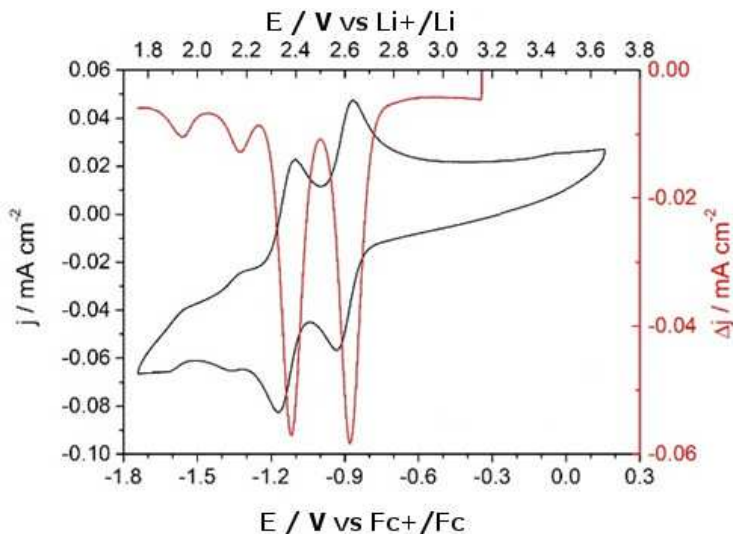


Figure 44 In Black, the 50mV/s cyclic voltammetry and, in red, the 20mV/s Differential Pulsed Voltammetry of the PDI soluble derivative are reported. The two single electron redox reactions, at 2.6V and 2.4V respectively, are clearly visible.

In Figure 44, both the CV (in black, 50mV/s on glassy carbon WE) and DPV (in red, 20mV/s on GC WE) reported. The two single electron redox reactions, at 2.6V and 2.4V respectively, are clearly visible and both are thermodynamically reversible. Because of the narrow stability window, no oxidation peak related to p-doping of the two imides has been identified at more positive potentials.

The composition of the PDI:SuperP:PVDF ink was 75:15:10 by weight. Powders have been preliminary mixed in a mortar and then anhydrous NMP (MERK) has been added in order to achieve the honey like viscosity. The mixture was subsequently homogenized at 30k rpm for 5 minutes. The obtained slurry was casted on an Al current collector with a blade coater (50 cm/min, 125 microns wet thickness). The electrode was then dried at 70°C in vacuum overnight. Coin cell, MTI SS304L, has been assembled with Li metal (Alfa Aesar) and fiberglass separator (Wattman GC/C) and sealed in Ar filled glove box (MBraun O₂<1ppm). Both CV and GCPL analysis were performed in ambient condition. Biologic VMP3 and VSP300 potentiostat were used to perform the measurements. Swagelok™ cell have been assembled as well.

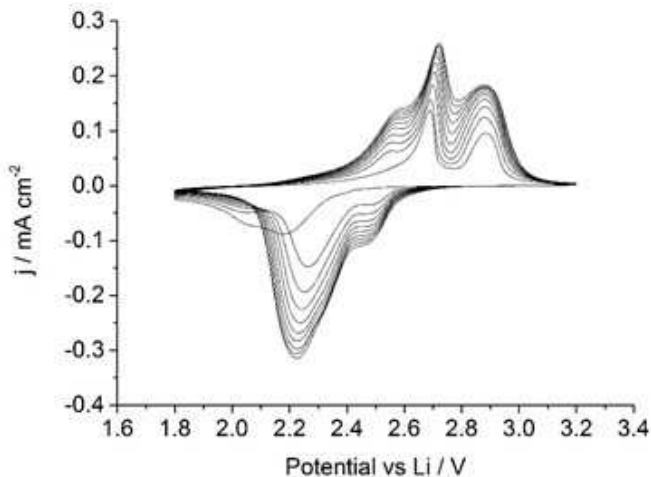


Figure 45 0.1mV/s cyclicvoltammety of a CR2032 coin cell. The current intensity increases upon cycling showing the presence of an activation mechanism.

In Figure 45, one CR2032 PDI coin cell with Li CE and LP30 electrode is tested. The CV shows that the PDI solid-state electrode works similarly to the soluble derivative but the growing of the current signal upon cycling underline the existence of an activation mechanism. This could be simply related to the wetting of the materials that “sucks” electrolyte upon charge/discharge volume changes (i.e. like a sponge), thus exposing more material available to the reaction.

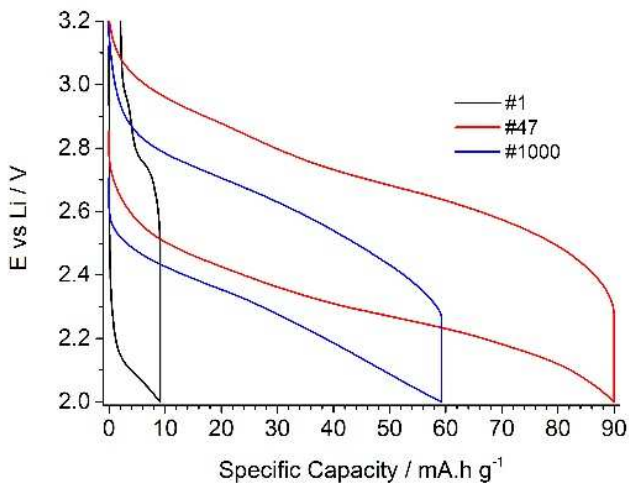


Figure 46 CR2032 PDI coin cell cycled at 1C for one thousand charge/discharge runs.

In Figure 46, charge discharge profiles of a PDI coin cell are reported. The slope in the potential suggests the presence of a two components one-phase reaction. The first cycle has a practical capacity of only 10mAh/g but after 47 cycles it reaches the maximum of 90mAh/g and subsequently it decreases for unknown, at the

moment, reasons to a value of 60mAh/g. Considering it as a discharged anode, it charges at 2.4V while the discharge happens at 2.6V. This 200mV charge/discharge overpotential at 1C is considerably high but it follows what we saw in the CV in Figure 45. Probably, this value can be improved (i.e. lowered) increasing the carbon to active material ration in the electrode formulation.

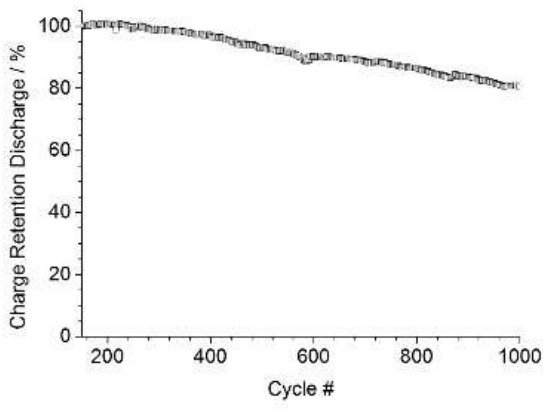
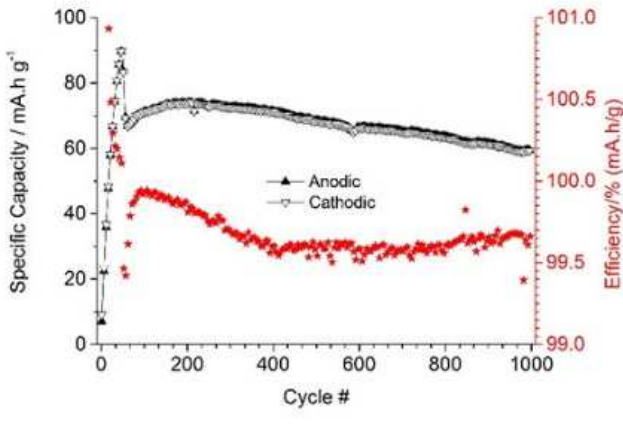


Figure 47 GCIPL of one PDI coin cell cycled at 1C rate in LP30 for one thousand cycles. In the first one hundred cycles, an unknown activation process happens. However, the Charge efficiency, in red, is reported to be very close to 100% meaning that the reversibility of the reactions involved is high. The charge capacity fades slowly upon cycling.

In Figure 47, the specific capacity and the charge efficiency of a PDI electrode is presented. Charge efficiency is close to 99.5% for almost all the 1000 cycles meaning that all the reaction involved are reversible. Although, the charge behavior is strange; in fact, during the first 50 cycles it grows from 10mAh/g to the maximum value of 90mAh/g and then it rapidly decreases down to a minimum of 65mAh/g. The charge capacity then slowly gains 10mAh/g more in 150 cycles for subsequently starting the natural fade related to the normal ageing of the material.

We previously suggested a “breathing” mechanism upon cycling, but this rollercoaster behavior can be hardly explained with that. To exclude any kind of mechanical hindrance caused by the continuous cycling we performed another experiment in which, after activating the material for 100 cycles, we let it rest for 48h before performing other few cycles.

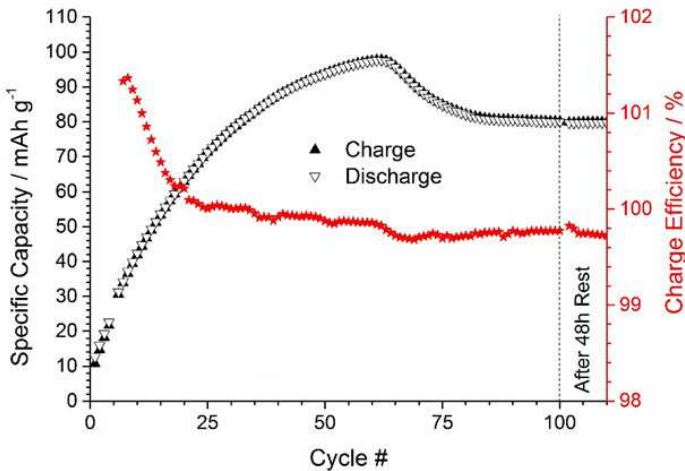


Figure 48 PDI GCPL at 1C, 136mA/g, is plotted. After 100 cycles, the cell is left resting for 48h and the cycled again. No big changes in both capacity and charge efficiency are recorded.

Referring to Figure 48, it is clear that resting after cycling does not bring back the material to any of its previous states. An *in-situ* XRD analysis, as well as *ex situ* SEM imaging would be of help in defining if any morphological or structural change related to the ageing of the material takes place.

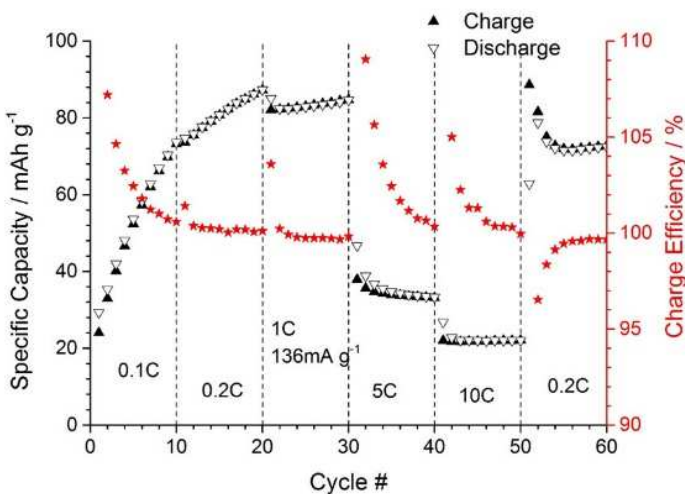


Figure 49 PDI pristine coin cell GCPL experiment in Li-based electrolyte at different C-rates.

In Figure 49, a GCPL experiment at different C-rates, ranging between C/10 to 10C (i.e. 10h and six minutes charge/discharge currents were applied, respectively), is reported. This experiment shows that the electrode material behaves well up to 1C, while for higher currents the charge drops down to one third of the nominal value. However, going back to slower rates recover the available charge. At slow C-rates, the Charge efficiency moves quickly in the 100% region, while for faster rates the evolution is a little bit worst.

As announced by Haupler et alii in their review⁶⁷, cycling organic compounds in Na-based electrolytes is of great interest because we can thus tackle two issues at the same time: Li scarcity and inorganic electrodic materials high costs. Therefore, PDI has been cycled in Na-

based electrolyte as well and the preliminary results are reported as follow.

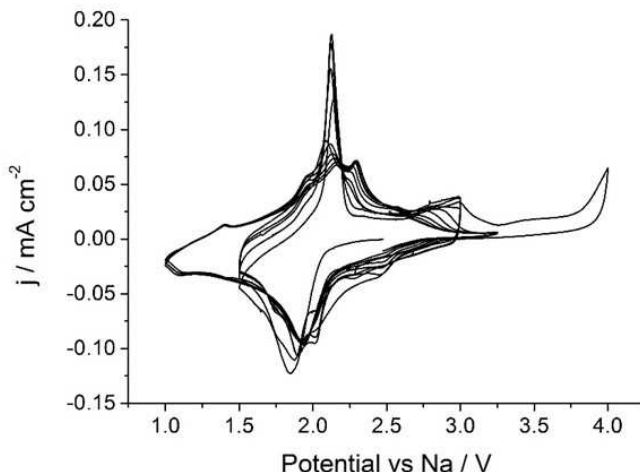


Figure 50 0.1mV/s cyclicvoltammetry of a PDI coin cell cycled in 1M NaClO₄ in EC:PC 1:1_v electrolyte.

Figure 49 shows the electrochemical behavior of the PDI in Na-based electrolyte. Instead of several peaks as in Li-based electrolytes, PDI shows less and sharper peaks when cycled in sodium; even though, the sharp oxidative peak in return quickly disappears after few cycles in favor of contiguous three peaks. Moreover, the thermodynamic reversibility of the n-doping process is better compared to the one in lithium. Broadening the cycling potential window does not show any other redox reaction of interest, but using the 1.0÷2.7V cycling potential window increases the practical charge capacity without

introducing any unwanted reaction (e.g. the irreversible oxidative tail starting at potentials higher than 2.7V vs Na).

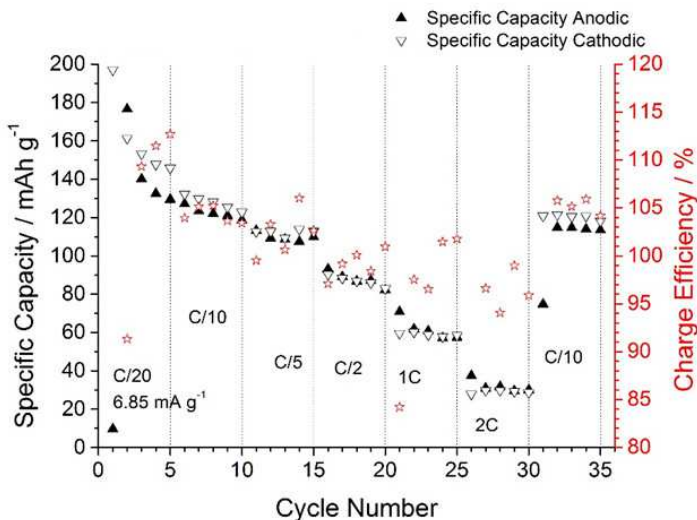


Figure 51 GCPL analysis at different C-rates, $C/20 \div 2C$, of a PDI based electrode in NaClO_4 1M in EC:PC 1:1_v electrolyte.

In Figure 51, PDI is galvanostatically cycled in sodium electrolyte at different C-rates, ranging from C/20 to 2C. Surprisingly, at low C-rate q reaches 120 mA h/g, a value very close to the theoretical one of 134 mA h/g. First cycles show high charge irreversibility and fading but it does not seem that an “activation” phenomenon takes place as in lithium. The scattered charge efficiency values, i.e. reversibility, are probably related to the not optimized electrolyte of choice. In fact, it is reported in several works that upon reduction the Na-based electrolyte do not form a stable SEI on the electrode surface, thus some charge is lost during every cycle.

Indanthrone

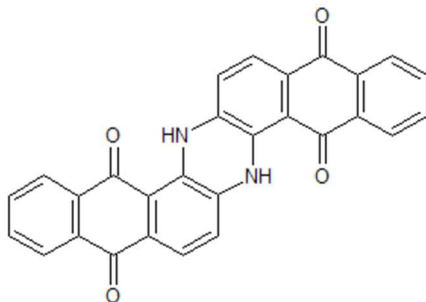


Figure 52 Indanthrone “Blue 60” structure, Mw 442g/mol. It comes as a blue thin powder.

Vat dyes of the highest quality have derived their name from indanthrone, a blue compound, which was originally known as Indanthrene Blue. The compound has been used for a long time as a pigment and is registered in the Color Index as Pigment. Indanthrone exists in four crystal modifications, of which the α - and the β -modification afford greenish and reddish blue shades, respectively, while the γ -form provides reddish hues. The δ -modification has no coloristic importance. Being the most stable thermodynamically, the α -form is most suitable for use as a pigment. The unsubstituted compound is a blue powder called “Blue 60”.

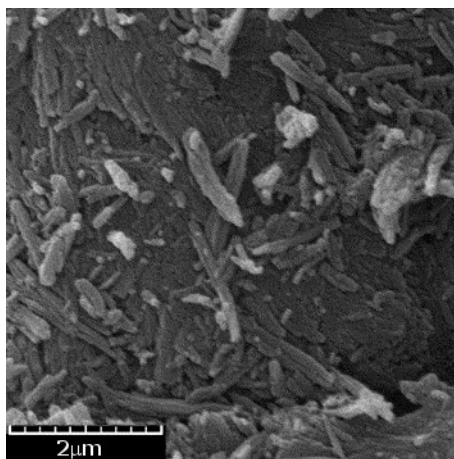


Figure 53 SEM image of an indanthrone washed sample. The material is close packed agglomerates of needle-like crystallites of $2\mu\text{m}$ long and few hundreds of nanometers wide.

Morphology resemble the one of PDI but the needles are smaller, Figure 53, $2\mu\text{m}$ long and few hundreds of nanometers wide, and agglomerates are more close-packed. The crystal structure is monoclinic $P2_1/a$ space group with cell parameters of $a=30.83$ $b=3.83$ $c=7.85$ $\beta=91^\circ 55'$ ¹¹⁴.

Indanthrone is the heaviest of the group and thus it has been analyzed briefly. Its theoretical specific capacity is, considering one e^- in oxidation and two e^- in reduction, 60mAh/g and 120mAh/g respectively.

IND was purchased from Sigma Aldrich and then washed under stirring for 2h in CH_2Cl_2 at room temperature for removing impurities and amorphous material. The preparation of the electrodes followed the procedure described in the previous paragraph.

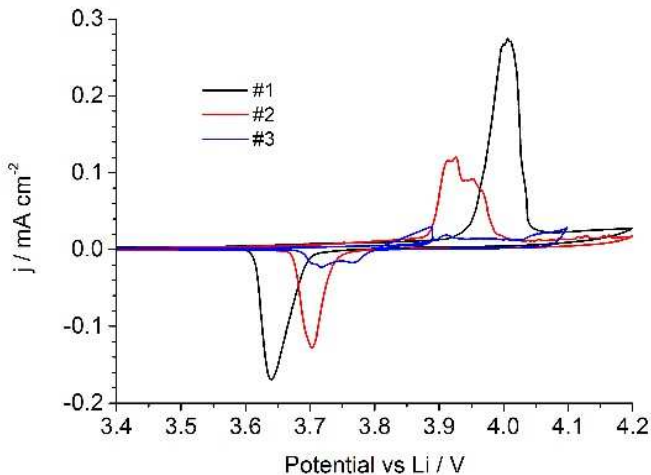


Figure 54 Cyclic voltammetry of a Swagelok™ containing an IND electrode. Scan speed is 0.1 mV/s while the electrolyte is LP30.

The cycle voltammetry in Figure 54 shows that IND is electroactive and can incorporate lithium in its structure. The potential at the first cycle is appealing, +4.0V, makes IND appealing as cathode material for LIBs. However, the following reduction happens at 3.6V and therefore the polarization of the electrode is very high and a lot of energy is wasted. The following cycles highlight a serious drop in capacity meaning that some irreversible reaction or loss of active material is happening.

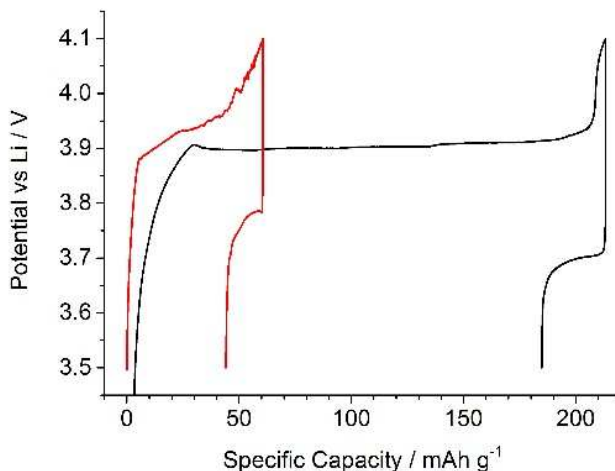


Figure 55 CR 2032 Galvanostatic cyclation at C/10 of IND electrode in LP30 electrolyte. 1st, black, and 2nd, red, cycles.

The same electrode material has been assembled in a coin cell and then cycled galvanostatically at C/10. The first oxidation peak seen in Figure 54 is now a very long plateau at 3.9V but the total capacity exceeds three times the theoretical one meaning for sure that an irreversible reaction is happening at the surface of the electrode. Further cycles shows similar irreversibility and almost no charge is delivered during the second discharge.

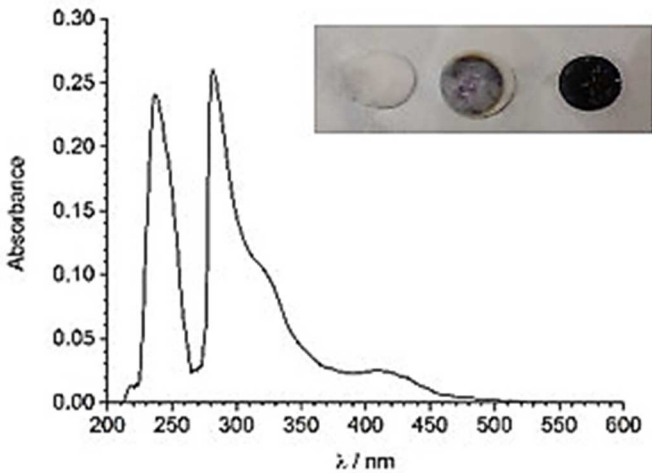


Figure 56 inset: View of the glass fiber separators after being cycled in a Swagelok™ cell. RE separator is clean, while WE/CE one is stained. UV-Vis spectrum of LP30 solution after 48h in contact with an IND electrode in the neutral state.

In Figure 56 the evidence that IND is soluble in carbonates based material is clear. The electrode material or the chemical compound must be protected somehow from dissolution. Different approaches have been undertaken and their results follows.

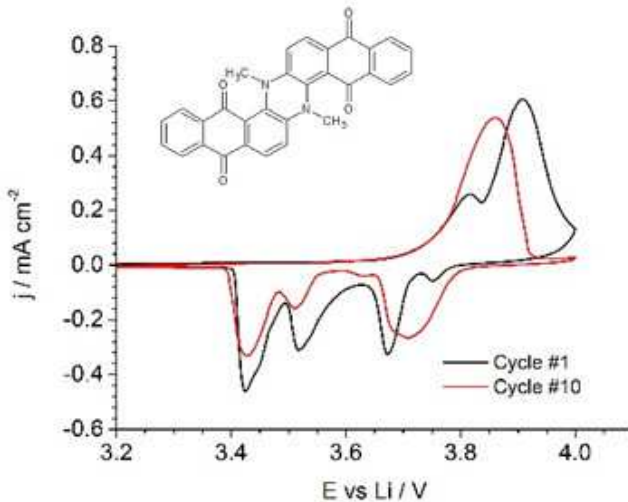


Figure 57 IND-Me methyl derivative molecular structure and, Right, its 0.1mV/s cyclic voltammetry in LP30 using both polymeric Celgard™ and glass-fiber separators.

It is known in imide compounds that, upon oxidation, one of the nitrogen can suffer deprotonation and consequently the diimide ring opens to stabilize the structure. Because the new decomposition compound is different and the imide group is “missing”, this could explain the irreversible cathodic scan of Figure 54. Therefore, a methyl derivative has been synthesized, Figure 57 inset, and analyzed, but even though it looks more stable, the discharge electrochemistry mechanism is not clear as too many peaks, 3.7V 3.5V and 3.4V, appear in the reverse scan, Figure 56.

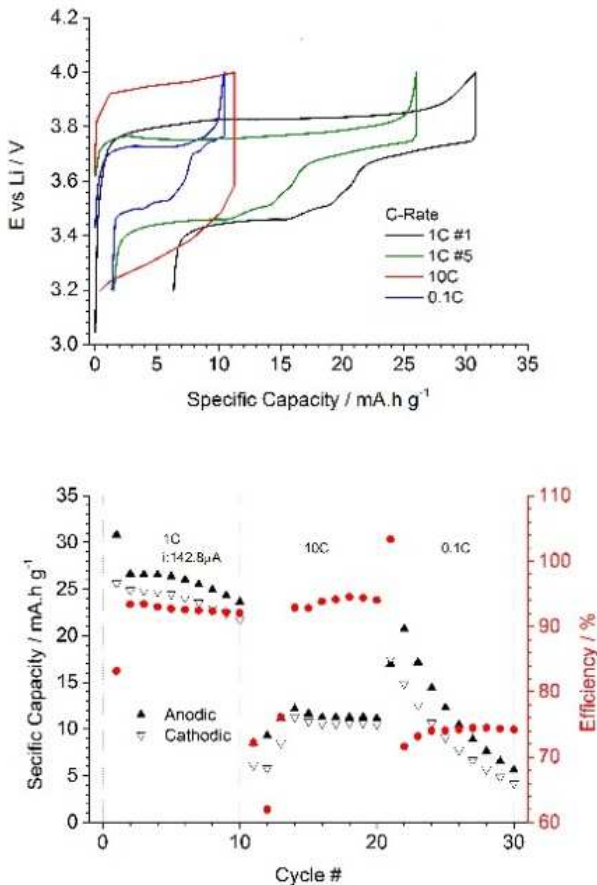


Figure 58 GCPL profiles, Left, and charge capacity as well as efficiency at different C-rates.

In Figure 58, GCPL analysis of IND-Me is reported. At low C-rates the main charging plateau happens around 3.8V and the discharge profile follows a two-steps mechanism, 3.6V and 3.4V, close to the CV one.

The charge capacity is half of the expected, 25mAh/g, and the overpotential is high, 200-400mV at low C-rates and 800mV at 10C. However, the charge efficiency, at low rates, is higher than 95% but it drastically decreases at 10C. To reduce the polarization a higher content of carbon in the slurry formulation is advised.

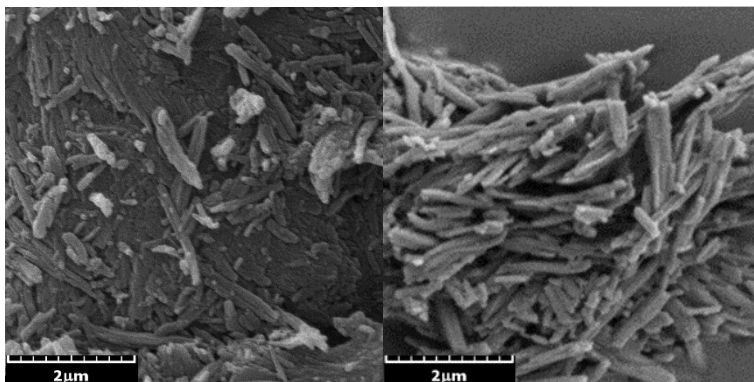


Figure 59 SEM image of pristine IND, Left, and carbon coated IND, Right.

As the thermal stability of pigments is reported to be as high as hundreds of °C, commercial IND, blue powder, was mixed with 10%w of D-glucose and everything diluted with water. The slurry was then dried and grounded in mortar. The obtained powder was transferred in a vacuum tube and heated at 340 °C in vacuum, using a two stages membrane pump, for 4h ¹¹⁵. The resulting black powder was characterized (SEM in Figure 59), processed in an electrode and cycled in LP30, Figure 60.

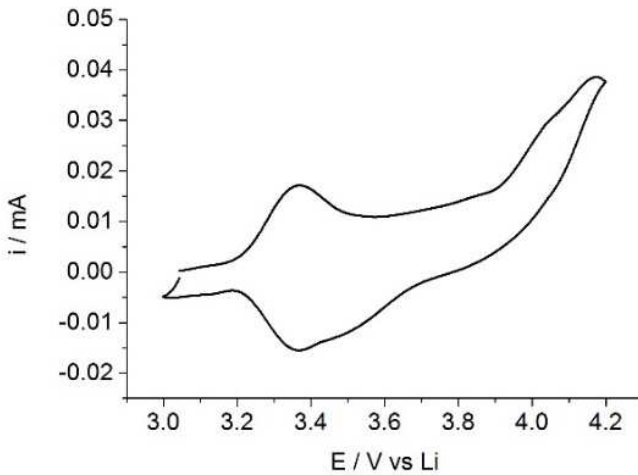


Figure 60 carbon coated IND, 0.1mV/s cyclicvoltammetry in LP30.

The cycling of the carbon coated derivative shows, Figure 60, that the material is no more responding after the carbon coating treatment.

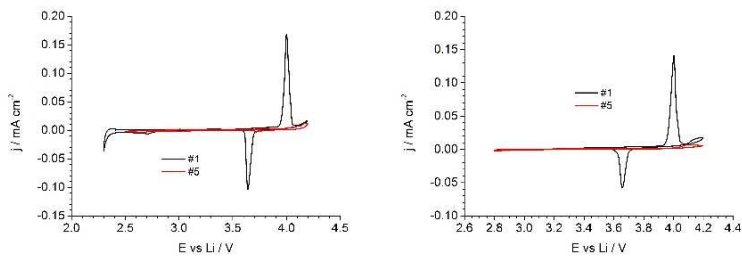


Figure 61 Silver, Left, and Silicon, Right, cladded IND, 0.1mV/s cyclicvoltammetry in LP30.

In order to protect the IND crystallites from dilution in the carbonate-based electrolyte when cycled, a self-assembling cladding approach was proposed as well. The IND powder was dispersed in a suitable media and then the corresponding Silver or Silicon precursor, namely an oxide, was added to the colloidal mixture. It is supposed that, because of the higher redox potential of the cladding precursor, the oxides would tend to be spontaneously reduced to the corresponding metals at the surface of the pigment crystallites, oxidizing it. This approach was tried but no evidence of the success of it are available. However, the produced materials were processed in electrodes and tested in a cell. In Figure 61, the results are reported but no improvements, respect to the bare IND, are visible in terms of cycling stability. However, the cladding procedure improved the shape of the voltammetry and single sharp peak is now present. Nevertheless, it has to be noticed the shift at higher potential of the oxidation peak, 4.1V, suggesting that maybe a sort of protecting layer covers the crystallites increasing the reaction overpotentials.

Quinacridone Pigments

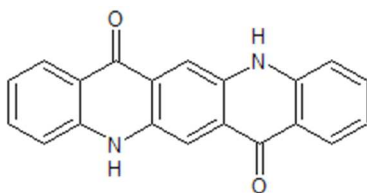


Figure 62 Quinacridone “Violet 19” structure, Mw 312g/mol. It is a purplish powder.

The quinacridone structure is a linear system of five annellated rings. These pigments perform largely like phthalocyanine pigments. Outstanding light- and weatherfastness, resistance to solvents and migration resistance justify the somewhat higher market price in

applications for high-grade industrial coatings, such as automotive finishes, for plastics, and special printing inks. Unsubstituted QA pigments are commercially available in a reddish violet beta and a red gamma crystal modification. One of the more important substituted pigments is the 2,9-dimethyl derivative, which affords a clean bluish red shade in combination with excellent fastness properties. The basic molecule is “Violet 19” and it is in the form of purplish fine particles.

QA is more appealing compared to IND because of the lower molecular weight and hence the higher theoretical capacity: 85mAh/g related to the reversible oxidation of one imide and 170mAh/g from the reversible reduction of the two carbonyls.

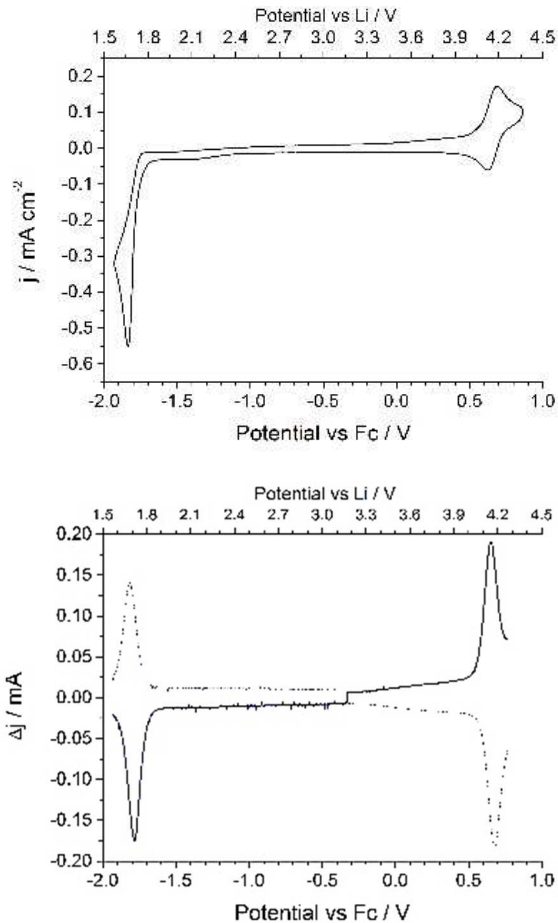


Figure 63 Left: 50mV/s cyclic voltammetry of the soluble derivative of quinacridone. Right: 20mV/s DPV analysis. WE is a GC pin and the electrolyte of choice in LiClO_4 0.1M CH_2Cl_2 :MeCN 1:1v.

Figure 63 shows the electrochemical performance of the soluble derivative of the QA pigment. It is clear from both CV and DPV that

QA is reversibly oxidized and reduced in a Li-based electrolyte. The redox potentials are impressive as well: 4.2V cathodic and 1.7V anodic. Moreover, the polarization is small for both processes.

Translating such performance in solid state opens to the possibility of building a symmetric QA-QA battery with a nominal potential of 2.5V, fast kinetic, good efficiency and low need of material. As a matter of fact Ox:Red reactions have 1:2 electrons ratio, thus only half of the material needed at the cathode must be used at the anode side. Nevertheless, because of the high anodic potential of 1.7V, Al current collector can be used saving weight and costs. Moreover, such a battery would be cheap too.

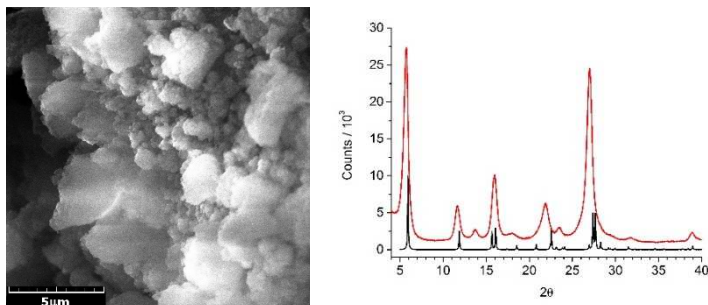


Figure 64 SEM image, Left, of the commercial QA purple powder after being washed in CH_2Cl_2 and XRD, Right, thereof. Experimental data in red, while theoretical one, monoclinic C P21/c crystal structure, in black.

Figure 64. After being washed, the morphological aspect of the commercial QA powder resemble that of an amorphous packed fine powder with no preferential orientation grow of particles. However, the XRD analysis confirms that it still maintain a crystalline structure and comparing that with the database the monoclinic C P21/c space group is the one that fits better our sample. However, peaks are

shifted to higher angles (i.e. smaller cell parameters) and the 14° peak has no correspondence in theoretical data (i.e. impurity?).

Consequently, we tailored the macroscopic morphology of QA simply following different precipitation experiments in presence of different media and H-bonding compounds. In Figure 65 the self-organization of QA in presence of the 4-amminopyridine (4AP) is reported. Other template used were 2-amminopyridine (2AP), diketopyrrolepyrrole (DPP) and benzylalcohol (BA).

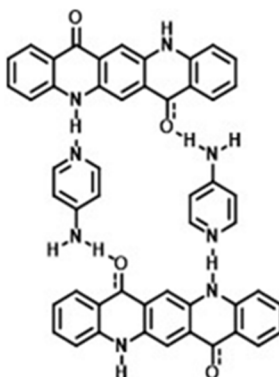


Figure 65 Self-assembled quinacridone/4aminopyridine supramolecular structure.

2AP, 4AP, DPP and BA, like others, can form H-bonding with other molecules as shown in Figure 65. Once the supramolecular structure is formed, the supporting media can be removed. In this step, the main molecule can reorganize its solid-state packing forming new macrostructure and thus new morphologies. The H-bonding agent is then removed from the structure with the help of the proper solvent. During this latter phase, some changes can happen too.

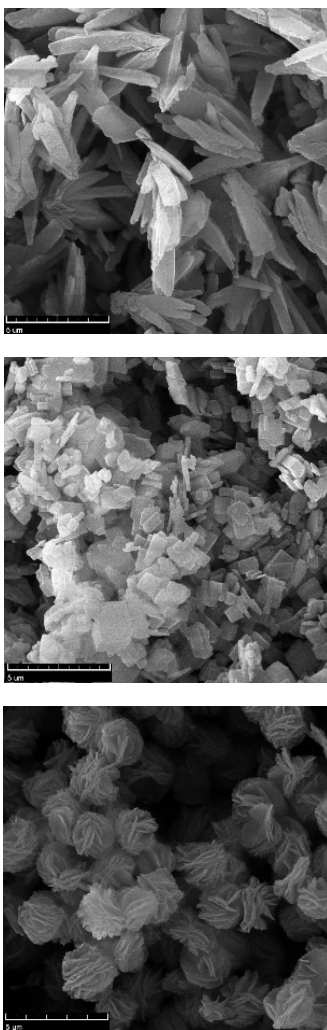


Figure 66 SEM images of three different morphologies of the QA after riprecipitation with, from top to bottom: 2-amminopyridine (QA-2AP), diketopyrrolepyrrole (QA-DPP) or benzylalcohol (QA-BA) and 4-amminopyridine (4AP). Scale is 5 μ m.

Figure 66 shows the diverse possibilities in shaping the morphology of pigments simply using riprecipitation techniques. In pigments application this is a well-known technique to tune finely the color (i.e. altering micro/nano morphology changes the light/matter interaction at the surface). 2AP gives elongated needles, while using BA as solvents or DPP as H-bonding agent bring to squared shape micro-tiles and 4AP creates what we have named “Desert Rose” morphology. Among the available one, the latter was the one we decided to use in the electrochemical characterization because of the high surface area and low density.

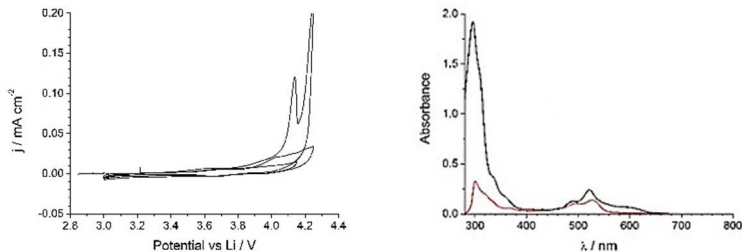


Figure 67 Left: 0.1mV/s cyclicvoltammetry of solid state QA electrodes cycled in LP30. Right: UV-Vis spectrum of soluble (in black), in dichloromethane, and insoluble (in red), in LP30, QA moieties.

Despite all the promising expectations, the preliminary electrochemical characterization returned bad results. The CV in Figure 67 shows that an oxidative peak appears at 4.1V and then an irreversible tail, due to the electrolyte decomposition, happens as well. However, in the reverse scan no charge is exchanged meaning that an important irreversible side-reaction take place during oxidation.

To tackle this issue, as for IND pigment, different approaches have been tried as well. Protecting the imide nitrogen with a propyl substituent as well as carbon coating claddings did not work out.

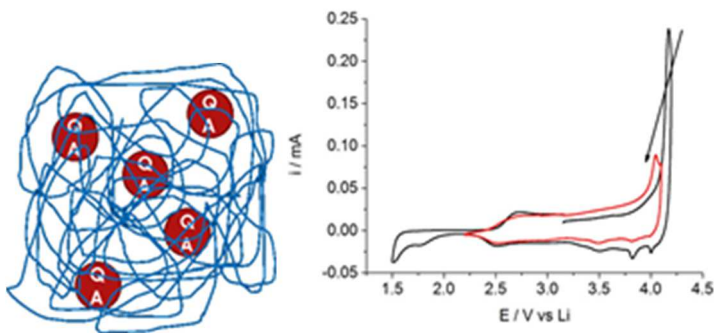


Figure 68 The “meatball spaghetti” approach sketch, Left, and cyclic voltammetry, Right.

Therefore, we decided to disperse the QA moiety in an electroconductive polymer such as pEDOT in order to avoid any hindrance and favoring ion diffusion in the bulky electrode. Hence, EDOT monomer was chemically polymerized in a solution containing dispersed QA. The obtained material was processed as a bulky electrode and then electrochemically analyzed. The CV in Figure 68 presents the standard p-doping electrochemistry of the pEDOT material followed at higher potential by an oxidative peak at 4.1V. The latter potential is compatible with the expected QA one but except for two low current peaks at 4.0V and 3.8V, no signals are recorded in reduction. After 10 cycles, the oxidative peak at 4.1V lowers (black arrow) meaning that a better stability of the system is achieved.

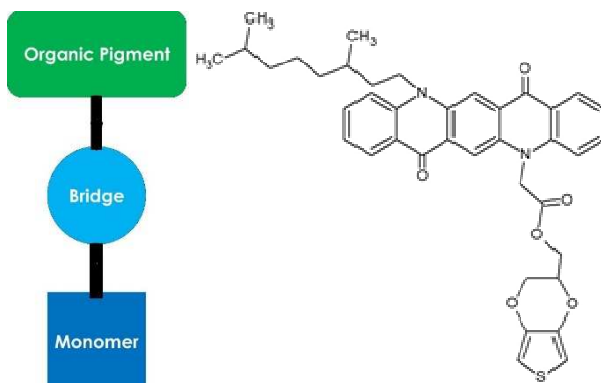


Figure 69 The polymerogenic approach idea and the QA derived molecule of choice.

In order to focus on the stabilization of the QA electrochemistry, we decided to explore the polymerogenic approach to bond chemically the pigment molecule to the polymer backbone. In Figure 69, the polymerogenic QA is reported. This approach has no practical application because the M_w of the molecule is too high, 682g/mol, lowering the theoretical specific capacity at the value of 86mAh/g (the 0.3-0.4 e^- from the pEDOT backbone must be taken into account). To minimize this loss of performance a very small and light bridge has been chosen.

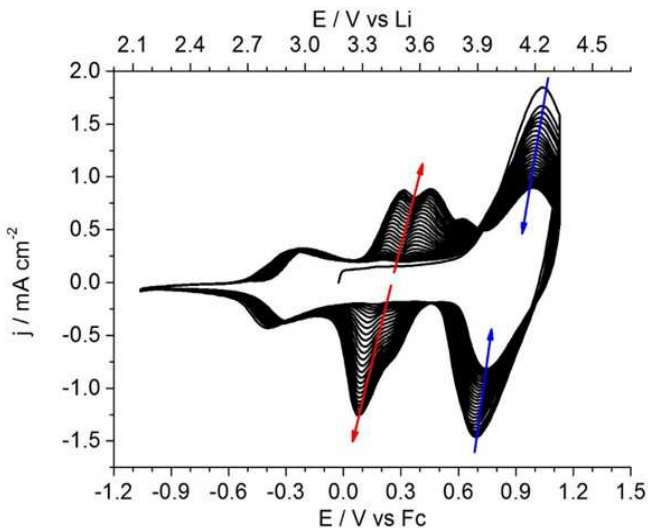


Figure 70 1mV/s cyclic voltammetry of an electrochemically polymerized pEDOT-QA sample in LiClO_4 0.1M MeCN. The arrows indicate the evolution of the peaks.

The obtained material was diluted in LiClO_4 0.1M CH_2Cl_2 :MeCN electrolyte and then electropolymerized by the mean of different techniques such as CV, GS and GP. The obtained thin film layers were then transferred and tested in a monomer free electrolyte, LiClO_4 0.1M MeCN.

Figure 70 shows that atop of the pEDOT electrochemistry the QA one is clearly visible. Moreover it takes place at the expected potential and it is somehow reversible. However, one unknown side reaction take place. The QA signal fades upon cycling while an intermediate one, respect the pEDOT and QA ones, appears. The nature of this new peak is unclear and can be ascribed to either QA-QA dimerization or QA-pEDOT coupling.

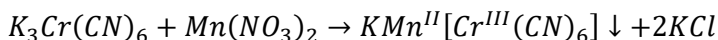
Pigments – Prussian Blue Analogues

Among all the different combinations of transition metals in the II or III valence state, we decided to focus our attention on the best combination to achieve the optimum PBAs based negative electrode. In fact, there are several options at the cathode side but not as much on the anode one.

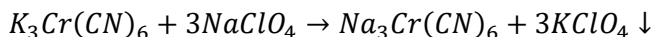
We have synthesized two chromium analogues: the manganese hexacyanochromate $KMn^{II}[Cr^{III}(CN)_6]$, MnHCCr, and its symmetric analogous chromium hexacyanochromate $KCr^{II}[Cr^{III}(CN)_6]$, CrHCCr .

Manganese Hexacyanochromate – MnHCCr

MnHCCr was synthesized by co-precipitation of a 0.269mM Mn(II)-based solution into the same volume of 0.154M $K_3[Cr(CN)_6]$ at 30 °C under vigorous stirring. As solvent we used Millipore™ water purged 1h with N_2 gas, NaCl 5M and corrected to pH 6 with HCl. The reaction is the following:



To get rid of the potassium from the hexacyanate product it is possible to perform a cation exchange using a ClO_4^- or IO_4^- salt, for example:



The obtained powder was then washed several times with, slightly acidic N_2 -purged, water and once with anhydrous MeCN. It has been dried at 70 °C overnight in an oven or using a hot plate and then manually grounded in a mortar into flour-like powder.

Before performing electrochemical analysis, the material went through a series of tests.

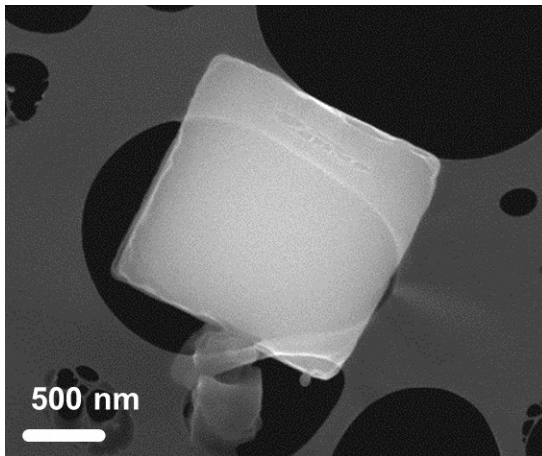
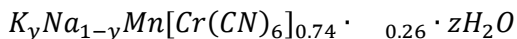


Figure 71 SEM image of a single cubic particle of MnHCCr.

SEM was performed and it has been possible to identify some single crystal cubic particles, Figure 71. The shape is extremely regular and the edge length is between 500nm and 1500nm, depending on the crystallite. At the same time, EDX composition analysis was done and the relative abundance of the searched elements was calculated by the software. Considering unitary the N-coordinated metal, Mn in this case, the chemical composition of the MnHCCr is:



zH_2O is the coordinated water and \square the vacancies in the structure. Therefore, it is clear that one fourth of the cyanide complexes is missing and, thus, the specific capacity cannot exceed 75% of the theoretical one. There are several techniques to improve this aspect:

- Synthesize the “full” (of cation) II/II compound
- Work in high concentration of cation salt (e.g. NaCl 5M)

- Slowing down the reaction speed

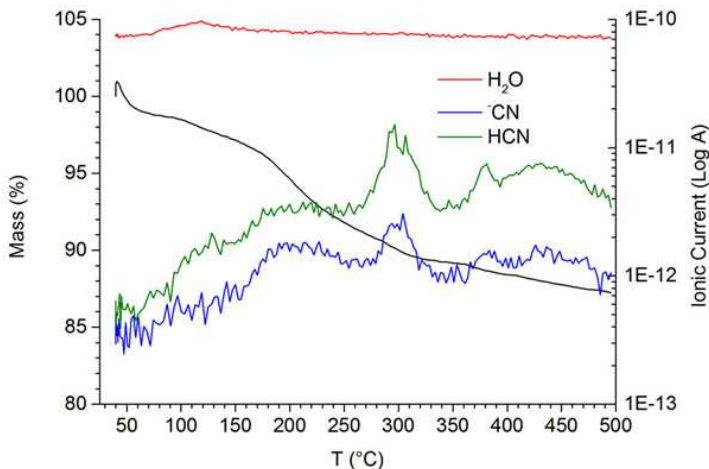


Figure 72 TGA-MS analysis of MnHCCr. As only a 15% loss is recorded, the material seems to be stable in air up to 500 °C.

In figure 72 TGA-MS shows the thermal stability of the MnHCCr compound. Only 15% of the initial mass is lost when heated to 500 °C in Ar. At 130 °C water, probably the coordinated one, leaves the material and less than 5% of the material is lost. Exceeding 200°C, the MS ionic current of ⁻CN and HCN increases and 10% of the weight is lost. I believe that this loss is not coming from the thermal decomposition of the compound, but from some unreacted reagents or not completed unit cells.

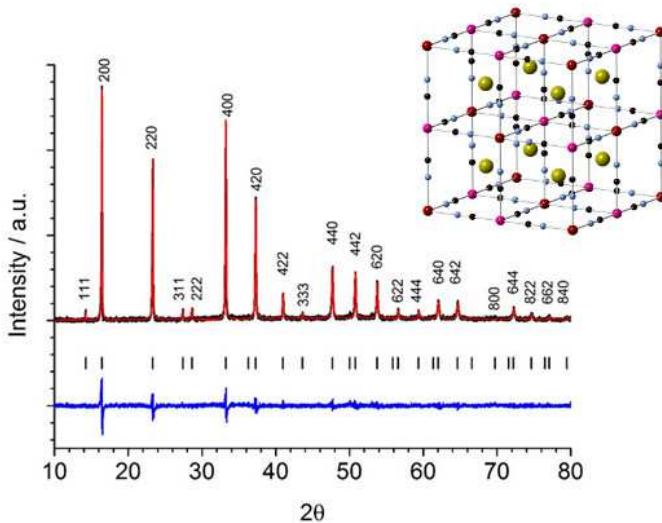


Figure 73 XRD of MnHCCr compound. The experimental data, in Black, fits well the theoretical one, in Red. The calculated crystal structure correspond to the cubic $m-3m$ space group and the unit cell parameter is 10.76\AA . In the inset is reported the crystal structure model: black Cr, light blue N, pink Cr, bordeaux Mn and lime Na.

XRD analysis of MnHCCr, Figure 73, confirms the cubic structure typical of this class of materials. The space group is $m-3m$ and the unit cell parameter is 10.76\AA . During fitting, monoclinic crystal systems having cell parameters close to a slightly distorted cube, $\beta > 90$ and $c > a = b$, was fitting the experimental data as well.

The ionic conductivity has been evaluated as well using a special two electrodes cell filled with 10mg of materials and then kept under a pressure of 0.5GPa (1t weight force over 0.785cm^2). As the material cannot be sintered and no binders are preferred in conductivity evaluation. The cell is designed to stand high pressure, up to 1GPa,

and airtight. The impedance spectroscopy analysis has been performed in the 1MHz-1Hz range with an amplitude of 20mV.

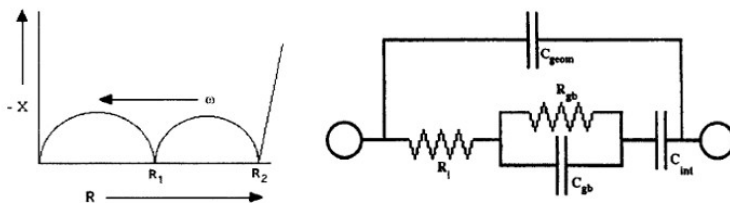


Figure 74 “Internal transverse interface impedance as well as partial electronic conduction” theoretical Nyquist plot, Left, and circuit, Right. $R_1=R_{gb}$ ¹¹⁶.

The proposed equivalent circuit is the one proposed by B. Huggins and called “Internal transverse interface impedance as well as partial electronic conduction” as described in Figure 74¹¹⁶. If the electronic conductivity is too high, the straight slope at low frequencies turns into a third semicircle and the equivalent circuit is modified adding a resistance R_c in parallel to the other two branches of the circuit described in Figure 74.

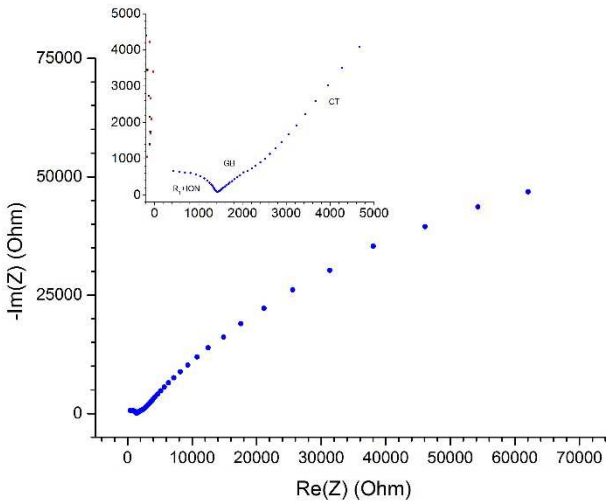


Figure 75 MnHCCr 1MHz-1Hz EIS at 0.5GPa of applied pressure. The inset enlighten the contacts and electrolyte resistance R_{EL} , as well as the ionic ION, grain boundary GB and charge transfer CT contributes.

The first semicircle in Figure 75 is the one related to the ionic conductivity of the material and it can be easily fitted using a $R_{EL}(R_1C_{geom})$ equivalent circuit. The R_1 value is the one used to calculate the conductivity σ :

$$\sigma = R_1 l / A$$

With R_1 the fitted resistance, l , the pellet thickness and A the pellet area. The calculated value for this material is $9.6 \cdot 10^{-5} \Omega/\text{cm}$. If conductivity, composition and other structural parameters are known, it is possible to calculate the Diffusion coefficient D , Figure 76.

Cell parameter a :	10.50	Angstrom
Na ions per formula unit :	1.80	#
Ionic conductivity :	2.70E-03	S/m
Ionic charge number z:	1	#
Temperature :	298	K
RT/z^2F^2 :	3.57E-04	mol/sS
Vcell :	1.16E-27	m ³
Number of cells :	8.64E+26	cells/m ³
Number of Na ions :	1.24E+28	Na/m ³
Moles of Na ions :	2.07E+04	mol/m ³
Molar conductivity :	1.31E-07	Sm ² /mol
Diffusion coefficient :	4.67E-07	cm ² /s

Figure 76 Example of diffusion coefficient calculation knowing the conductivity, composition and structure of the given material.

The material has been processed as described in Chapter 3, but because of the small amount, the mortar route was preferred. carbon cloth was the WE of choice and to make it hydrophilic it has been treated with 1M nitric acid overnight. The electrodes were then cycled in aqueous electrolytes.

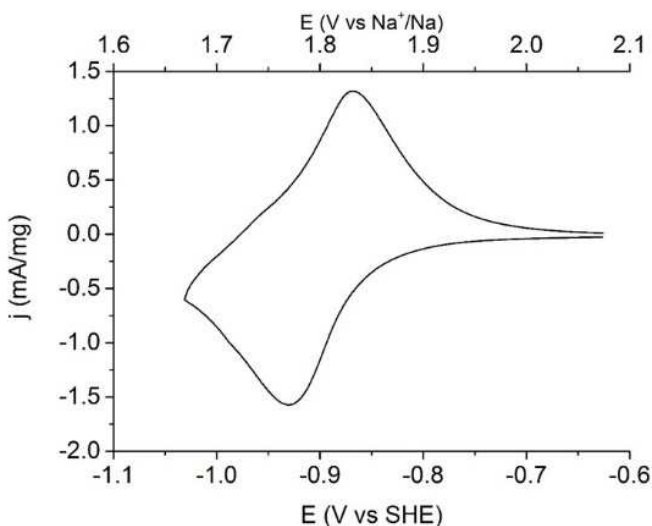
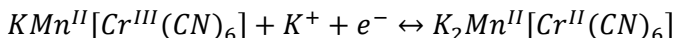


Figure 77 1mV/s cyclic voltammetry. 1st cycle of MnHCCr carbon cloth electrode in aqueous 8M NaClO₄.

The CV in Figure 77 shows the reversible intercalation reaction of sodium in the crystal structure. The redox reaction is the following:



It must be noticed the very low potential at which the reaction occurs, -0.9V vs SHE, that is much less than the thermodynamic stability of water at pH 7, -419mV vs SHE. Consequently, the following cycles show irreversibility probably due to the loss of electronic contact between the material and the current collector as consequence of hydrogen evolution (i.e. bubbles).

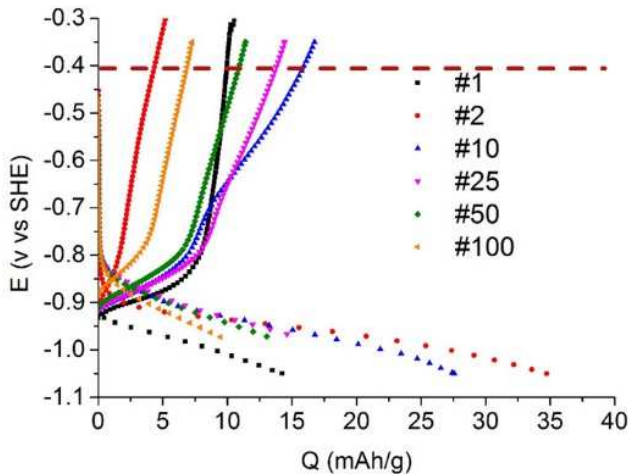


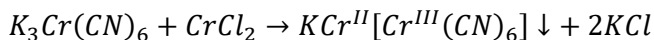
Figure 78 MnHCCr GCPL cycling 100 times at 1C rate. The dotted red line represent the cathodic thermodynamic stability of water at pH 7.

GCPL analysis, Figure 78, confirms the irreversible behavior of the hexacyanate material when cycled in water.

By any mean, water cannot be stabilized to this very low potential¹¹⁷. Increasing the pH can help but at alkali pH the PBAs structure decomposes. So, the only solution is increasing the reduction potential of the anode material choosing the proper N-coordinate metal.

Chromium hexacyanochromate - CrHCCr

CrHCCr was synthesized by co-precipitation of a 0.269mM Mn(II)-based solution into the same volume of 0.154M $K_3[Cr(CN)_6]$ at 30 °C under vigorous stirring. As solvent we used Millipore™ water purged 1h with N_2 gas, NaCl 5M and corrected to pH 4 with HCl. The reaction is the following:



The need of working at this low pH is because Cr(II) salts are not stable in water and tend to oxidize to Cr(III) and acidic conditions stabilize the reduced valence state.

The material has been processed similarly to the manganese derivative described previously and preliminarily analyzed before being electrochemically tested.

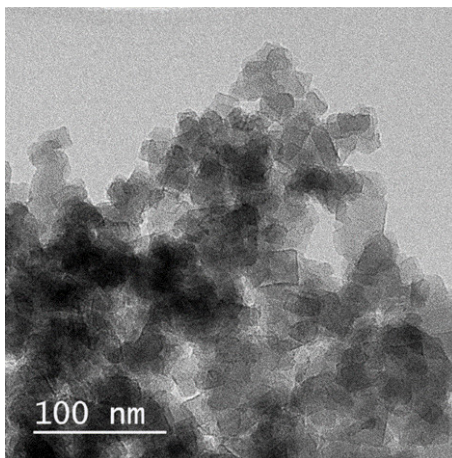


Figure 79 TEM image of CrHCCr. The cubic particles are as small as few tens of nanometers each.

In Figure 79 is presented the TEM image of CrHCCr. It is clear from the picture that particles are small cubes and their dimension, few tens of nanometers, are even distributed through the sample. EDX compositional analysis has been performed as well, but, being impossible recognized with this technique the C- and N-coordinated chromium, the chemical formula and the number of vacancies cannot be guessed.

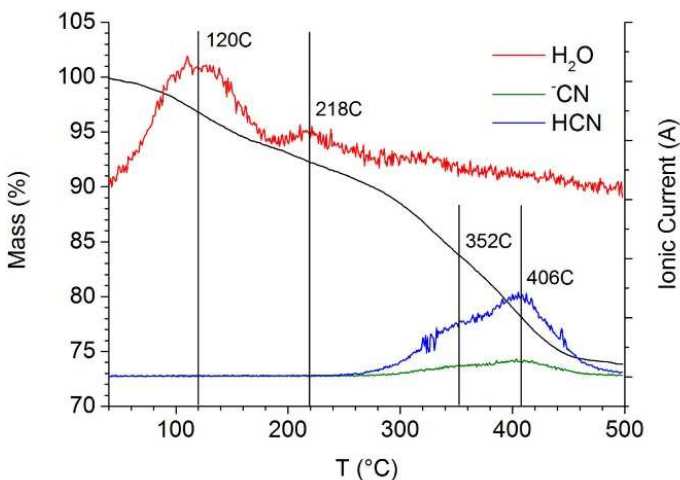
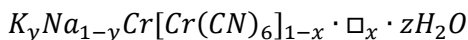


Figure 80 TGA-MS analysis of CrHCCr. The material loses 25% of the initial weight when heated to 500 °C. The mass spectrometer link the loss to the elimination of adsorbed and zeolitic water and decomposition of cyanide compounds.

TGA, Figure 80, shows that CrHCCr loses both water, 10%, and cyanides, 15%. From MS signals, it is possible to recognized at least two types of water in the material: the physically adsorbed, at 120 °C,

and the zeolitic coordinated in the structure, at 218 °C. While cyanides decomposes from 250 °C.

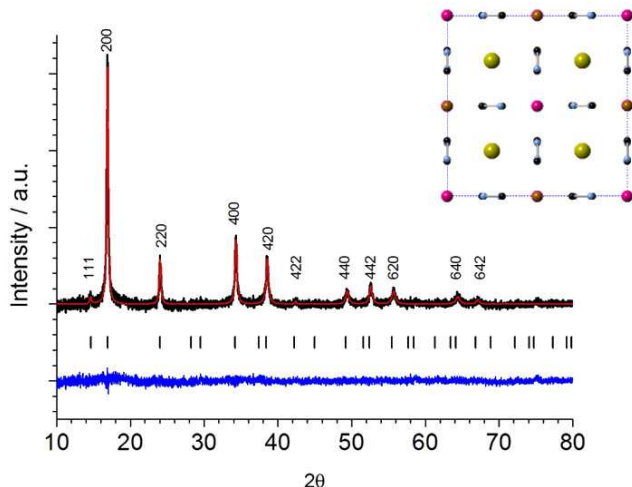


Figure 81 CrHCCr XRD analysis. The experimental data, in black, fits the theoretical one, in Red. The material possesses a cubic $m\bar{3}m$ crystal structure with cell parameter $a = 10.41\text{\AA}$

In Figure 81 the XRD structural analysis is reported. Similarly to MnHCCr, CrHCCr has a FCC $m\bar{3}m$ cubic structure with the cell parameter corresponding to $a = 10.41\text{\AA}$ and the diffractogram can be fitted with a slightly distorted cubic structure as well. This distortion is common in PBAs, in fact the III/III “empty” compound is perfectly cubic and starts to modify its structure while the material is reduced to III/II, half occupied, and eventually II/II, fully occupied.

The powder has been processed into an ink, deposited on carbon cloths current collectors and then cycled in NaClO_4 8M aqueous electrolyte.

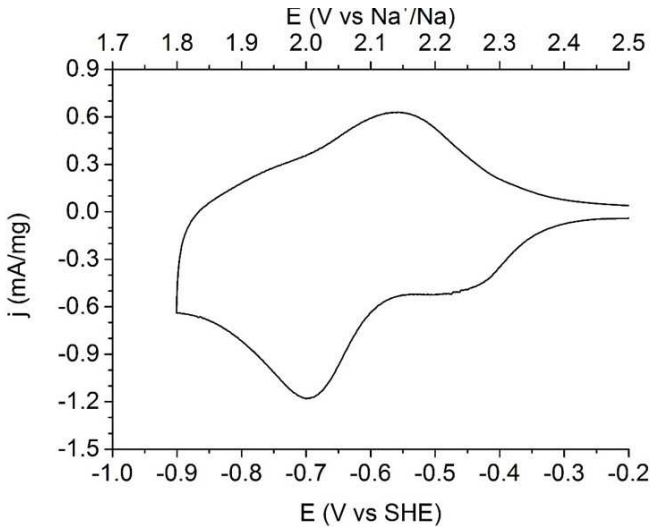


Figure 82 CrHCCr 1mV/s cyclic voltammetry of a carbon cloth electrode cycled in NaClO_4 8M aqueous electrolyte.

The CV in Figure 82 shows the behavior of CrHCCr cycled in aqueous electrolyte. It is clear from the picture that we succeeded in moving the reaction at higher potential, in fact now the redox potential is something like 250mV towards more positive potential. This results is promising but not enough for being out of the hydrogen evolution zone, -0.4V vs SHE at pH 7. Following cycles show high irreversibility and the current signal rapidly fades away.

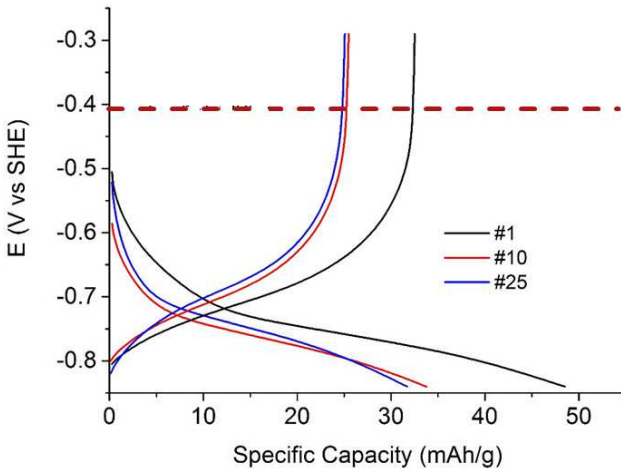


Figure 83 CrHCr GCPL analysis at 1C in NaClO_4 8M H_2O . The red line represents the stability of water.

Even though, the reversibility and stability of the electrode material is better compared to the manganese analogue but a lot of charge is still lost upon cycling and only one third of the expected theoretical value is moved in and out from the material. The reaction potential lies somewhere in the $-0.8 \div -0.7\text{V}$ vs SHE range.

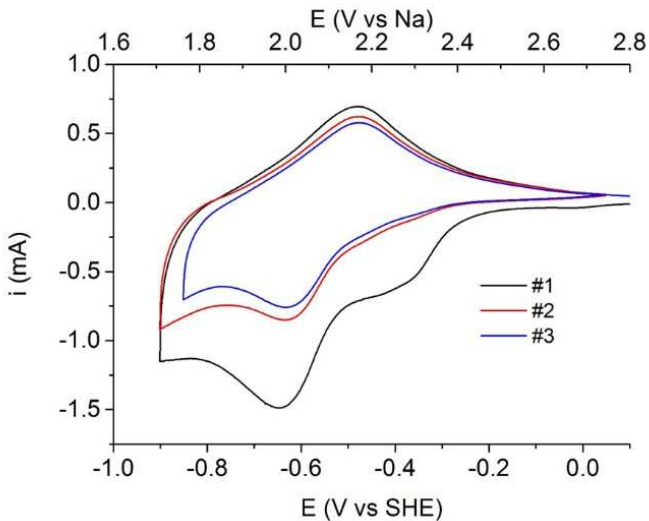


Figure 84 CrHCCr deposited on glassy carbon bulk working electrode. The cyclic voltammetry is performed at 1mV/s and the material is run in NaClO₄ 8M H₂O.

As graphitic carbon cloth is electroactive in H₂ evolution, we casted some slurry material atop of a piece of bulky glassy carbon that is not. As expected, during the first three cycles the current signal decreased but the shape of the CV was kept, Figure 84.

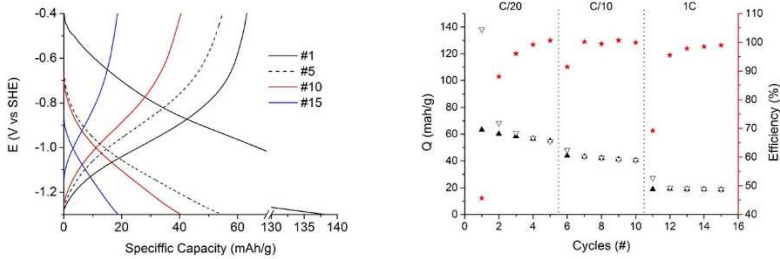
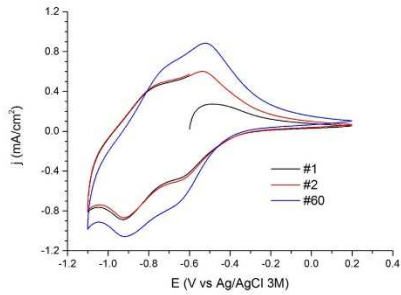
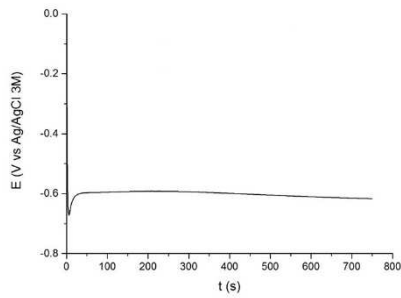


Figure 85 CrHCCr cycling in organic NaClO_4 1M PC electrolyte. Both the charge/discharge profiles and charge/efficiency plots are reported.

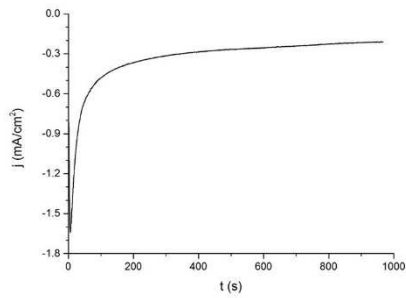
We got rid of all the water presents in the cell cycling the chromium based material in NaClO_4 1M in anhydrous PC and the outcomes are visible in Figure 85. The situation improved respect in water but some kind of water reduction is still going on. We agree with Ohkoshi et alii¹¹⁸, that coordinated zeolitic water can have a key role in the diffusion of the ionic species in the material. Moreover, we believe that zeolitic water can undergo electrochemical reaction as well. Additionally, where H_2 -evolution happens the pH can grow at values at which PBAs are not stable and the structure can decompose.



(a)



(b)



(c)

Figure 86 CrHCCr electrodeposition on carbon cloth with different techniques, from the to: (a) 50mV/s CV, (b) -13.3 μ A GS and (c) -0.7V vs Ag/AgCl 3M PS.

PBAs can be electrodeposited in situ starting from an aqueous solution of the III/III metals. In fact, the III/III derivative is the soluble one and normally does not precipitate spontaneously. Therefore, applying a negative current or potential the reduction of one of the two metals take place and the III/II material is deposited at the surface of the WE. In Figure 86, three different successful electrochemical deposition techniques, CV, GS and PS, are shown.

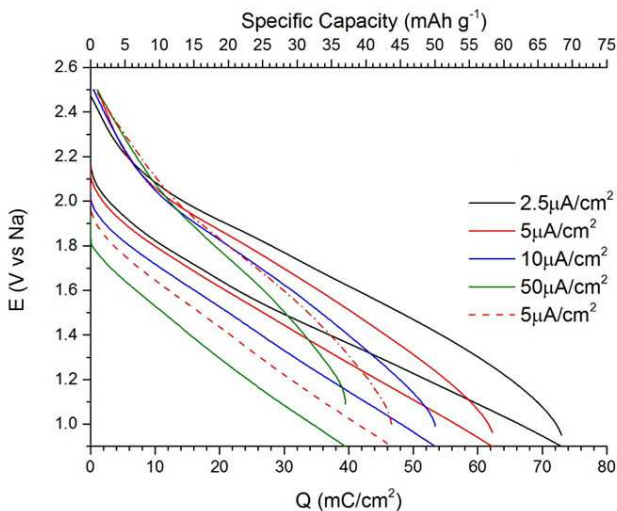


Figure 87 GCPL of CrHCCr deposited by potentiostatic mean, the charge/discharge current densities are varied every five cycles and the 5th cycle of every rate is plotted. The material is cycled in NaClO₄ 1M EC:DMC organic electrolyte.

In Figure 87 the charge/discharge behavior of the electrodeposited Cr-PBA is reported for different current density. There is not a well defined plateau and the potential varies between 2.0V and 1.2V vs Na. The reversibility, stability and charge capacity seem to be better respect to the chemical synthesized counterpart but the reader have

to keep in mind that electrodeposited material is a thin layer and not a bulky one.

Chapter 5

Conclusions and Future Work

Conclusions

The world's growing and increasing demand for energy is one of the major challenges of the 21st century. With regard to rising environmental issues, the requirements for efficient and clean power sources such as solar and wind power and, especially, the need for sustainable energy storage systems led to ongoing research to improve the existing battery techniques.

In particular, the rising market for small, thin and bendable mobile devices requires compact, lightweight and flexible battery systems. The research of an efficient, reliable and cheap system for leveling the natural fluctuation of renewable energy technology as well as the irregular surplus or deficit demand of energy is of high interest.

LIBs are for sure the best tool humanity owns to face the problem. Albeit is well known that the amount of lithium is not limitless, for sure the easy available one. Therefore, alternative technologies or materials must be pursuit.

The application of organic compounds as active materials in secondary batteries is still at the very beginning and to date no material or system has reached commercialization. Flow system based on radical compounds seems now the closest one to the shelf.

In this work, we focused our attention on organic conjugated carbonyl/imide b-type systems because they have the potential to reach both discrete energy and power densities. Moreover they are counter-ion independent, so the employment of Li is not compulsory. In particular, we concentrated our efforts on a precise family of organic compounds, the pigments. Pigments are a special class of carbonyl materials normally employed in the paints and varnishes

market. Their key point are that, by definition, they are insoluble, possess a crystal structure and they are extremely cheap because of the huge availability as colorants. Perylenedimide PDI, Indanthrone IND and quinacridone QA are our systems of choice.

In PDI only the n-doping process is accessible at around 2.5V while the p-doping one is out of the stability potential window of the electrolyte. The practical charge capacity is only 70mAh/g, 55% of the theoretical one, but it retain 85% of the charge after 1000 cycles and the charge efficiency at 1C is 99.5%. Moreover, preliminary test showed that being cycled in Na-based electrolyte (2V vs Na) increases the practical capacity to 90% of the theoretical one at low C-rates, although the redox processes suffer of unwanted side reaction that lower down efficiency and reversibility.

IND system showed an interesting p-doping redox process at 3.9V but the high M_w lower down the theoretical specific capacity to 60mAh/g in oxidation. Moreover early electrochemical tests showed severe problems due to both side reactions and solubility of the oxidized molecule. Different approaches have been pursuit, i.e. carbon coating and Ag or Si cladding, but none of them turned out to be successful.

QA is, at least the soluble derivative, a perfect b-type material that oxidized at 4.1V and reduces at 1.6V. The lower M_w , 312 g/mol, gives a theoretical value of 85mAh/g and 170mAh/g in oxidation and reduction, respectively. Thus, in principle, QA can be employed in a 2.5V symmetric battery. Unfortunately, quinacridone showed similar issues as IND but, because of the easier chemistry, we decided to face the problem differently. QA has been embedded firstly in a polymer pEDOT matrix and then a polymerogenic precursor was synthesized.

However, even though the two approaches partially limited the solubility, none of them improved the cyclability and reversibility of the p-doping process.

Prussian Blue Analogues is another class of pigments and, because the similarities to MOFs, their organic-inorganic classification is still debated. PB is used in paints, cell staining, metal filtration, electrochromism and, recently, energy storage. The main advantages of PBAs are: facile chemistry, tunability, cycling stability and open framework. In this work, we decide to find new low potential redox systems to be applied as anode in a full PBAs aqueous battery.

MnHCCr and CrHCCr have been synthesized and fully characterized. Both share a cubic morphology with $0.5\div 1.5\mu\text{m}$ edges and their crystal structure corresponds to the cubic $m\bar{3}m$ space group with a little distorted $\beta > 90$ and $c > a = b$ cell parameters. The calculated cell parameter is 10.76\AA and 10.71\AA for the Mn and Cr analogues, respectively. The practical capacity in both cases is not stellar because of the high content, 25%, of vacancies in the structure (i.e. theoretical 90mAh/g and practical $< 60\text{mAh/g}$ at 1st cycle). Unfortunately the redox potential of both materials, -0.9V the Mn and -0.7V the Cr vs SHE, is lower than the thermodynamic stability of water at pH7, -0.4V vs SHE. Hence, important irreversible processes (e.g. H_2 -evolution) fade the capacity down to zero in few cycles. Cycling them in organic electrolyte improved the cycling performance but did not solve the problem. We believe that working at that low potential decomposes the zeolitic coordinated water inside the structure as well and this water is supposed to be involved in the cation diffusion through the structure.

Outlook

Although it is forty years since first works on electroconductive polymers and small molecules, the interest and efforts in organic compounds has to be considered at its early stages. The number of pigments available on the market or simply published is in the order of thousands of fully described organic carbonyl/imide small molecules. Hence, the scouting of suitable molecules is far to an end. In particular, as there are plenty of option at the n-doping side, we think efforts must be focused on new p-doping systems with low M_w , high oxidation potential and cycling stability. In PDI, the “activation mechanism” should be studied and addressed and its cyclability in sodium should be optimized finding a suitable electrolyte. QA and IND needs an effective morphological, compositional or chemical approach to avoid the dissolution of the material in the liquid electrolyte. The polymerogenic way is slightly effective but, because of the increase in weight, the capacity is low. However, in polymerogenic quinacridone the unwanted coupling reactions, QA-QA or QA-pEDOT, must be investigated further.

PBAs are nowadays a hot topic and their use in real application is not far away. However, the goal of a full PBAs aqueous battery is far to be realized because of the lack of low potential, hence high energy, anode material. As it is not possible to lower the water thermodynamic stability down to the MnHCCr and CrHCCr compounds reduction potential, the research of a chromate-based PBAs alternative with a redox potential of -0.4V vs SHE is needed. Moreover the role of zeolitic coordinated water inside the structure should be fully addressed, specially in anodic PBAs. In fact Goodenough asserts that cathodic materials gets benefits from water removal¹¹⁹, while our outcomes on the negative side are the

opposite. We think that a deep evaluation of the mobility of interstitial water as well ions by the mean of NMR PFG (Pulsed Field Gradient) ¹²⁰ solid state techniques could help in finding an answer.

Annex

Bibliography

1. Huggins, R. A. *Energy Storage*. (Springer US, 2010). doi:10.1007/978-1-4419-1024-0
2. EIA. Primary Energy Consumption. (2012). Available at: https://www.eia.gov/totalenergy/data/annual/pecss_diagram.php.
3. Eurostat. Energy production and imports. (2016). Available at: http://ec.europa.eu/eurostat/statistics-explained/index.php/Energy_production_and_imports.
4. Kostková, K., Omelina, L., Kyčina, P. & Jamrich, P. An introduction to load management. *Electr. Power Syst. Res.* **95**, 184–191 (2013).
5. University of Michigan. Energy Institute. Available at: <http://energy.umich.edu/>.
6. The Economist. Packing some power. (2012).
7. Harby, A. *et al.* in *Transition to Renewable Energy Systems* 597–618 (Wiley-VCH Verlag GmbH & Co. KGaA, 2013). doi:10.1002/9783527673872.ch29
8. Wang, C. *et al.* C-MEMS for the Manufacture of 3D Microbatteries. *Electrochem. Solid-State Lett.* **7**, A435 (2004).
9. W. R. Salzman. Electrical Work and the Nernst Equation. (2006). Available at: <http://cbc.arizona.edu/~salzmanr/480a/480ants/elecwork/elecwork.html>. (Accessed: 24th February 2017)
10. Atkins, P. W. *Physical Chemistry*. (Oxford University Press, 1978).

11. Rosciano, F. In Situ Synchrotron and Neutron Diffraction Based Methods for the Characterization of Cathodic Materials for Lithium-Ion Batteries. (ETH, Zurich, 2008).
12. Frood, A. Riddle of Baghdad's batteries. (2003).
13. Winter, M. & Brodd*, R. J. What Are Batteries, Fuel Cells, and Supercapacitors? (2004). doi:10.1021/CR020730K
14. Wikipedia. Voltaic Pile. Available at: https://en.wikipedia.org/wiki/Voltaic_pile#/media/File:Voltaic_pile.svg.
15. Groove, W. Philosophical Magazine and Journal of Science. *RCS Meet. Proc.* 272 (1843).
16. Howard, B. Low voltage electrolytic capacitor. (1954).
17. Meng, C., Gall, O. Z. & Irazoqui, P. P. A flexible supercapacitive solid-state power supply for miniature implantable medical devices. *Biomed. Microdevices* **15**, 973–983 (2013).
18. Wikipedia. Daniell Cell. Available at: https://en.wikipedia.org/wiki/Galvanic_cell#/media/File:Galvanic_cell_with_no_cation_flow.png.
19. Duffy, S. J. & others. *Environmental chemistry: a global perspective*. (Oxford university press, 2011).
20. Li, Q., Chen, J., Fan, L., Kong, X. & Lu, Y. Progress in electrolytes for rechargeable Li-based batteries and beyond. *Green Energy Environ.* **1**, 18–42 (2016).
21. Roth, E. P. & Orendorff, C. J. How electrolytes influence battery safety. *Electrochem. Soc. Interface* **21**, 45–49 (2012).

-
22. Chen, R. *et al.* The pursuit of solid-state electrolytes for lithium batteries: from comprehensive insight to emerging horizons. *Mater. Horiz.* **3**, 487–516 (2016).
 23. Electropaedia. Energy densities of different battery types. Available at: <http://www.mpoweruk.com/>.
 24. Robert A. Huggins. *Advanced Batteries*. (Springer US, 2009). doi:10.1007/978-0-387-76424-5
 25. Luntz, A. C. & McCloskey, B. D. Nonaqueous Li–Air Batteries: A Status Report. *Chem. Rev.* **114**, 11721–11750 (2014).
 26. Manthiram, A., Fu, Y., Chung, S.-H., Zu, C. & Su, Y.-S. Rechargeable Lithium–Sulfur Batteries. *Chem. Rev.* **114**, 11751–11787 (2014).
 27. Linden, D. Handbook of batteries. *Fuel Energy Abstr.* **4**, 265 (1995).
 28. VARTA. *Primary battery handbook - LiMnOx*.
 29. WHITTINGHAM, M. S. Electrical Energy Storage and Intercalation Chemistry. *Science (80-)*. **192**, (1976).
 30. Rechargeable battery. (1980).
 31. Ozawa, K. Lithium-ion rechargeable batteries with LiCoO₂ and carbon electrodes: the LiCoO₂/C system. *Solid State Ionics* **69**, 212–221 (1994).
 32. Brissot, C., Rosso, M., Chazalviel, J.-N., Baudry, P. & Lascaud, S. In situ study of dendritic growth in lithium/PEO-salt/lithium cells. *Electrochim. Acta* **43**, 1569–1574 (1998).
 33. Balbuena, P. B. & Wang, Y. *Lithium-Ion Batteries: Solid-*
-

- Electrolyte Interphase*. (2004).
34. Dey, A. N. & Sullivan, B. P. The Electrochemical Decomposition of Propylene Carbonate on Graphite. *J. Electrochem. Soc.* **117**, 222 (1970).
 35. Wang, J., Manga, K. K., Bao, Q. & Loh, K. P. High-Yield Synthesis of Few-Layer Graphene Flakes through Electrochemical Expansion of Graphite in Propylene Carbonate Electrolyte. *J. Am. Chem. Soc.* **133**, 8888–8891 (2011).
 36. Komaba, S. *et al.* Polyacrylate Modifier for Graphite Anode of Lithium-Ion Batteries. *Electrochem. Solid-State Lett.* **12**, A107 (2009).
 37. Ohzuku, T., Ueda, A. & Yamamoto, N. Zero-Strain Insertion Material of $\text{Li}[\text{Li}_{1/3}\text{Ti}_{5/3}]\text{O}_4$ for Rechargeable Lithium Cells. *J. Electrochem. Soc.* **142**, 1431 (1995).
 38. Hawkins, P. $\text{Li}_4\text{Ti}_5\text{O}_{12}$ crystal structure. (2014). Available at: <http://www.iycr2014.org/learn/crystallography365/articles/20140131>.
 39. Huggins, R. A. & Nix, W. D. Decepritation model for capacity loss during cycling of alloys in rechargeable electrochemical systems. *Ionics (Kiel)*. **6**, 57–63 (2000).
 40. Liu, N. *et al.* A Yolk-Shell Design for Stabilized and Scalable Li-Ion Battery Alloy Anodes. *Nano Lett.* **12**, 3315–3321 (2012).
 41. Fujifilm Photo. http://www.fujifilm.co.jp/eng/news_e/nr079.html. (1996).
 42. Yoon, Y. S., Lee, S. H., Cho, S. B. & Nam, S. C. Influence of Two-Step Heat Treatment on Sputtered Lithium Cobalt Oxide

- Thin Films. *J. Electrochem. Soc.* **158**, A1313 (2011).
43. Ohzuku, T. & Ueda, A. Solid-State Redox Reactions of LiCoO_2 (R3m) for 4 Volt Secondary Lithium Cells. *J. Electrochem. Soc.* **141**, 2972 (1994).
 44. Morales, J., Pérez-Vicente, C. & Tirado, J. L. Cation distribution and chemical deintercalation of $\text{Li}_{1-x}\text{Ni}_{1+x}\text{O}_2$. *Mater. Res. Bull.* **25**, 623–630 (1990).
 45. Delmas, C. *et al.* An overview of the $\text{Li}(\text{Ni},\text{M})\text{O}_2$ systems: syntheses, structures and properties. *Electrochim. Acta* **45**, 243–253 (1999).
 46. Liu, Z., Yu, A. & Lee, J. Y. Synthesis and characterization of $\text{LiNi}_{1-x-y}\text{Co}_x\text{Mn}_y\text{O}_2$ as the cathode materials of secondary lithium batteries. *J. Power Sources* **81**, 416–419 (1999).
 47. Ohzuku, T. & Makimura, Y. Layered Lithium Insertion Material of $\text{LiCo}_{1/3}\text{Ni}_{1/3}\text{Mn}_{1/3}\text{O}_2$ for Lithium-Ion Batteries. *Chem. Lett.* **30**, 642–643 (2001).
 48. Lu, Z. & Dahn, J. R. Understanding the Anomalous Capacity of $\text{Li}/\text{Li}[\text{Ni}_{x/3}\text{Li}_{(1/3-2x/3)}]\text{Mn}_{(2/3-x/3)}\text{O}_2$ Cells Using In Situ X-Ray Diffraction and Electrochemical Studies. *J. Electrochem. Soc.* **149**, A815 (2002).
 49. Thackeray, M. M. Manganese oxides for lithium batteries. *Prog. Solid State Chem.* **25**, 1–71 (1997).
 50. Jugović, D. & Uskoković, D. A review of recent developments in the synthesis procedures of lithium iron phosphate powders. *J. Power Sources* **190**, 538–544 (2009).
 51. Chen, J. & Whittingham, M. S. *Hydrothermal synthesis of lithium iron phosphate. Electrochemistry Communications* **8**,

- (2006).
52. Armand, M., Endres, F., MacFarlane, D. R., Ohno, H. & Scrosati, B. Ionic-liquid materials for the electrochemical challenges of the future. *Nat. Mater.* **8**, 621–9 (2009).
 53. Fergus, J. W. Ceramic and polymeric solid electrolytes for lithium-ion batteries. *J. Power Sources* **195**, 4554–4569 (2010).
 54. Sapunkov, O. *et al.* Quantifying the promise of ‘beyond’ Li-ion batteries. *Transl. Mater. Res.* **2**, 45002 (2015).
 55. Van Noorden, R. The rechargeable revolution: A better battery. *Nature* **507**, 26–28 (2014).
 56. Lee, J.-H., Ali, G., Kim, D. H. & Chung, K. Y. Metal-Organic Framework Cathodes Based on a Vanadium Hexacyanoferrate Prussian Blue Analogue for High-Performance Aqueous Rechargeable Batteries. *Adv. Energy Mater.* 1601491 (2016). doi:10.1002/aenm.201601491
 57. Barnhart, C. J. *et al.* On the importance of reducing the energetic and material demands of electrical energy storage. *Energy Environ. Sci.* **6**, 1083 (2013).
 58. Poizot, P. & Dolhem, F. Clean energy new deal for a sustainable world: from non-CO₂ generating energy sources to greener electrochemical storage devices. *Energy Environ. Sci.* **4**, 2003 (2011).
 59. Tarascon, J.-M. Is lithium the new gold? *Nat. Publ. Gr.* **2**, (2010).
 60. Chen, H. *et al.* From Biomass to a Renewable LiXC₆O₆ Organic Electrode for Sustainable Li-Ion Batteries.
-

ChemSusChem **1**, 348–355 (2008).

61. Azuma, H., Imoto, H., Yamada, S. & Sekai, K. Advanced carbon anode materials for lithium ion cells. *J. Power Sources* **81**, 1–7 (1999).
62. Liu, N. *et al.* Rice husks as a sustainable source of nanostructured silicon for high performance Li-ion battery anodes. *Sci. Rep.* **3**, 497–501 (2013).
63. Novák, P., Müller, K., Santhanam, K. S. V. & Haas*, O. Electrochemically Active Polymers for Rechargeable Batteries. (1997). doi:10.1021/CR941181O
64. Lowe, M. A., Kiya, Y., Henderson, J. C. & Abruña, H. D. *Pendant thioether polymer for redox capacitor cathodes. Electrochemistry Communications* **13**, (2011).
65. Liu, M., Visco, S. J. & Jonghe, L. C. De. Electrode Kinetics of Organodisulfide Cathodes for Storage Batteries. *J. Electrochem. Soc.* **137**, 750 (1990).
66. Wei, X. *et al.* TEMPO-Based Catholyte for High-Energy Density Nonaqueous Redox Flow Batteries. *Adv. Mater.* **26**, 7649–7653 (2014).
67. Häupler, B., Wild, A. & Schubert, U. S. Carbonyls: Powerful organic materials for secondary batteries. *Adv. Energy Mater.* (2015). doi:10.1002/aenm.201402034
68. *Paints and varnishes -- Vocabulary -- Part 1: General terms. Second* (1984).
69. Colors and pigments directory. Pigments. Available at: <http://colors-and-pigments.regionaldirectory.us/colors-pigments-720.jpg>.

-
70. Willy Herbst, K. H. *Industrial Organic Pigments*. (WILEY-VCH Verlag GmbH & Co. KGaA, Weinheim, 2004).
 71. Ke, F.-S., Wu, Y.-S. & Deng, H. Metal-organic frameworks for lithium ion batteries and supercapacitors. *J. Solid State Chem.* **223**, 109–121 (2015).
 72. Kraft, A. ON THE DISCOVERY AND HISTORY OF PRUSSIAN BLUE. *Bull. Hist. Chem* **33**, (2008).
 73. Vincent van Gogh. The Starry Night. (1889). Available at: https://www.moma.org/learn/moma_learning/vincent-van-gogh-the-starry-night-1889.
 74. Luo, C. *et al.* Graphene oxide wrapped croconic acid disodium salt for sodium ion battery electrodes. *J. Power Sources* **250**, 372–378 (2014).
 75. Verdejo, R. *et al.* Graphene filled polymer nanocomposites. *J. Mater. Chem.* **21**, 3301–3310 (2011).
 76. Cassatt, D. R. *et al.* Medical Countermeasures against Nuclear Threats: Radionuclide Decorporation Agents. *Radiat. Res.* **170**, 540–548 (2008).
 77. Frank, J. A. *et al.* Clinically Applicable Labeling of Mammalian and Stem Cells by Combining Superparamagnetic Iron Oxides and Transfection Agents. *Radiology* **228**, 480–487 (2003).
 78. Ellis, D., Eckhoff, M. & Neff, V. D. Electrochromism in the mixed-valence hexacyanides. 1. Voltammetric and spectral studies of the oxidation and reduction of thin films of Prussian blue. *J. Phys. Chem.* **85**, 1225–1231 (1981).
 79. Karyakin, A. A. Prussian Blue and Its Analogues: Electrochemistry and Analytical Applications.
-

80. Pasta, M. *et al.* Manganese–cobalt hexacyanoferrate cathodes for sodium-ion batteries. *J. Mater. Chem. A* **4**, 4211–4223 (2016).
 81. Lee, H.-W. *et al.* Effect of the alkali insertion ion on the electrochemical properties of nickel hexacyanoferrate electrodes. *Faraday Discuss.* **176**, 69–81 (2014).
 82. Wang, R. Y. *et al.* Reversible Multivalent (Monovalent, Divalent, Trivalent) Ion Insertion in Open Framework Materials. *Adv. Energy Mater.* **5**, 1401869 (2015).
 83. Lee, H.-W. *et al.* Manganese hexacyanomanganate open framework as a high-capacity positive electrode material for sodium-ion batteries. *Nat. Commun.* **5**, 5280 (2014).
 84. Wessells, C. D. *et al.* Tunable Reaction Potentials in Open Framework Nanoparticle Battery Electrodes for Grid-Scale Energy Storage. *ACS Nano* **6**, 1688–1694 (2012).
 85. Pasta, M. *et al.* Full open-framework batteries for stationary energy storage. *Nat. Commun.* **5**, 3577–3613 (2014).
 86. Pasta, M. *et al.* A high-rate and long cycle life aqueous electrolyte battery for grid-scale energy storage. *Nat. Commun.* **3**, 1149 (2012).
 87. Parga, J. R., Shukla, S. S. & Carrillo-Pedroza, F. R. Destruction of cyanide waste solutions using chlorine dioxide, ozone and titania sol. doi:10.1016/S0956-053X(02)00064-8
 88. Scholz, F. & Dostal, A. The Formal Potentials of Solid Metal Hexacyanometalates. *Angew. Chemie Int. Ed. English* **34**, 2685–2687 (1996).
 89. Robin, M. B. The Color and Electronic Configurations of
-

- Prussian Blue. *Inorg. Chem.* **1**, 337–342 (1962).
90. Dostal, A., Kauschka, G., Reddy, S. J. & Scholz, F. Lattice contractions and expansions accompanying the electrochemical conversions of Prussian blue and the reversible and irreversible insertion of rubidium and thallium ions. *J. Electroanal. Chem.* **406**, 155–163 (1996).
 91. Wang, Z. *et al.* Stability improvement of Prussian blue in nonacidic solutions via an electrochemical post-treatment method and the shape evolution of Prussian blue from nanospheres to nanocubes. *Analyst* **139**, 1127 (2014).
 92. You, Y. *et al.* High-quality Prussian blue crystals as superior cathode materials for room-temperature sodium-ion batteries. *Energy Environ. Sci.* **7**, 1643 (2014).
 93. NPTEL. TGA scheme. Available at: <http://nptel.ac.in/courses/103103026/module2/lec14/images/8.png>.
 94. Skoog, D., Holler, J. & Crouch, S. *Principles of Instrumental Analysis*. (Brooks/Cole, 1985).
 95. Reusch, W. Mass Spectrometry. (2013). Available at: <https://www2.chemistry.msu.edu/faculty/reusch/virttxtjml/spectrpy/massspec/masspec1.htm>.
 96. University of Nebraska-Lincoln. SEM. Available at: <http://ncmn.unl.edu/enif/images/semoptic.gif>.
 97. Harvard University. Center for Nanoscale System. Available at: <http://cns.fas.harvard.edu/TEM>.
 98. Wikiwand. EDX. Available at: http://www.wikiwand.com/en/Energy-dispersive_X-

ray_spectroscopy.

99. ETH Zurich. XRD.
100. Amatucci, G. G., Badway, F., Du Pasquier, A. & Zheng, T. An Asymmetric Hybrid Nonaqueous Energy Storage Cell. *J. Electrochem. Soc.* **148**, A930 (2001).
101. Best Manufacturing Practice. Coin Cell. Available at: http://www.bmpcoe.org/library/books/navso_p-3676/932.html.
102. Intech. Potentiostat. Available at: <http://www.intechopen.com/source/html/43463/media/image4.png>.
103. Hamann, C. H. *Electrochemistry*. (Wiley-VCH, 2006).
104. RIBEIRO, D. V. *et al.* Use of Electrochemical Impedance Spectroscopy (EIS) to monitoring the corrosion of reinforced concrete. *Rev. IBRACON Estruturas e Mater.* **8**, 529–546 (2015).
105. FLEXIBLE TRANSPARENT ELECTROCHROMIC DEVICE, AND A METHOD FOR THE PREPARATION THEREOF.
106. Salamone, M. M. STUDIO DELLE PROPRIETÀ OTTICHE, ELETTRICHE ED ELETTOCHIMICHE DI DERIVATI POLITIOFENICI. (Università degli studi di Milano Bicocca, 2008).
107. Rosciano, F. *et al.* High Voltage Organic Materials for Energy Storage Applications. (2013).
108. Sassi, M. *et al.* Gray to colorless switching, crosslinked electrochromic polymers with outstanding stability and

- transmissivity from naphthalenediimide-functionalized EDOT. *Adv. Mater.* **24**, 2004–2008 (2012).
109. Salamone, M. M., Sassi, M., Beverina, L., Mari, C. M. & Ruffo, R. Investigation of redox activity in the naphthalenediimide-poly(3,4-ethylenedioxythiophene) cross-linked polymers. *Electrochim. Acta* **140**, 152–159 (2014).
 110. Rosciano, F., Salamone, M. M., Ruffo, R., Sassi, M. & Beverina, L. Crosslinked Electroactive Polymers Containing Naphthalene-Bisimide Redox Centers for Energy Storage. *J. Electrochem. Soc.* **160**, A1094–A1098 (2013).
 111. Rosciano, F., Ruffo, R., Beverina, L., Sassi, M. & Salamone, M. M. ORGANIC ACTIVE MATERIALS FOR ELECTROCHEMICAL ENERGY STORAGE. (2015).
 112. Luo, W., Allen, M., Raju, V. & Ji, X. An Organic Pigment as a High-Performance Cathode for Sodium-Ion Batteries. *Adv. Energy Mater.* **4**, 1400554 (2014).
 113. Sharma, P., Damien, D., Nagarajan, K., Shaijumon, M. M. & Hariharan, M. Perylene-polyimide-Based Organic Electrode Materials for Rechargeable Lithium Batteries. *J. Phys. Chem. Lett.* **4**, 3192–3197 (2013).
 114. Bailey, M. The crystal structure of indanthrone. *Acta Crystallogr.* **8**, 182–185 (1955).
 115. Moritomo, Y., Goto, K. & Shibata, T. Glucose-Treated Manganese Hexacyanoferrate for Sodium-Ion Secondary Battery. *Energies* **8**, 9486–9494 (2015).
 116. Huggins, R. A. Simple method to determine electronic and ionic components of the conductivity in mixed conductors a

- review. *Ionics (Kiel)*. **8**, 300–313 (2002).
117. Stojadinović, J., Dushina, A., Trócoli, R. & La Mantia, F. Electrochemical Characterization of Gel Electrolytes for Aqueous Lithium-Ion Batteries. *Chempluschem* **79**, 1507–1511 (2014).
118. Ohkoshi, S. *et al.* High Proton Conductivity in Prussian Blue Analogues and the Interference Effect by Magnetic Ordering. *J. Am. Chem. Soc.* **132**, 6620–6621 (2010).
119. Song, J. *et al.* Removal of Interstitial H₂O in Hexacyanometallates for a Superior Cathode of a Sodium-Ion Battery. *J. Am. Chem. Soc.* **137**, 2658–2664 (2015).
120. Johnson, C. S. Diffusion ordered nuclear magnetic resonance spectroscopy: principles and applications. *Prog. Nucl. Magn. Reson. Spectrosc.* **34**, 203–256 (1999).

Table of Figures

FIGURE 1 PRIMARY ENERGY CONSUMPTION BY SOURCE AND SECTOR IN US IN 2014 ² ...	16
FIGURE 2 DEVELOPMENT OF THE PRODUCTION OF PRIMARY ENERGY IN EU-28 DURING 2004-2014 TIMESPAN. ³	18
FIGURE 3 OFFER AND DEMAND OF ENERGY FLUCTUATIONS AND BUFFER MECHANISM ⁵ .	19
FIGURE 4 THE VOLTA'S PILE. LEFT: A REAL PROTOTYPE. RIGHT: THE ZN, CARDBOARD AND CU STACKING IS REPRESENTED ¹⁴ .	24
FIGURE 5 RAGONE CHART. DIFFERENT ELECTROCHEMICAL STORAGE TECHNOLOGIES ARE PLOT AGAINST THEIR POWER AND ENERGY DENSITY ¹⁷ .	26
FIGURE 6 DANIELL'S ZINC-COPPER SOLID-LIQUID-SOLID BATTERY ¹⁸ .	28
FIGURE 7 GRAVIMETRIC AND VOLUMETRIC ENERGY DENSITIES OF CONVENTIONAL BATTERY SYSTEMS ²³ .	31
FIGURE 8 SONY'S ROCKING-CHAIR BATTERY: LAYERED LITHIUM COBALT OXIDE CATHODE, GRAPHITIC ANODE AND A LI-SALT BASED ORGANIC ELECTROLYTE. THE BLACK ARROWS SHOWS THE DIRECTIONS OF THE Li^+ IONS (IN RED) DURING THE CHARGE AND DISCHARGE STEPS ³¹ .	37
FIGURE 9 LEFT: GRAPHITE STACKED STRUCTURE. RIGHT: INITIAL CHARGE (REDUCTION) AND DISCHARGE (OXIDATION) CURVES OF GRAPHITE AS A NEGATIVE ELECTRODE WITH SEVERAL BINDERS, (A) PVDF, (B) PAAH, (C) PAALi, AND (D) PAANA, IN LiClO_4 1M EC:DMC AT 50 mA G^{-1} ³⁶ .	39
FIGURE 10 LEFT: SPINEL STRUCTURE OF THE $\text{Li}_4\text{Ti}_5\text{O}_{12}$ ANODE MATERIAL. OCTAHEDRAL SITES ARE OCCUPIED RANDOMLY BY LITHIUM (1/6) (NOT SHOWN IN IMAGE) AND TITANIUM (5/6) ATOMS. TI ATOMS ARE BLUE, LI ATOMS GREEN AND O ATOMS ARE RED. RIGHT: CHARGE DISCHARGE PROFILES OF A 88:6:6 TITANATE ELECTRODE AT 0.5 mA/G AT 30 °C IN 1M LiClO_4 EC:DME 1:1v. CAPACITY FADES IN 100 CYCLES FROM 160 MAH/G TO 150 MAH/G . ³⁸	41
FIGURE 11 LEFT: LAYERED MIXED METAL OXIDE CRYSTAL STRUCTURE (MIT'S COURTESY). RIGHT: CHARGE-DISCHARGE CURVES OF LiCoO_2 THIN FILM IN HALF CELL TEST ⁴² .	43
FIGURE 12 LEFT: LiMn_2O_4 SPINEL CRYSTAL STRUCTURE LI IN RED, TETRAHEDRAL MN IN YELLOW AND OCTAHEDRAL OXYGEN IN BLUE. RIGHT CHARGE DISCHARGE PROFILE OF $\text{Li}_x\text{Mn}_2\text{O}_4$ HALF-CELL, BOTH PLATEAUS AT 4V AND 3V ARE VISIBLE ⁴⁹ .	46

FIGURE 13 LEFT: THE OLIVINE STRUCTURE OF LiFePO_4 : SHOWING THE FeO_6 OCTAHEDRA (YELLOW), PO_4 TETRAHEDRA (BLUE), AND THE ONE-DIMENSIONAL TUNNELS IN WHICH THE Li^+ IONS RESIDE ⁵⁰. RIGHT: FIRST ELECTROCHEMICAL CYCLE OF HYDROTHERMAL LiFePO_4 AT ROOM TEMPERATURE ⁵¹ 47

FIGURE 14 GARTNER TYPE HYPE CHART FOR BATTERY TECHNOLOGIES. A TYPICAL TECHNOLOGY GOES THROUGH FIVE PHASES: (I) INNOVATION TRIGGER, (II) PEAK OF INFLATED EXPECTATIONS, (III) TROUGH OF DISILLUSIONMENT, (IV) SLOPE OF ENLIGHTENMENT AND (V) PLATEAU OF PRODUCTIVITY. NA–AIR, MG–ION, NA–ION, REDOX–FLOW, LI–S, LI–AIR AND LI–ION BATTERIES ARE PLOTTED AT THEIR RESPECTIVE PHASE OF DEVELOPMENT [45] 50

FIGURE 15 PROGRESSES, LEFT, AND EXPECTATIONS, RIGHT, IN THE OPTIMIZATION OF STORAGE TECHNOLOGIES ⁵⁵ 51

FIGURE 16 ILLUSTRATION COMPARING CURRENT TECHNOLOGY USING METAL-BASED ELECTRODE MATERIALS WITH A SIMPLIFIED CYCLE LIFE OF A “GREENER” LI-ION BATTERY TAKING BENEFIT OF REDOX-ACTIVE ORGANIC ELECTRODE MATERIALS DERIVING TYPICALLY FROM BIOMASS ⁶⁰ 55

FIGURE 17 AVERAGE VOLTAGE VS. NA AND CAPACITY FOR SOME FAMILIES OF ORGANIC ELECTRODE MATERIALS [17] 56

FIGURE 18 REPRESENTATIVE STRUCTURES OF THE CARBONYL-BASED ACTIVE ELECTRODE MATERIALS AND THEIR DIFFERENT STABILIZATION MECHANISM OF THE CHARGE ⁶⁷. 59

FIGURE 19 YELLOW, PURPLE, BLUE, GREEN AND RED PIGMENTS ⁶⁹ 61

FIGURE 20 THE STARRY NIGHT -1889 VAN GOGH. IN THIS PAINTING PRUSSIAN BLUE AND OTHER BLUE-HUE PIGMENTS HAVE BEEN USED ⁷³ 65

FIGURE 21 CYCLIC VOLTAMMETRY OF PB, 40MV/S IN 0.1M KCL AQUEOUS ELECTROLYTE ⁷⁹ 68

FIGURE 22 PRUSSIAN BLUE CUBIC CRYSTAL STRUCTURE: IN BLUE THE N-COORDINATED Me_1 , IN GREEN THE C-COORDINATED Me_2 AND IN RED THE INTERCALATED IONS ⁸⁹. 71

FIGURE 23 THERMAL GRAVIMETRIC ANALYSIS GENERAL WORKING SCHEME ⁹³. 73

FIGURE 24 TYPICAL DSC/DTA DIAGRAM. STEP-LIKE VARIATIONS ARE CHANGES IN THE SPECIFIC HEAT, E.G. GLASS TRANSITION. UPWARDS PEAKS CORRESPOND TO ENDOTHERMIC REACTIONS OR TRANSITIONS, WHILE DOWNWARDS ONES ARE EXOTHERMIC ⁹⁴ 75

-
- FIGURE 25 MASS SPECTROMETRY ANALYSIS OF PROPANE GAS. THE MS GRAPH REPRESENTS THE RELATIVE ABUNDANCE OF THE POSSIBLE M/Z DECOMPOSITION PRODUCTS PRESENTED ⁹⁵. 75
- FIGURE 26 LEFT: SCHEMATIC VIEW OF A SEM MACHINE. RIGHT: ELECTRON BEAM TO THE SAMPLE MATTER INTERACTION. ALL OF THOSE DIFFERENT SIGNALS ARE PECULIAR AND CAN BE USED TO BOTH CONSTRUCT THE IMAGE AND ANALYZE THE CHEMICAL AND STRUCTURAL COMPOSITION OF THE SAMPLE. THE BEAM INTERACTS ONLY WITH THE FIRST FEW MICRONS FROM THE SURFACE ⁹⁶. 77
- FIGURE 27 LEFT: TEM BUILDING SKETCH. THE SAMPLE IS PLACED BETWEEN THE PROJECTOR LENS AND THE SCREEN (I.E. THE DETECTOR), IN THE BEAM FOCUS. RIGHT: AN EXAMPLE OF THE TEM ANALYSIS. BOTH MORPHOLOGICAL AND STRUCTURAL INFORMATION ARE ACCESSIBLE FROM A SINGLE TEM MEASURE ⁹⁷. 79
- FIGURE 28 LEFT: SCHEMATIC OF THE MECHANISM OF GENERATION OF $K\alpha$, $K\beta$ AND $L\alpha$ PHOTO EMITTED X-RAYS. RIGHT: EDX PLOT EXAMPLE. IT IS CLEAR THE OVERLAPPING OF SIGNALS, ESPECIALLY AT LOW KEV ⁹⁸. 80
- FIGURE 29 LEFT: θ - 2θ GONIOMETER CONFIGURATION, BOTH THE X-RAY SOURCE AND DETECTOR MOVE FOLLOWING THE PERIMETER OF A CIRCUMFERENCE CENTERED IN THE SAMPLE. RIGHT: GEOMETRICAL REPRESENTATION OF THE INCIDENT AND REFLECTED BEAM. IF THE BRAGG'S LAW IS SATISFIED, A MAXIMUM OF INTERFERENCE HAPPENS AND A DIFFRACTION PEAK IS RECORDED. COURTESY OF ETH ZURICH ⁹⁹. 81
- FIGURE 30 THREE ELECTRODES FLOODED CELL. THE WORKING, WE, THE COUNTER, CE, AND THE REFERENCE ELECTRODES, RE, ARE SUBMERGED IN THE ELECTROLYTE. 86
- FIGURE 31 SWAGELOK™ CELLS. TWO ELECTRODES CONFIGURATION, LEFT, AND THREE ELECTRODES SETUP, RIGHT. METAL CURRENT COLLECTORS (SS, AL, AND CU) PROVIDE THE ELECTRICAL CONTACT. NOTE THE SPRING TO PROVIDE THE SAME PRESSURE TO THE STACKED MATERIALS AND THUS MAKING THE EXPERIMENT REPRODUCIBLE ¹⁰⁰. 87
- FIGURE 32 SECTION VIEW OF THE COIN CELL. NOTE THE GASKET PLACED BETWEEN THE ANODE AND CATHODE CASES THAT PROVIDES BOTH ELECTRICAL INSULATION AND PROTECTION FROM MOISTURE AND OXYGEN ¹⁰¹. 88
- FIGURE 33 VERY BASIC CONFIGURATION OF A THREE ELECTRODES CELL COUPLED TO A POTENTIOSTAT. THE CURRENT FLOWS BETWEEN WE AND CE, WHILE THE POTENTIAL IS CONTROLLED BETWEEN WE AND CE ¹⁰². 89
-

FIGURE 34 REPRESENTATION OF A SINGLE CYCLICVOLTAMMETRY SCAN, EUROPEAN CONVENTION ¹⁰³	90
FIGURE 35 GENERIC GALVANOSTATIC PLOT. DIFFERENT POLARIZATION CONTRIBUTES AS WELL AS IR DROP ARE HIGHLIGHTED. FOR SIMPLICITY THE OCV IS CONSIDERED CONSTANT ¹³	92
FIGURE 36 LEFT: DUAL COMPONENTS, SINGLE-PHASE TRANSFORMATION. RIGHT: SINGLE COMPONENT, SINGLE-PHASE REACTION ¹	94
FIGURE 37 ELECTROCHEMICAL IMPEDANCE SPECTROSCOPY OF A MIXED DIFFUSION AND CHARGE TRANSFER REACTION. LEFT: THE OBTAINED NYQUIST PLOT; LEFT: THE EQUIVALENT CIRCUIT ¹⁰⁴	96
FIGURE 38 LEFT: POLY(3,4-ETHYLENEDIOXYTHIOPHENE) (PEDOT) POLYMER STRUCTURE IN THE AROMATIC OXIDIZED COLORLESS STATE. RIGHT: 10 TH CYCLE OF ELECTRODEPOSITED PEDOT THIN LAYER, 50MC/CM ² , ON TOP OF GOLD PIN ELECTRODES CYCLED IN DIFFERENT ACETONITRILE-BASED ELECTROLYTES.	98
FIGURE 39 (A) POLYINDOLIZINE AROMATIC NEUTRAL STRUCTURE. (B) CYCLIC VOLTAMMETRY BEHAVIOUR OF POLYIND ELECTRODEPOSITED THIN FILM. (C) CYCLIC VOLTAMMETRY RESPONSE OF A THICK CHEMICALLY POLYMERIZED BULK POLYIND ELECTRODE.	99
FIGURE 40 (A) CAPACITY RETENTION OVER ONE THOUSAND CYCLES; INSET THE MONOMER STRUCTURE. (B) CYCLICVOLTAMMETRY RESPONSE OVER ONE THOUSAND CYCLES. ADD 3.7V TO CALCULATE THE POTENTIAL VS LI.	100
FIGURE 41 PERYLENEDIIMIDE “VIOLET 29” STRUCTURE, M _w 392G/MOL. IT IS A REDDISH POWDER.....	101
FIGURE 42 LEFT: THE PDI FIVE RINGS CORE PRESERVE ITS AROMATICITY AND THE MOLECULE IS IN THE NEUTRAL STATE. MIDDLE: UPON REVERSIBLE REDUCTION OF TWO ELECTRONS AT AROUND 2.5V, THE ELECTRONIC CONFIGURATION CHANGES AND O-LI, IONIC, GROUPS ARE FORMED AT THE CARBONYLS. RIGHT: A SECOND REDUCTION HAPPENS, ALL THE CARBONYLS ARE REDUCED AND THE CORE RINGS ARE IN QUINOID CONFIGURATION. THIS REDUCTION REACTION IS REPORTED TO HAPPEN CLOSE TO 0.5V AND BEING NOT FULLY REVERSIBLE.....	102
FIGURE 43 LEFT: SEM IMAGE OF COMMERCIAL UNTREATED PDI SHOWING THE NEEDLE SHAPE OF THE MICROMETRIC CRYSTALLITES: LENGTH 10 MICRONS, WIDTH 2	

MICRONS. RIGHT: THE XRD SPECTRUM, BLACK, OF THE COMMERCIAL SAMPLE IS COMPARED TO THE THEORETICAL ONE, RED.	103
FIGURE 44 IN BLACK, THE 50MV/S CYCLICVOLTAMMETRY AND, IN RED, THE 20MV/S DIFFERENTIAL PULSED VOLTAMMETRY OF THE PDI SOLUBLE DERIVATIVE ARE REPORTED. THE TWO SINGLE ELECTRON REDOX REACTIONS, AT 2.6V AND 2.4V RESPECTIVELY, ARE CLEARLY VISIBLE.	104
FIGURE 45 0.1MV/S CYCLICVOLTAMMETRY OF A CR2032 COIN CELL. THE CURRENT INTENSITY INCREASES UPON CYCLING SHOWING THE PRESENCE OF AN ACTIVATION MECHANISM.....	105
FIGURE 46 CR2032 PDI COIN CELL CYCLED AT 1C FOR ONE THOUSAND CHARGE/DISCHARGE RUNS.	106
FIGURE 47 GCPL OF ONE PDI COIN CELL CYCLED AT 1C RATE IN LP30 FOR ONE THOUSAND CYCLES. IN THE FIRST ONE HUNDRED CYCLES, AN UNKNOWN ACTIVATION PROCESS HAPPENS. HOWEVER, THE CHARGE EFFICIENCY, IN RED, IS REPORTED TO BE VERY CLOSE TO 100% MEANING THAT THE REVERSIBILITY OF THE REACTIONS INVOLVED IS HIGH. THE CHARGE CAPACITY FADES SLOWLY UPON CYCLING.....	108
FIGURE 48 PDI GCPL AT 1C, 136MA/G, IS PLOTTED. AFTER 100 CYCLES, THE CELL IS LEFT RESTING FOR 48H AND THE CYCLED AGAIN. NO BIG CHANGES IN BOTH CAPACITY AND CHARGE EFFICIENCY ARE RECORDED.....	110
FIGURE 49 PDI PRISTINE COIN CELL GCPL EXPERIMENT IN LI-BASED ELECTROLYTE AT DIFFERENT C-RATES.	111
FIGURE 50 0.1MV/S CYCLICVOLTAMMETRY OF A PDI COIN CELL CYCLED IN 1M NaClO ₄ IN EC:PC 1:1 _v ELECTROLYTE.	112
FIGURE 51 GCPL ANALYSIS AT DIFFERENT C-RATES, C/20 ÷ 2C, OF A PDI BASED ELECTRODE IN NaClO ₄ 1M IN EC:PC 1:1 _v ELECTROLYTE.	113
FIGURE 52 INDANTHRONE “BLUE 60” STRUCTURE, Mw 442g/mol. IT COMES AS A BLUE THIN POWDER.	114
FIGURE 53 SEM IMAGE OF AN INDANTHRONE WASHED SAMPLE. THE MATERIAL IS CLOSE PACKED AGGLOMERATES OF NEEDLE-LIKE CRYSTALLITES OF 2μm LONG AND FEW HUNDREDS OF NANOMETERS WIDE.	115
FIGURE 54 CYCLICVOLTAMMETRY OF A SWAGELOK™ CONTAINING AN IND ELECTRODE. SCAN SPEED IS 0.1MV/S WHILE THE ELECTROLYTE IS LP30.....	116

FIGURE 55 CR 2032 GALVANOSTATIC CYCLATION AT C/10 OF IND ELECTRODE IN LP30 ELECTROLYTE. 1 ST , BLACK, AND 2 ND , RED, CYCLES.	117
FIGURE 56 INSET: VIEW OF THE GLASS FIBER SEPARATORS AFTER BEING CYCLED IN A SWAGelok™ CELL. RE SEPARATOR IS CLEAN, WHILE WE/CE ONE IS STAINED. UV-VIS SPECTRUM OF LP30 SOLUTION AFTER 48H IN CONTACT WITH AN IND ELECTRODE IN THE NEUTRAL STATE.....	118
FIGURE 57 IND-ME METHYL DERIVATIVE MOLECULAR STRUCTURE AND, RIGHT, ITS 0.1mV/s CYCLIC VOLTAMMETRY IN LP30 USING BOTH POLYMERIC CELGARD™ AND GLASS-FIBER SEPARATORS.	119
FIGURE 58 GCPL PROFILES, LEFT, AND CHARGE CAPACITY AS WELL AS EFFICIENCY AT DIFFERENT C-RATES.	120
FIGURE 59 SEM IMAGE OF PRISTINE IND, LEFT, AND CARBON COATED IND, RIGHT... ..	121
FIGURE 60 CARBON COATED IND, 0.1mV/s CYCLICVOLTAMMETRY IN LP30.....	122
FIGURE 61 SILVER, LEFT, AND SILICON, RIGHT, CLADDED IND, 0.1mV/s CYCLICVOLTAMMETRY IN LP30.	122
FIGURE 62 QUINACRIDONE “VIOLET 19” STRUCTURE, MW 312G/MOL. IT IS A PURPLISH POWDER.....	123
FIGURE 63 LEFT: 50mV/s CYCLIC VOLTAMMETRY OF THE SOLUBLE DERIVATIVE OF QUINACRIDONE. RIGHT: 20mV/s DPV ANALYSIS. WE IS A GC PIN AND THE ELECTROLYTE OF CHOICE IN LiClO ₄ 0.1M CH ₂ Cl ₂ :MECN 1:1v.	125
FIGURE 64 SEM IMAGE, LEFT, OF THE COMMERCIAL QA PURPLE POWDER AFTER BEING WASHED IN CH ₂ Cl ₂ AND XRD, RIGHT, THEREOF. EXPERIMENTAL DATA IN RED, WHILE THEORETICAL ONE, MONOCLINIC C P2 ₁ /C CRYSTAL STRUCTURE, IN BLACK.	126
FIGURE 65 SELF-ASSEMBLED QUINACRIDONE/4AMMINOPYRIDINE SUPRAMOLECULAR STRUCTURE.	127
FIGURE 66 SEM IMAGES OF THREE DIFFERENT MORPHOLOGIES OF THE QA AFTER RIPRECIPIATION WITH, FROM TOP TO BOTTOM: 2-AMMINOPYRIDINE (QA-2AP), DIKETOPYRROLEPYRROLE (QA-DPP) OR BENZYLALCOHOL (QA-BA) AND 4-AMMINOPYRIDINE (4AP). SCALE IS 5μm.	128
FIGURE 67 LEFT: 0.1mV/s CYCLICVOLTAMMETRY OF SOLID STATE QA ELECTRODES CYCLED IN LP30. RIGHT: UV-VIS SPECTRUM OF SOLUBLE (IN BLACK), IN DICHLOROMETHANE, AND INSOLUBLE (IN RED), IN LP30, QA MOIETIES.	129

FIGURE 68 THE “MEATBALL SPAGHETTI” APPROACH SKETCH, LEFT, AND CYCLICVOLTAMMETRY, RIGHT.	130
FIGURE 69 THE POLYMERGENIC APPROACH IDEA AND THE QA DERIVED MOLECULE OF CHOICE.....	131
FIGURE 70 1mV/S CYCLIC VOLTAMMETRY OF AN ELECTROCHEMICALLY POLYMERIZED PEDOT-QA SAMPLE IN LiClO ₄ 0.1M MeCN. THE ARROWS INDICATE THE EVOLUTION OF THE PEAKS.	132
FIGURE 71 SEM IMAGE OF A SINGLE CUBIC PARTICLE OF MnHCCr.	134
FIGURE 72 TGA-MS ANALYSIS OF MnHCCr. AS ONLY A 15% LOSS IS RECORDED, THE MATERIAL SEEMS TO BE STABLE IN AIR UP TO 500 °C.....	135
FIGURE 73 XRD OF MnHCCr COMPOUND. THE EXPERIMENTAL DATA, IN BLACK, FITS WELL THE THEORETICAL ONE, IN RED. THE CALCULATED CRYSTAL STRUCTURE CORRESPOND TO THE CUBIC M-3M SPACE GROUP AND THE UNIT CELL PARAMETER IS 10.76Å. IN THE INSET IS REPORTED THE CRYSTAL STRUCTURE MODEL: BLACK Cr, LIGHT BLUE N, PINK Cr, BORDEAUX Mn AND LIME Na.	136
FIGURE 74 “INTERNAL TRANSVERSE INTERFACE IMPEDANCE AS WELL AS PARTIAL ELECTRONIC CONDUCTION” THEORETICAL NYQUIST PLOT, LEFT, AND CIRCUIT, RIGHT. $R_i=R_{GB}^{116}$	137
FIGURE 75 MnHCCr 1MHz-1Hz EIS AT 0.5GPa OF APPLIED PRESSURE. THE INSET ENLIGHTEN THE CONTACTS AND ELECTROLYTE RESISTANCE R_{el} , AS WELL AS THE IONIC ION, GRAIN BOUNDARY GB AND CHARGE TRANSFER CT CONTRIBUTES.	138
FIGURE 76 EXAMPLE OF DIFFUSION COEFFICIENT CALCULATION KNOWING THE CONDUCTIVITY, COMPOSITION AND STRUCTURE OF THE GIVEN MATERIAL.	139
FIGURE 77 1mV/S CYCLIC VOLTAMMETRY. 1 ST CYCLE OF MnHCCr CARBON CLOTH ELECTRODE IN AQUEOUS 8M NaClO ₄	140
FIGURE 78 MnHCCr GCPL CYCLING 100 TIMES AT 1C RATE. THE DOTTED RED LINE REPRESENT THE CATHODIC THERMODYNAMIC STABILITY OF WATER AT PH 7.	141
FIGURE 79 TEM IMAGE OF CrHCCr. THE CUBIC PARTICLES ARE AS SMALL AS FEW TENS OF NANOMETERS EACH.	142
FIGURE 80 TGA-MS ANALYSIS OF CrHCCr. THE MATERIAL LOSES 25% OF THE INITIAL WEIGHT WHEN HEATED TO 500 °C. THE MASS SPECTROMETER LINK THE LOSS TO THE ELIMINATION OF ADSORBED AND ZEOLITIC WATER AND DECOMPOSITION OF CYANIDE COMPOUNDS.....	143

FIGURE 81 CrHCCr XRD ANALYSIS. THE EXPERIMENTAL DATA, IN BLACK, FITS THE THEORETICAL ONE, IN RED. THE MATERIAL POSSES A CUBIC M-3M CRYSTAL STRUCTURE WITH CELL PARAMETER $a = 10.41\text{\AA}$	144
FIGURE 82 CrHCCr 1MV/S CYCLIC VOLTAMMETRY OF A CARBON CLOTH ELECTRODE CYCLED IN NaClO_4 8M AQUEOUS ELECTROLYTE.	145
FIGURE 83 CrHCCr GCPL ANALYSIS AT 1C IN NaClO_4 8M H_2O . THE RED LINE REPRESENTS THE STABILITY OF WATER.....	146
FIGURE 84 CrHCCr DEPOSITED ON GLASSY CARBON BULK WORKING ELECTRODE. THE CYCLICVOLTAMMETRY IS PERFORMED AT 1MV/S AND THE MATERIAL IS RUN IN NaClO_4 8M H_2O	147
FIGURE 85 CrHCCr CYCLING IN ORGANIC NaClO_4 1M PC ELECTROLYTE. BOTH THE CHARGE/DISCHARGE PROFILES AND CHARGE/EFFICIENCY PLOTS ARE REPORTED..	148
FIGURE 86 CrHCCr ELECTRODEPOSITION ON CARBON CLOTH WITH DIFFERENT TECHNIQUES, FROM THE TO: (A) 50MV/S CV, (B) -13.3 μA GS AND (C) -0.7V vs Ag/AgCl 3M PS.	149
FIGURE 87 GCPL OF CrHCCr DEPOSITED BY POTENTIOSTATIC MEAN, THE CHARGE/DISCHARGE CURRENT DENSITIES ARE VARIED EVERY FIVE CYCLES AND THE 5 TH CYCLE OF EVERY RATE IS PLOTTED. THE MATERIAL IS CYCLED IN NaClO_4 1M EC:DMC ORGANIC ELECTROLYTE.	150

List of Symbols, Fundamental Constants and Abbreviations

Symbol	Name	Unit
a_i	Activity of species i	mol dm^{-3}
C-rate	Rate of charge	Ah
c_i	Concentration of species	mol dm^{-3}
E°	Standard electrode potential	V or mV
ΔE°	Cell potential	V or mV
ΔG°	Standard Gibbs' free energy	J mol^{-1}
i	Electric current	μA , mA or A
M, m	Mass	g or kg
M_w	Molar mass	g mol^{-1}
n	Number of exchanged electrons	
Q	Practical charge capacity	mAh g^{-1} or Ah kg^{-1}
R	Resistance	Ω
T	Temperature	K
t	time	s
V	Volume	dm^3 or l
S	Conductivity	mS cm^{-1} or S cm^{-1}
D	Diffusion coefficient	$\text{cm}^2 \text{s}^{-1}$

Quantity	Symbol	Value	Power of Ten	Units
Faraday constant	F	9.6485	10^4	C mol^{-1}
Gas constant	R	8.3145		$\text{J K}^{-1} \text{mol}^{-1}$
Boltzmann	k	1.3806	10^{-23}	J K^{-1}
Avogadro constant	N_A	6.0221	10^{23}	mol^{-1}

2AP	2-amminopyridine
4AP	4-amminopyridine

BA	Benzylalcohol
CE	Counter Electrode
CH ₂ Cl ₂	Dichloro Methane
CV	Cyclic Voltammetry
DPP	Diketopyrrolepyrrole
DTA	Differential Temperature Analysis
EDX	Energy Dispersive X-ray Spectroscopy
emf	Electro-Motive Force
FEV	Full Electric Vehicle
GC	Glassy carbon
GS	GalvanoStatic
HEV	Hybrid Electric Vehicle
IND	Indanthrone
LIB	lithium Ion Battery
LiPO	lithium Polymer
LP30	EC:DMC 1M LiPF ₆
MeCN	Acetonitrile
MOF	Metal-Organic Framework
MS	Mass Spectroscopy
M _w	Molecular Weight
NIB	sodium Ion Battery
OSM	Organic Small Molecules
OSM	Organic Small Molecule
PB	Prussian Blue
PBA	Prussian Blue Analogue
PC	Propylene Carobnate
PDI	Perylenediimide
PS	PotentialStatic
PSH	Pumped-Storage Hydroelectricity
QA	Quinacridone
REF	REference electrode

SEI	Solid Electrolyte Interface
SEM	Scanning Electron Microscopy
SS	Stainless Steel
TEM	Tunnel Electron Microscopy
TGA	Thermal Gravimetric Analysis
WE	Working Electrode
XRD	X-ray Diffraction

Publications, Posters, Conferences

2014

- Investigation of $\text{Na}_x\text{Mn}_{0.5}\text{Fe}_{0.5}\text{O}_2$ Cathode Materials from Low Cost Preparation Route
IMLB 2014 - Poster Contribution
- Neutron Diffraction and Electrochemical Study of $\text{FeNb}_{11}\text{O}_{29}/\text{Li}_{11}\text{FeNb}_{11}\text{O}_{29}$ for lithium Battery Anode Applications.
Ilya Pinus, Michele Catti, Riccardo Ruffo, Matteo M. Salamone, and Claudio M. Mari
Chem. Mater., 2014, 26 (6), pp 2203–2209
- Investigation of redox activity in the naphthalenediimide-poly(3,4-ethylenedioxythiophene) cross-linked polymers.
Matteo M. Salamone, Mauro Sassi, Luca Beverina, Claudio M. Mari, Riccardo Ruffo
Electrochemical Acta (2014), 140, 152-159
- Organic Active Materials for Electrochemical Energy Storage
Toyota Motor Europe, Milano Bicocca University
Fabio Rosciano, Riccardo Ruffo, Luca Beverina, Mauro Sassi, Matteo Marco Salamone
PCT WO2014067574 (A1) — 2014-05-08

2015

- Materials, large-scale production technique of layers and spectro-electrochemical characterization of plastic based EC devices.
Poster session – WSED 2015
- Stokes shift/emission efficiency trade-off in donor–acceptor perylenemonoimides for luminescent solar concentrators.

Riccardo Turrisi, Alessandro Sanguineti, Mauro Sassi, Brett Savoie, Atsuro Takai, Giorgio E Patriarca, Matteo M Salamone, Riccardo Ruffo, Gianfranco Vaccaro, Francesco Meinardi, Tobin J Marks, Antonio Facchetti, Luca Beverina
Journal of Materials Chemistry A 3 (15), 8045-8054

2016

- chromium Hexacyanochromates: A New Anode Materials for sodium-Ion Batteries.
UK Korean Symposium 2016 – Poster Contribution
- A novel layered lithium niobium titanate as battery anode material: Crystal structure and charge-discharge properties.
Catti, M., Pinus, I., Ruffo, R., Salamone, M. M., & Mari, C. M. Solid State Ionics, 295, 72–77(2016)
- State-of-the-Art Neutral Tint Multichromophoric Polymers for High Contrast See-Through Electrochromic Devices.
Mauro Sassi, Matteo M. Salamone, Riccardo Ruffo, Giorgio E. Patriarca, Claudio M. Mari, Giorgio A. Pagani, Uwe Posset, Luca Beverina
Advanced Functional Materials (2016)
- Molecular Level Factors Affecting the Efficiency of Organic Chromophores for p-Type Dye Sensitized Solar Cells.
Svitlana Karamshuk, Stefano Caramori, Norberto Manfredi, Matteo Salamone, Riccardo Ruffo, Stefano Carli, Carlo A Bignozzi, Alessandro Abbotto
Energies (2016), 9
- Edge-Enriched 2D MoS₂ Thin Films Grown by Chemical Vapor Deposition for Enhanced Catalytic Performance.
Li, S., Wang, S., Salamone, M. M., Robertson, A. W., Nayak,

S., Kim, H., Pasta, M., Warner, J. H.

ACS Catalysis, 7(1), 877–886 (accepted 2016)

- Hexacyanochromates: New Anode Materials for sodium-Ion Batteries.

GEI-E3 2016 – Oral Contribution

Curriculum Vitae

Matteo Marco SALAMONE

26-11-1979 // Male // Italian

Via Angelo Cazzaniga 161, 20861, Brugherio (MB), ITALY

Mobile: +39 347 3065515 || Email: matteo.salamone@yahoo.it

EXPERIENCE

R&D Technologist 2009 – ongoing
INNOSHADE EU FP7 and EELICON EU FP7
Italian research consortium INSTM

- Electrochemical and chemical polymerization of electrochromic materials
- Evaluation of the optical and electrochemical properties
- Building of prototypes with different size and configuration
- Lifetime evaluation and climate-test ageing
- Drafting of standardized protocols for electrochromic materials and devices evaluation
- Production process scale-up

International collaborations:

- Six months at Hydro-Québec's Research Institute (Canada)
- Short periods at CIDETEC (Spain), Fraunhofer ISC and Coatema GmbH (Germany)

Ph.D. Research 2014 – 2016

Organic Materials for Energy Storage Applications
Università degli studi di Milano Bicocca and University of Oxford

- Evaluation of commercially-available organic dyes and tailoring thereof
- Synthesis of new optimized Prussian Blue analogues
- Chemical, structural, morphological, optical and electrochemical characterization
- Assembling of Na and Li battery prototypes
- Evaluation of the electrochemical performance

Side projects:

- Synthesis and characterization of sodium transition metal bronzes for Na-ion batteries
- Quantification of HOMO and LUMO in organic molecule for solar energy harvesting

Other Activities:

- Set up and management of new laboratories for electrochemical analysis
- Laboratory assistant during the Chemistry of Materials course and supervisor of undergraduate students' bachelor and master thesis
- Multi-year experience in promoting Hi-Tech companies during marketing campaigns and expositions

EDUCATION

- Jan 2014 - Dec 2016 (to be obtained in 2017)
Ph.D. in Materials Science and Nanotechnology
Università degli studi di Milano Bicocca

- Aug 2015 - Jun 2016
Visiting Ph.D. student
University of Oxford
- Oct 2008
M.Sc. in Materials Science
Università degli studi di Milano Bicocca

TECHNICAL SKILLS

- Techniques: basic and advanced electrochemical techniques, impedance, battery testing, SEM, EDS, XRD, TGA/DTA, DSC, DMA, UV-Vis, FTIR
- Thin-film deposition (blade, spin, deep, sputter coating)
- Chemical and electrochemical deposition of conductive polymers
- Wet and solid-state synthesis of inorganic compounds
- Slurry compounding optimization and battery prototypes assembling
- Expert worker in controlled environment: glove box and dry room
- Computer: Windows and (basic) Linux, Office suite, Origin and various instrument software

PERSONAL SKILLS

- Languages: Italian: mother tongue; English: C1 “proficient User”
- Team player, Communicative, Problem solver, Small group team leader

Acknowledgements

Professor Riccardo Ruffo and Professor Claudio Maria Mari for hosting me again in their lab and office during this new adventure and for the scientific and personal support they gave me.

Professor Luca Beverina et al. for helping me with the chemical aspects.

Professor Mauro Pasta for letting me be part of his group at Oxford Materials.

MY FAMILY that grew along with my Ph.D. Laura, my delightful wife, and little Giacomo, the reason why I'm here. I did all of this because of you, I hope that I will be able to provide you a peaceful and carefree future.

My mother.

My father Giovanni, my sister Diana and the whole family Massimo, Marco, Margherita and Riccardo.

Nonna Maria, Zia Giusi, Zia Rina, Zio Adri, Zio Franco and all the cousins Stefania, Alice, Barbara, Clara and Gianluca.

The Erbissonis, my family-in-law: Valter, Pinuccia, Luis, Mina, Elena, Andrea, Gaia Jr, Giulia Jr.

The reason why my mind didn't blow up during these three years is that I have wonderful friends. So, thank you for letting me be part of your life!

Fabio, seventeen years are passed and we are still friends even though all the kilometers and all the borders between us. Cheers mate!

Croce, if you did not exist, someone should take care of inventing you.

Cisco, you are a great friend. We had great food and rides together.

Luca, please come back!

Conan, we should hang out more often together.

Robbo, it's good having you back in the group.

Giangi, it's something like twenty-five years we know each other, remarkable.

Albert1, I'm glad to have you still around. Don't forget to smile sometime!

Riccardo, it's good sharing the same office with my "broken" nose.

Daniela & Mattia Jr, Sara & Bruno Jr, Tosca & Marco Jr, Kate & Federico Jr (..under construction), Melissa, Laura & Simone Jr, Madoka & Leandro Jr, Kona, Alessia & Dafne Jr, Ale, Angelo, Irene, Il Fra, Ciprea, Giafranco, Robi, Luca G, Massimiliano, Il Pasta, Erin, Nicoletta, Nor, Antonella, Gianluca L., Fabrizio, The Mangiagallis, ...

Gianluca, it has been a pleasure being your lab mate in this three-year adventure. I wish you the best for the future.

The lunch crew.

The people from the lab.

All the SdMs.

The Canadians "ECDs".

The MTB syndicate.

The organic dream team.

Oxford PBG's.

The housemates from Oxford Brookes University.

Cuba and Spritz, the cats.

Bender B. Rodriguez, Philosopher.